GW_CLASS: Cosmological Gravitational Wave Background in the cosmic linear anisotropy solving system

Journal of Cosmology and Astroparticle Physics
An IOP and SISSA journal

GW_CLASS: Cosmological Gravitational Wave Background in the cosmic linear anisotropy solving system

Florian Schulze,[a,b] **Lorenzo Valbusa Dall'Armi,**[c,d] **Julien Lesgourgues,**[b] **Angelo Ricciardone,**[e,f,c] **Nicola Bartolo,**[c,d,g] **Daniele Bertacca,**[c,d,g] **Christian Fidler**[b] **and Sabino Matarrese**[c,d,g,h]

[a]Max-Planck-Institut für Kernphysik,
Saupfercheckweg 1, 69117 Heidelberg, Germany
[b]Institute for Theoretical Particle Physics and Cosmology (TTK), RWTH Aachen University,
D-52056 Aachen, Germany
[c]Dipartimento di Fisica e Astronomia "Galileo Galilei",
Università degli Studi di Padova,
via Marzolo 8, I-35131, Padova, Italy
[d]INFN, Sezione di Padova,
via Marzolo 8, I-35131, Padova, Italy
[e]Dipartimento di Fisica "Enrico Fermi", Università di Pisa,
Pisa I-56127, Italy
[f]INFN sezione di Pisa, Pisa I-56127, Italy
[g]INAF- Osservatorio Astronomico di Padova,
Vicolo dell'Osservatorio 5, I-35122 Padova, Italy
[h]Gran Sasso Science Institute,
Viale F. Crispi 7, I-67100 L'Aquila, Italy

E-mail: florian.schulze@mpi-hd.mpg.de, lorenzo.valbusadallarmi@phd.unipd.it, lesgourg@physik.rwth-aachen.de, angelo.ricciardone@pd.infn.it, nicola.bartolo@pd.infn.it, daniele.bertacca@pd.infn.it, fidler@physik.rwth-aachen.de, sabino.matarrese@pd.infn.it

Received June 19, 2023
Accepted August 27, 2023
Published October 6, 2023

Abstract. The anisotropies of the Cosmological Gravitational Wave Background (CGWB) retain information about the primordial mechanisms that source the gravitational waves and about the geometry and the particle content of the universe at early times. In this work, we discuss in detail the computation of the angular power spectra of CGWB anisotropies and of their cross correlation with Cosmic Microwave Background (CMB) anisotropies, assuming different processes for the generation of these primordial signals. We present

https://doi.org/10.1088/1475-7516/2023/10/025

JCAP10(2023)025

an efficient implementation of our results in a modified version of `CLASS` which will be publicly available. By combining our new code `GW_CLASS` with `MontePython`, we forecast the combined sensitivity of future gravitational wave interferometers and CMB experiments to the cosmological parameters that characterize the cosmological gravitational wave background.

Keywords: cosmological perturbation theory, gravitational waves / sources, primordial gravitational waves (theory), physics of the early universe

ArXiv ePrint: 2305.01602

JCAP10(2023)025

Contents

JCAP10(2023)025

1 Introduction

The Cosmological Background of Gravitational Waves (CGWB) is probably the most fascinating target of future Cosmic Microwave Background (CMB) and Gravitational Wave (GW) detectors. It can be produced by different mechanisms in the early universe such as inflation, phase transitions (PTs), cosmic strings (CSs), primordial black holes (PBHs), etc. (see [1–4] for reviews). Each of these sources leads to a peculiar frequency spectrum that can be used to discriminate among them [5, 6]. Thanks to their remarkable sensitivity, the next generation of detectors — such as the Einstein Telescope (ET) [7–9], Cosmic Explorer (CE) [10, 11] or LISA [12], BBO [13] and DECIGO [14] — will detect the sum of a large number of individual black hole and neutron star mergers plus various relevant sources of astrophysical and cosmological backgrounds. In such a situation, the detection of the stochastic background of gravitational waves from the data will be challenging. For this reason, it is important to introduce as many observables characterizing the Stochastic Gravitational Wave Background (SGWB) signal as possible.

It has been shown in the literature that mapping anisotropies in the SGWB [15–18] would provide a powerful way to distinguish between (different contributions to) the astrophysical background (generated by many overlapping or faint sources) [19–25] and the cosmological one [2–4] (see [26] for a recent forecast about detection of anisotropies with future ground-based detectors.). Like for CMB photons, the energy density of GWs exhibits small spatial fluctuations, which carry information both on the GW production mechanism and on the properties of the universe along each line of sight.

The astrophysical background has been thoroughly studied in the literature. A complete gauge invariant treatment of its anisotropies has been carried out in [27]. The authors of [28] have recently released a branch of the Einstein-Boltzmann solver (EBS) `CLASS` [29] that allows to predict the statistics of anisotropies in the Astrophysical Gravitational Wave Background (AGWB), taking into account astrophysical dependencies and projection effects. Meanwhile, reference [30–33] has provided a framework to describe the statistics of anisotropies in the CGWB, which shares many common features with CMB anisotropies. Reference [34] shows that the CGWB contains information about the abundance of ultra-relativistic relics in the very early universe and about pre-recombination physics that is not accessible with other means. It also shows that CGWB anisotropies are significantly correlated with CMB anisotropies [35, 36]. This can be used to test systematic errors and/or new physics in both CMB and SGWB measurements, or to assess the significance of CMB anomalies [37].

In this paper, we present and release[1] `GW_CLASS`, a code able to compute the one-point and two-point statistics of the CGWB anisotropies generated by a list of plausible mechanisms. This code is an extension of the publicly available EBS `CLASS`,[2] which has been developed to compute mainly CMB, cosmic shear and galaxy number count anisotropies [29, 38].

The `GW_CLASS` code takes into account the production mechanism of the GW background in the very early universe (i.e. GW decoupling) and its propagation through large-scale cosmic inhomogeneities. It incorporates the computation of the CGWB angular power spectrum $C_\ell^{\mathrm{CGWB}\times\mathrm{CGWB}}$, of the CMB×CGWB angular cross-correlation spectrum and of the spatially-averaged energy density spectrum $\bar{\Omega}_{\mathrm{GW}}(f)$.

[1] As soon as this paper is accepted, the code will be publicly accessible as a new branch `GW_CLASS` on the `CLASS` repository www.github.com/lesgourg/class_public. The repository will include an explanatory jupyter notebook, allowing to reproduce the most important figures of this work.

[2] http://www.class-code.net.

JCAP10(2023)025

The CGWB anisotropies do not carry directly an information on the GW monopole $\bar{\Omega}_{\rm GW}(f)$. However, since gravitons do not thermalise, the knowledge of $\bar{\Omega}_{\rm GW}(f)$ is necessary to compute the spectrum $C_\ell^{\rm CGWB\times CGWB}$ observable at a given GW detector frequency f [30]. One can actually play with the f-dependency to optimize the detection of anisotropies [39].

Among many possible cosmological mechanisms of GW production, we focus here on inflationary models with a blue tilt ($n_T > 0$), first-order phase transitions and scalar-induced GWs that may lead to the formation of PBHs. According to current knowledge, these mechanisms are the most likely to be detectable by GW interferometers like ET [7, 8], CE [10, 11] and LISA [12, 40, 41]. In a first step, the `GW_CLASS` code can be used to predict the monopole $\bar{\Omega}_{\rm GW}(f)$, to compare it with the sensitivity of the detector, and to check whether the chosen generation mechanism may lead to a detection. If this is the case, `GW_CLASS` is used again to compute the angular power spectrum $C_\ell^{\rm CGWB\times CGWB}$ and then, in combination with the parameter inference package `MontePython` [42, 43], to forecast the sensitivity of the detector to model parameters.

An important feature of `GW_CLASS` is that it takes into account any possible ultra-relativistic relics that may have decoupled at very high energy scales — much larger than those usually probed by CMB observations. This allows to use CGWB anisotropies as a new tool to probe physics beyond the Standard Model [34]. Furthermore, `GW_CLASS` computes efficiently the angular power spectrum of the CGWB at different frequencies, including the auto- and cross-correlation of the spectra at a list of frequencies that can be specified by the user. This attribute would be extremely useful in any analysis that require a precise knowledge of the shape in frequency of the stochastic background, in order to do component separation with other signals [44] or to minimize the impact of instrumental noise on the estimate of the anisotropies.

In section 2, we summarize the formalism describing the two-point statistics of CGWB anisotropies. In section 3, we present our modelling of GW generation mechanisms. In section 4, we show how to compute the CMB×CGWB angular cross-correlation spectrum. In section 5, we show the results of a few sensitivity forecasts for the LIGO-Virgo-Kagra (LVK) network, for the ET+CE network and for even more futuristic experiments. Our conclusions are exposed in section 6. In appendix A we relate our notation to previous work. Appendix B and C detail our assumptions concerning the initial conditions for the GW anisotropies at the time of GW decoupling, while appendix D summarizes the formalism describing the generation of GWs during inflation. Appendix E presents a calculation that helps to understand the shape of the CMB×CGWB cross-correlation spectrum. Finally, appendix F contains technical details on the numerical implementation and accuracy of `GW_CLASS`.

2 Boltzmann approach to the SGWB anisotropies

The summary presented in this section is based on previous results from references [32–35]. However, we switch here to notations closer to those of the `CLASS` code and papers [29, 45]. Appendix A summarizes the correspondence between different sets of notations.

2.1 Basic formalism

In the limit of geometrical optics, the propagation of GWs (or gravitons) can be described using the Boltzmann equation [46]. The limit of geometrical optics is well justified if the shortwave approximation is valid, i.e., when the wavelength of the GWs under consideration is much smaller than the typical scales over which the background metric varies. In this work

JCAP10(2023)025

we are computing the anisotropies of cosmological GW background that can be detected by current and future GW interferometers, thus the smallest frequencies considered are in the Pulsar Timing Array (PTA) band (around the nHz) and the angular scales that can be probed (typically up to a multipole $\ell_{\rm max} \approx 10 - 15$ [26, 47]) are much larger than the wavelength of the GWs. Along each geodesic, GWs can be described by a distribution function $f_{\rm GW}(x^\mu, p^\mu)$, where x^μ denotes position and $p^\mu = dx^\mu/d\lambda$ momentum (which relates to the GW frequency). $f_{\rm GW}$ evolves according to the Boltzmann equation

$$\mathcal{L}[f_{\rm GW}] = \mathcal{C}[f_{\rm GW}(\lambda)] + \mathcal{I}[f_{\rm GW}(\lambda)]\,, \tag{2.1}$$

where $\mathcal{L} \equiv d/d\lambda$ is the Liouville operator along the geodesic, while $\mathcal{C}$ is the collision operator and $\mathcal{I}$ accounts for emissivity from cosmological and astrophysical sources [31]. In the case of the CGWB, the emissivity term can be treated as an initial condition on the GW distribution, while, in the case of the AGWB, it would be related, e.g., to black hole merging along the geodesic [31]. Typically, the GW collision term can be neglected, since it only affects the distribution at higher orders in the gravitational strength $M_{\rm Pl}^{-1}$ (where $M_{\rm Pl}$ is the reduced Planck mass). See e.g., [48] for a study of the AGWB anisotropies in presence of collision, accounting for gravitational Compton scattering off of massive objects.

We assume that our universe is well described by a perturbed Friedmann-Lemaitre-Robertson-Walker (FLRW) metric, and we adopt the Newtonian gauge in which

$$ds^2 = a^2(\eta)\left[-e^{2\psi}d\eta^2 + (e^{-2\phi}\delta_{ij} + h_{ij})dx^i dx^j\right]\,, \tag{2.2}$$

where $a(\eta)$ is the scale factor as a function of conformal time η, $\phi(\eta, x^i)$ and $\psi(\eta, x^i)$ account for scalar perturbations, and the transverse-traceless (TT) stress tensor $h_{ij}(\eta, x^i)$ for large-scale tensor perturbations. Then, we can solve the Boltzmann equation (2.1) at the background and linear levels.

Once the background distribution $\bar{f}_{\rm GW}$ is expressed as a function of η and of the comoving momentum $q = ap$ (left invariant by the expansion, while the physical momentum scales like $p \propto a^{-1}$), the background Boltzmann equation simply reads $\partial \bar{f}_{\rm GW}/\partial\eta = 0$. It is solved by any distribution that does not explicitly depend on time, namely $f_{\rm GW} = \bar{f}_{\rm GW}(q)$. Including the linear level, the equation becomes [31–33]

$$\frac{\partial f_{\rm GW}}{\partial \eta} + n^i \frac{\partial f_{\rm GW}}{\partial x^i} + \left[\frac{\partial \phi}{\partial \eta} - n^i \frac{\partial \psi}{\partial x^i} - \frac{1}{2} n^i n^j \frac{\partial h_{ij}}{\partial \eta}\right] q \frac{\partial f_{\rm GW}}{\partial q} = 0\,, \tag{2.3}$$

where the unit vector $\hat{n}$ of components $n^i = p^i/p$ denotes the direction of propagation of GWs.

The perturbed GW energy at a given time and location is given by integrating over momentum (or frequency) and direction,

$$\rho_{\rm GW}(\eta, \vec{x}) = \frac{1}{a^4(\eta)} \int d^2\hat{n} \int dq\; q^3\, f_{\rm GW}(\eta, \vec{x}, q, \hat{n})\,. \tag{2.4}$$

It is useful to introduce a dimensionless quantity $\omega_{\rm GW}$ that accounts for the contribution of GWs propagating at a given time, location, frequency and direction to the critical density:

$$\omega_{\rm GW}(\eta, \vec{x}, q, \hat{n}) = \frac{4\pi}{\rho_{\rm crit}(\eta)} \frac{q^4}{a^4(\eta)} f_{\rm GW}(\eta, \vec{x}, q, \hat{n})\,, \tag{2.5}$$

where $\rho_{\rm crit} = 3H^2 M_{\rm Pl}^2$ and H the Hubble rate. The monopole of $\omega_{\rm GW}$ is denoted as

$$\Omega_{\rm GW}(\eta, \vec{x}, q) = \int \frac{d^2\hat{n}}{4\pi}\, \omega_{\rm GW}(\eta, \vec{x}, q, \hat{n})\,, \tag{2.6}$$

JCAP10(2023)025

and the average value of this monopole as

$$\bar{\Omega}_{\rm GW}\left(\eta,\, q\right) = \langle \Omega_{\rm GW}\left(\eta,\, \vec{x},\, q\right)\rangle_{\vec{x}}\,. \tag{2.7}$$

With such definitions, the anisotropy of the CGWB density at the detector's time η_0, location $\vec{x}_0$ and momentum/frequency q can be simply defined as:

$$\delta_{\rm GW}(\eta_0, \vec{x}_0, q, \hat{n}) \equiv \frac{\omega_{\rm GW}(\eta_0,\, \vec{x}_0,\, q,\, \hat{n}) - \Omega_{\rm GW}(\eta_0,\, \vec{x}_0,\, q)}{\Omega_{\rm GW}(\eta_0,\, \vec{x}_0,\, q)}\,. \tag{2.8}$$

In very good approximation, we can assume that the detector occupies a typical position in the universe where $\Omega_{\rm GW}(\eta_0,\, \vec{x}_0,\, q) = \bar{\Omega}_{\rm GW}(\eta_0,\, q)$ and redefine the anisotropy as

$$\delta_{\rm GW}(\eta_0, \vec{x}_0, q, \hat{n}) \equiv \frac{\omega_{\rm GW}(\eta_0,\, \vec{x}_0,\, q,\, \hat{n}) - \bar{\Omega}_{\rm GW}(\eta_0,\, q)}{\bar{\Omega}_{\rm GW}(\eta_0,\, q)}\,. \tag{2.9}$$

Given that $[\Omega_{\rm GW}(\vec{x}) - \bar{\Omega}_{\rm GW}]$ is a linear perturbation — with random values at each $\vec{x}$ much smaller than $\bar{\Omega}_{\rm GW}$, typically by five orders of magnitude — the definitions given in (2.8) and (2.9) only differ by a stochastic multiplicative factor very peaked near one and a stochastic monopole term very peaked near zero, none of which are detectable. Thus, we can rely on the second definition, for which making theoretical predictions is more straightforward.[3]

At this point, as shown in [31–33], it is useful to re-define the perturbed graviton distribution function in terms of the phase-space relative perturbation Γ,

$$\delta f_{\rm GW} = f_{\rm GW} - \bar{f}_{\rm GW} \equiv -q\,\frac{\partial \bar{f}_{\rm GW}}{\partial q}\,\Gamma\left(\eta,\, \vec{x},\, q,\, \hat{n}\right), \tag{2.10}$$

such that the first order Boltzmann equation reads in Fourier space

$$\Gamma' + i\,k\,\mu\,\Gamma = \phi' - ik\,\mu\,\psi - \frac{1}{2} n^i n^j\, h'_{ij}\,, \tag{2.11}$$

where the terms on the r.h.s. define the so-called source function $S(\eta,\, \vec{k},\, \hat{n})$. A prime denotes a derivative with respect to conformal time, and μ is the cosine of the angle between $\vec{k}$ and $\hat{n}$. $\vec{k}$ and k are the wave vector and wave number of the (large-scale) cosmological perturbations and should not be confused with the graviton comoving momentum $\vec{q} = a\,\vec{p}$ which is orders of magnitudes larger. The solution of eq. (2.11) can be decomposed as

$$\Gamma(\eta,\, \vec{k},\, q,\, \hat{n}) = \Gamma_I(\eta,\, \vec{k},\, q,\, \hat{n}) + \Gamma_S(\eta,\, \vec{k},\, \hat{n}) + \Gamma_T(\eta,\, \vec{k},\, \hat{n})\,, \tag{2.12}$$

where I, S, and T stand for *Initial*, *Scalar* and *Tensor*. These indices refer to the mechanism *sourcing* the graviton perturbation. The *Initial* term is related to the anisotropies generated by the GW production mechanism before the free propagation of the waves. The scalar and tensor terms correspond to additional anisotropies induced by the propagation of GWs in a background with large-scale perturbations of scalar type (sourced by $\phi' - ik\,\mu\,\psi$) and/or tensor type (sourced by $-\frac{1}{2} n^i n^j\, h'_{ij}$). The scalar and tensor source terms are independent of

[3] The same approximation is always implicitly performed in the case of CMB anisotropies. For instance, the temperature anisotropy map $\delta T/\bar{T}$ should in principle be defined with respect the temperature monopole $T_{\rm CMB} = \langle T(\vec{x}_0, \hat{n})\rangle_{\hat{n}}$ at the detector's location. However, for the purpose of making theoretical predictions, the map is always implicitly assumed to be defined with respect to the spatially averaged temperature monopole $\bar{T} = \langle T(\vec{x}, \hat{n})\rangle_{\vec{x},\hat{n}}$.

JCAP10(2023)025

the GW momentum/frequency q, and so are the contributions Γ_S, Γ_T. On the other hand, as stressed in [32, 33] the initial anisotropies can have a large (order unity) dependence on the frequency (contrary to what happens for CMB photons at linear order).[4]

The GW energy density contrast $\delta_{\rm GW}$ of eq. (2.9) is related to the phase-space relative perturbation Γ and to the fractional background energy density contribution $\bar{\Omega}_{\rm GW}$ [32, 33] through

$$\delta_{\rm GW}\left(\eta_0,\,\vec{x}_0,\,q,\,\hat{n}\right) = \left(4 - \frac{\partial \ln \bar{\Omega}_{\rm GW}\left(\eta_0,\,q\right)}{\partial \ln\, q}\right) \Gamma\left(\eta_0,\,\vec{x}_0,\,q,\,\hat{n}\right) \equiv \left(4 - n_{\rm gwb}\right) \Gamma\,, \tag{2.13}$$

where we define the Gravitational Wave Background (GWB) spectral index

$$n_{\rm gwb}(q) \equiv \frac{\partial \ln \bar{\Omega}_{\rm GW}\left(\eta_0,\,q\right)}{\partial \ln\, q}. \tag{2.14}$$

In this relation, $n_{\rm gwb}(q)$ should be evaluated at the detector momentum/frequency q at which $\delta_{\rm GW}$ is measured. Many cosmological GW production mechanisms (see section 3.2) have a GW frequency spectrum well described by a simple power law (i.e., $\bar{\Omega}_{\rm GW} \propto q^{n_{\rm GWB}}$) such that $n_{\rm gwb}$ is independent of the considered frequency.

Like in the case of the CMB temperature anisotropies, we can expand the GW density contrast in spherical harmonics $Y_{\ell m}(\hat{n})$,

$$\delta_{\rm GW}(\eta_0, \vec{x}_0, q, \hat{n}) = \sum_{\ell} \sum_{m=-\ell}^{\ell} \delta_{{\rm GW},\,\ell m}(\eta_0,\,\vec{x}_0,\,q)\, Y_{\ell m}(\hat{n})\,. \tag{2.15}$$

As we will see in the next sections, the scalar and tensor contributions are ubiquitous for all cosmological production mechanisms, since they are generated by the propagation itself, while the initial contribution should depend on each specific scenario. Following [32, 33], in harmonic space, the three contributions to the solution of the linear Boltzmann equation read

$$\begin{aligned}
\delta_{{\rm GW},\,\ell m,\,I}\left(q\right) &= 4\pi\,(-i)^{\ell}\,(4 - n_{\rm gwb}) \int \frac{d^3k}{(2\pi)^3}\, {\rm e}^{i\vec{k}\cdot\vec{x}_0}\, Y^*_{\ell m}(\hat{k})\, \Gamma(\eta_{\rm in},\,\vec{k},\,q)\, j_{\ell}\left[k\left(\eta_0 - \eta_{\rm in}\right]\right)\,, \\
\delta_{{\rm GW},\,\ell m,\,S} &= 4\pi\,(-i)^{\ell}\,\left(4 - n_{\rm gwb}\right) \int \frac{d^3k}{(2\pi)^3}\, {\rm e}^{i\vec{k}\cdot\vec{x}_0}\, Y^*_{\ell m}(\hat{k})\, \mathcal{R}(\vec{k})\, \Delta^S_{\ell}\left(k,\,\eta_0,\,\eta_{\rm in}\right)\,, \\
\delta_{{\rm GW},\,\ell m,\,T} &= 4\pi\,(-i)^{\ell}\,\left(4 - n_{\rm gwb}\right) \int \frac{d^3k}{(2\pi)^3}\, {\rm e}^{i\vec{k}\cdot\vec{x}_0} \sum_{\lambda=\pm 2} {}_{-\lambda}Y^*_{\ell m}(\hat{k})\, h_{\lambda}(\vec{k})\, \Delta^T_{\ell}\left(k,\,\eta_0,\,\eta_{\rm in}\right)\,,
\end{aligned} \tag{2.16}$$

where $\eta_{\rm in}$ is an initial time after which the GWs propagate freely (defined in the next subsection) and $j_{\ell}(x)$ are the spherical Bessel functions. For concision, on the left-hand side, we omitted the detector's time and location $(\eta_0, \vec{x}_0)$ in the argument of the multipoles.

In order to derive the first integral, one needs to assume that the initial phase-space perturbation — that would read in general $\Gamma(\eta_{\rm in},\,\vec{k},\,q,\,\hat{n})$ — does not depend on the direction $\hat{n}$. Such a dependence might arise in the case of a breaking of statistical isotropy, as mentioned in ref. [33], even though this is not the only possibility. In any case, we do assume here

[4]The initial anisotropies could be sourced by both scalar and tensor perturbations, depending on the mechanism considered.

JCAP10(2023)025

that $\Gamma(\eta_{\rm in},\,\vec{k},\,q,\,\hat{n})$ does not depend on $\hat{n}$, giving a plausible physical example on how this condition can be satisfied in section 2.3 and appendix C.

In the next two terms accounting for scalar and tensor contributions, we have factorized out the primordial scalar (comoving curvature) perturbation $\mathcal{R}(\vec{k})$ and the primordial tensor perturbation $h_\lambda(\vec{k})$ (where $\lambda=\pm2$ accounts for the two polarisation degrees of freedom) at a given wavevector $\vec{k}$, defined at very early times on super-Hubble scales. The scalar and tensor transfer functions Δ_ℓ^X, with $X=S,T$, account for the sourcing of graviton fluctuations by metric perturbations at a given wavenumber k between $\eta_{\rm in}$ and η_0. They depend on the metric transfer functions T_ϕ, T_ψ, T_h normalised to

$$\phi(\eta,\vec{k}) = T_\phi(\eta,k)\mathcal{R}(\vec{k})\,, \tag{2.17}$$

$$\psi(\eta,\vec{k}) = T_\psi(\eta,k)\mathcal{R}(\vec{k})\,, \tag{2.18}$$

$$h_{ij}(\eta,\vec{k}) = \sum_{\lambda=\pm2} e_{ij,\lambda}(\hat{k})\,T_h(\eta,\,k)\,h_\lambda(\vec{k})\,, \tag{2.19}$$

where $e_{ij,\lambda}(\hat{k})$ is the polarisation tensor normalised to one, $e_{ij,\lambda}(\hat{k})e_{ij,\lambda'}(\hat{k})=\delta_{\lambda\lambda'}$. The scalar and tensor transfer functions can be expressed as line-of-sight integrals,

$$\begin{aligned}
\Delta_\ell^S\,(k,\,\eta_0,\,\eta_{\rm in}) &\equiv T_\psi\,(\eta_{\rm in},\,k)\;j_\ell\,(k\,(\eta_0-\eta_{\rm in}))+\int_{\eta_{\rm in}}^{\eta_0}d\eta\,\frac{\partial\,[T_\phi\,(\eta,\,k)+T_\psi\,(\eta,\,k)]}{\partial\eta}\,j_\ell\,(k\,(\eta_0-\eta))\,,\\
\Delta_\ell^T\,(k,\,\eta_0,\,\eta_{\rm in}) &\equiv \sqrt{\frac{(\ell+2)!}{(\ell-2)!}}\,\frac{1}{4}\int_{\eta_{\rm in}}^{\eta_0}d\eta\,\frac{\partial T_h\,(\eta,\,k)}{\partial\eta}\,\frac{j_\ell\,(k\,(\eta_0-\eta))}{k^2\,(\eta_0-\eta)^2}\,.
\end{aligned} \tag{2.20}$$

Under the assumption of statistical isotropy and in absence of statistical correlations between the three GW density multipoles ($\delta_{{\rm GW},\,\ell m,\,I}$, $\delta_{{\rm GW},\,\ell m,\,S}$, $\delta_{{\rm GW},\,\ell m,\,T}$), we can decompose the harmonic power spectrum of GW density as

$$\delta_{\ell\ell'}\;\delta_{mm'}C_\ell^{\rm CGWB\times CGWB} \equiv \left\langle\delta_{{\rm GW},\ell m}\delta^*_{{\rm GW},\ell' m'}\right\rangle \equiv \delta_{\ell\ell'}\;\delta_{mm'}\;\left[C_{\ell,I}\,(q)+C_{\ell,S}+C_{\ell,T}\right]\,, \tag{2.21}$$

where the three contributions are given by

$$C_{\ell,I}\,(q) = 4\pi\,(4-n_{\rm gwb})^2\int\frac{dk}{k}\;\left[j_\ell\,(k\,(\eta_0-\eta_{\rm in}))\right]^2\;P_I\,(q,\,k)\;, \tag{2.22}$$

$$C_{\ell,S} = 4\pi\,(4-n_{\rm gwb})^2\int\frac{dk}{k}\;\left[\Delta_\ell^S\,(k,\,\eta_0,\,\eta_{\rm in})\right]^2\;P_{\mathcal{R}}\,(k)\;, \tag{2.23}$$

$$C_{\ell,T} = 4\pi\,(4-n_{\rm gwb})^2\int\frac{dk}{k}\;\left[\Delta_\ell^T\,(k,\,\eta_0,\,\eta_{\rm in})\right]^2\;\sum_{\lambda=\pm2}P_{h_\lambda}\,(k)\;. \tag{2.24}$$

Here, we have introduced the primordial power spectrum $P_I\,(q,\,k)$ of the initial phase-space perturbation $\Gamma(\eta_{\rm in},\,\vec{k},\,q)$, the primordial scalar spectrum $P_{\mathcal{R}}\,(k)$, and the primordial tensor spectra $P_{h_\lambda}\,(k)$ for $\lambda=\pm2$. In a FLRW universe, for standard models, the latter are equal to each other and usually parametrized as $P_{h_1}(k)=P_{h_2}(k)=\frac{1}{4}P_T(k)$, where $P_T(k)$ is the primordial tensor spectrum (defined in more details in appendix D). Since the two-point function $\langle\mathcal{R}(\vec{k})h_\lambda(\vec{k}')\rangle$ vanishes as a consequence of statistical isotropy conservation, the scalar and tensor contributions are uncorrelated and their spectra can be summed in quadrature. On the other hand, the initial anisotropy of the stochastic background could depend on the scalar perturbation $\mathcal{R}$, leading to a cross-correlation between $\delta_{{\rm GW},\,\ell m,\,I}$ and $\delta_{{\rm GW},\,\ell m,\,S}$ that was neglected above for simplicity. A more general analysis of this correlation is performed

JCAP10(2023)025

in section 2.3. We will see that in the case of pure adiabatic initial conditions, the initial and scalar-induced contributions are actually maximally correlated, which implies that the angular power spectrum must be written differently than in eq. (2.21).

The expression of the GW scalar transfer function in eq. (2.20) allows to draw an analogy with the CMB: GWs are affected by a Sachs-Wolfe (SW) contribution, which represents the energy lost by a graviton escaping from a potential well $\psi(\eta_{\rm in}, \vec{x})$, and by an Integrated Sachs-Wolfe (ISW) contribution that depends on the variation of the potentials $(\psi + \phi)$ along the line of sight. However, for all GW production mechanisms, the decoupling time is considerably smaller than the photon decoupling time, leading to very different values of the SW and ISW terms in the GW and CMB cases.

The main goal of our new code `GW_CLASS` is to evaluate the angular power spectra of eqs. (2.21)–(2.24) for different CGWB production mechanisms.

2.2 Initial time

In principle, the choice of initial time $\eta_{\rm in}$ should be very different for the purpose of CMB and CGWB calculations. For the CMB, it is sufficient to pick up an initial time corresponding to a few e-folds of expansion before the smallest observable wavelength crosses the Hubble radius. This condition is met with an initial conformal time $\eta_{\rm min} \sim \mathcal{O}(10^{-1})$ Mpc, that corresponds roughly to a redshift $z_{\rm max} \sim \mathcal{O}(10^6)$.[5]

Instead, the CGWB allows us to probe much earlier times in the cosmic history. In this work, we consider a CGWB of frequency f produced at some time $\eta_{\rm prod}$ and decoupled afterwards (e.g. $\eta_{\rm prod}$ could be the end of inflation or of a phase transition). If at this time the CGWB of frequency f is already inside the horizon, $\eta_{\rm in}$ should in principle be set to $\eta_{\rm prod}$. Otherwise, since GWs start to propagate and transport energy when they enter the Hubble radius, $\eta_{\rm in}$ should in principle be set to the Hubble crossing time $\eta_{\rm h.c.}$. For a GW of momentum q — related to the observed frequency today f through $q = 2\pi\, a_0\, f/c$ — this time reads

$$\frac{q}{\mathcal{H}(\eta_{\rm h.c.})} = 1 \qquad \Rightarrow \qquad \eta_{\rm h.c.} = \begin{cases} 1/q & \text{Radiation Domination} \\ 2/q & \text{Matter Domination} \end{cases} \tag{2.25}$$

where $\mathcal{H}$ is the conformal Hubble rate. Thus, in principle, the initial time should be adjusted to

$$\eta_{\rm in}(f) = \max\left[\eta_{\rm prod}, \eta_{\rm h.c.}(f)\right] . \tag{2.26}$$

For instance, the network ET+CE is expected to probe a frequency range $f \in [1, 3000]$ Hz, leading approximately to

$$\eta_{\rm h.c.} \in \left[10^{-18}, 10^{-15}\right] \text{ Mpc}\,, \tag{2.27}$$

which is considerably smaller than the time of equality $\eta_{\rm eq} \approx 112\,$Mpc, or even than the initial time of CMB calculations $\eta_{\rm min} \simeq 10^{-1}$ Mpc. This is also true for other GW detectors such as LISA, BBO, DECIGO and Taiji, which are expected to work in the milli-Hertz frequency range.

[5] `CLASS` makes a conservative choice of integrating background and thermodynamical equations starting from a much earlier time, but what really matters is the time at which the perturbation equations start to be followed. For simple cosmologies, default precision and CMB calculations, this time is indeed close to $\eta_{\rm min} \simeq 10^{-1}$ Mpc.

JCAP10(2023)025

In practice, at the code level, the situation is different for two reasons:

- On super-Hubble scales $k \ll \mathcal{H}$, the metric fluctuations $\phi(\eta, \vec{k})$, $\psi(\eta, \vec{k})$, $h_{ij}(\eta, \vec{k})$ have a trivial evolution that can be computed analytically. The same holds for the GW perturbations $\Gamma(\eta, \vec{k}, q)$ and their power spectrum $P_I(q, k)$. Thus, it would be a waste of time to integrate numerically some perturbation equations between $\eta_{\rm in}$ and the usual EBS initial time $\eta_{\rm min}$.

- Besides the evolution of perturbations, $\eta_{\rm in}$ appears either in the integral boundary or in the argument of the spherical Bessel function in eqs. (2.20), (2.22), and thus, plays a role in projection effects from Fourier to multipole space. However, from this point of view, as long as $\eta_{\rm in}$ is very small compared to η_0, its precise value does not affect the final angular power spectra. In particular, we checked that for all the production mechanisms considered in the next section, $\eta_{\rm in}$ can be substituted in the Bessel function by any value smaller or equal to $\eta_{\rm min}$ without changing the spectra.

The conclusion is that, in the code, it is possible to integrate all perturbation equations starting from the usual time $\eta_{\rm min} \simeq 10^{-1}$ Mpc and to set $\eta_{\rm in}$ in spherical Bessel functions to any arbitrary value smaller or equal to $\eta_{\rm min}$ — as long as the super-Hubble evolution of perturbations between the time $\eta_{\rm in}$ and $\eta_{\rm min}$ is correctly modelled analytically. The next sections will show how to account for this evolution in different cases. As a result of this discussion, we see that the smallness of $\eta_{\rm in}$ has no impact on the structure nor computational cost of EBSs like `CLASS`.[6]

2.3 Adiabatic initial conditions for GWs

We now come back to the expression of the first (initial) contribution to the angular power spectrum in eq. (2.22).

Let us assume for a while that the initial perturbation Γ of the graviton phase-space distribution $f_{\rm GW}$ has non-negligible anisotropies that depend on the angle between the wavevector $\vec{k}$ and the direction of propagation $\hat{n}$, such that $\vec{k} \cdot \hat{n} = k\,\mu$. It can then be expanded in multipoles,

$$\Gamma(\eta_{\rm in}, \vec{k}, q, \hat{n}) = \sum_{\ell} (-i)^{\ell} (2\ell + 1)\, \Gamma_l(\eta_{\rm in}, \vec{k}, q)\, \mathcal{P}_\ell(\mu)\,, \tag{2.28}$$

where $\mathcal{P}_\ell(\mu)$ stands for Legendre polynomials. The evolution of these multipoles obeys to a Boltzmann hierarchy. We can make progress under the assumption that, at some very early times, only the first multipoles survive, for instance because of some tight coupling regime between GW modes. (One can draw an analogy with the CMB for which, as long as photons are tightly coupled, higher multipoles are suppressed by powers of $k\eta/\kappa$, where κ is the photon optical depth, see e.g. [46]). Later on, during the free-streaming regime, higher multipoles grow, but remain very small on super-Hubble scales, since the structure of the Boltzmann hierarchy requires

$$\Gamma_\ell(\eta, \vec{k}, q) \approx k\eta\, \Gamma_{\ell-1}(\eta, \vec{k}, q)\,. \tag{2.29}$$

[6] Still notice that, as already mentioned at the end of the previous section, and as we will detail later, the fact that $\eta_{\rm prod}$ and $\eta_{\rm in}$ for the CGWB are much smaller that the decoupling time of CMB photons, *does* indeed lead to significant differences in the corresponding final angular power spectra.

JCAP10(2023)025

At the initial time $\eta_{\rm in}$ defined in section 2.2, Fourier modes of interest are particularly far outside the Hubble scale, $k\eta_{\rm in} \ll 1$, and thus the multipoles $\ell \geq 2$ can be safely neglected. This argument does not hold for the dipole Γ_1, which is a gauge-dependent quantity, and which also depends on momentum exchanges during a possible early tight coupling regime. It does hold for the quadrupole Γ_2, which could be sourced by tensor perturbations on cosmological scales, but remains very small as long as these scales are super-Hubble.

In a next step, we can decompose as usual the possible solutions of the system of perturbation equations (including the Boltzmann hierarchy for Γ_ℓ) in one growing adiabatic mode and several non-adiabatic and/or decaying modes. If we consider only the growing adiabatic mode (and neglect any decaying mode) we are compatible with the "separate universe assumption" [49]. As a matter of fact, in this case, each Hubble patch evolves like a separate universe, where it is possible to foliate the space-time in spatial hypersurfaces of uniform density in which the curvature perturbation is conserved. Then, on super-Hubble scales, all quantities, such as e.g. the density of GWs $\rho_{\rm GW}(\eta, \vec{x})$, have spatial fluctuations (whatever gauge one chooses) related to a unique time-shifting function $\delta\eta(\vec{x})$ via the time-derivative of the background solution, like in

$$\delta\rho_{\rm GW}(\eta, \vec{x}) = \dot{\bar{\rho}}_{\rm GW}(\eta)\ \delta\eta(\vec{x})\,. \tag{2.30}$$

If a single-clock mechanism generates primordial curvature perturbations $\mathcal{R}(\vec{k})$ in the universe, the presence of the adiabatic mode is unavoidable. Non-adiabatic modes may appear in cases where the generation of GWs leads additionally to intrinsic primordial fluctuations in Γ that are not captured by the "separate universe assumption". Such a GW generation mechanism should involve a local time-shifting function (that is, a local random process) on top of the time-shifting function that describes primordial curvature perturbations. Such a mechanism is difficult to realize on super-Hubble scales. However, we will see later an explicit example based on GWs generated by the formation of primordial black holes triggered by non-Gaussian perturbations [50].

We already argued that multipoles $\ell \geq 2$ should be vanishingly small on super-Hubble scales obeying $k\eta_{\rm in} \ll 1$. In the case of the adiabatic mode, it is also possible to relate the monopole Γ_0 to metric perturbations (in the Newtonian gauge, to ψ, see appendix B) and to prove that $\Gamma_1 \ll \Gamma_0$ (see appendix C for a proof in the same gauge). For non-adiabatic modes, it is not obvious that the dipole can be neglected, but for simplicity, we assume that this is true in this work and in our `CLASS` implementation. Thus, we always assume that Γ reduces to its monopole component Γ_0, and we can expand the initial perturbation Γ of the graviton phase-space distribution into an adiabatic and non-adiabatic contribution,

$$\Gamma(\eta_{\rm in}, \vec{k}, q, \hat{n}) = \Gamma_0(\eta_{\rm in}, \vec{k}, q) = T_\Gamma^{\rm AD}(\eta_{\rm in}, k, q)\,\mathcal{R}(\vec{k}) + \Gamma_0^{\rm NAD}(\eta_{\rm in}, \vec{k}, q)\,. \tag{2.31}$$

In the Newtonian gauge and for the adiabatic contribution, we can use the relation

$$\Gamma_0(\eta_{\rm in}, \vec{k}, q) = -\frac{2}{4 - n_{\rm gwb}(q)}\psi(\eta_{\rm in}, \vec{k}) \tag{2.32}$$

shown in appendix B, and express the adiabatic transfer function of Γ at a given momentum/frequency q as

$$T_\Gamma^{\rm AD}(\eta_{\rm in}, k, q) = -\frac{2}{4 - n_{\rm gwb}(q)}T_\psi(\eta_{\rm in}, k)\,. \tag{2.33}$$

JCAP10(2023)025

Finally, the total angular power spectrum of the CGWB can be expressed in a handy form,

$$\frac{C_\ell^{\rm CGWB\times CGWB}}{(4-n_{\rm gwb})^2} = 4\pi \int \frac{dk}{k} \Bigg\{ \left[\Delta_\ell^{\rm AD}(k,\eta_0,\eta_{\rm in},q) + \Delta_\ell^{\rm SW}(k,\eta_0,\eta_{\rm in}) + \Delta_\ell^{\rm ISW}(k,\eta_0,\eta_{\rm in})\right]^2 P_{\mathcal{R}}(k) \\ + \left[j_\ell\left(k\left(\eta_0-\eta_{\rm in}\right)\right)\right]^2 P_\Gamma^{\rm NAD}(k,q) \\ + j_\ell\left(k\left(\eta_0-\eta_{\rm in}\right)\right)\left[\Delta_\ell^{\rm AD}+\Delta_\ell^{\rm SW}+\Delta_\ell^{\rm ISW}\right] P^\times(k,q) \\ + \left[\Delta_\ell^T(k,\eta_0,\eta_{\rm in})\right]^2 \sum_{\lambda=\pm 2} P_{h_\lambda}(k) \Bigg\}, \tag{2.34}$$

where, in addition to eq. (2.20), we defined the GW anisotropy transfer functions

$$\begin{aligned} \Delta_\ell^{\rm AD}(k,\eta_0,\eta_{\rm in},q) &\equiv -\frac{2}{4-n_{\rm gwb}(q)}\, T_\psi\left(\eta_{\rm in},\, k\right)\, j_\ell\left(k\left(\eta_0-\eta_{\rm in}\right)\right)\,, \\ \Delta_\ell^{\rm SW}(k,\eta_0,\eta_{\rm in}) &\equiv T_\psi\left(\eta_{\rm in},\, k\right)\, j_\ell\left(k\left(\eta_0-\eta_{\rm in}\right)\right)\,, \\ \Delta_\ell^{\rm ISW}(k,\eta_0,\eta_{\rm in}) &\equiv \int_{\eta_{\rm in}}^{\eta_0} d\eta\, \frac{\partial\left[T_\phi\left(\eta,\, k\right)+T_\psi\left(\eta,\, k\right)\right]}{\partial\eta}\, j_\ell\left(k\left(\eta_0-\eta\right)\right)\,, \end{aligned} \tag{2.35}$$

and the non-adiabatic and cross-correlation primordial spectra

$$\begin{aligned} P_\Gamma^{\rm NAD}(k,q) &= \left\langle \left|\Gamma_0^{\rm NAD}(\eta_{\rm in},\vec{k},q)\right|^2 \right\rangle\,, \\ P^\times(k,q) &= \left\langle \mathcal{R}(\vec{k})\,\Gamma_0^{\rm NAD*}(\eta_{\rm in},\vec{k},q)\, + \mathcal{R}^*(\vec{k})\,\Gamma_0^{\rm NAD}(\eta_{\rm in},\vec{k},q) \right\rangle\,. \end{aligned} \tag{2.36}$$

The re-writing of eq. (2.21) in the form of eq. (2.34) can be seen as a change of basis from the modes "initial, scalar" (I,S) to the modes "adiabatic, non-adiabatic" (AD, NAD), leaving the tensor contribution unchanged. The latter decomposition better captures the statistical correlation between the adiabatic component of the initial contribution $\delta_{{\rm GW},\,\ell m,I}$ and the scalar-induced contribution $\delta_{{\rm GW},\,\ell m,\,S}$.

In figure 1, we show two examples of CGWB angular power spectra generated by scalar perturbations with adiabatic initial conditions — that is, considering only the first line in (2.34) — with two different tilts $n_{\rm gwb}$. As already explained in [34], these spectra do not feature acoustic peaks like the CMB ones. As a matter of fact, GW anisotropies arise from metric perturbations, rather than fluctuations in a fluid featuring pressure and acoustic waves. The ISW contribution and the total angular power spectrum are enhanced at small angular scales ($\ell > 100$), because Fourier modes crossing the Hubble radius during radiation domination experience a variation of metric fluctuations that boosts the ISW term. At larger angular scales, the ISW term also picks up a contribution from the variation of metric perturbations around the time of equality between radiation and matter. Indeed, during the transition from a radiation-dominated universe to a matter-dominated one, the large-scale scalar metric perturbations get damped by a factor close to 9/10 [46, 51, 52]. In the CMB case, this variation does not contribute to the ISW term since it occurs before recombination.

In figure 2, we show the angular power spectrum of the CGWB generated by scalar and tensor perturbations with adiabatic initial conditions and $n_{\rm gwb}(q) = 0.4$. The tensor power spectrum $P_T(k)$ has been computed by assuming the Planck constraints on the tensor-to-scalar ratio, $r = 0.03$, and $n_{\rm t}(k) = -r/8(2-r/8-n_S) \approx -0.003$.[7] In analogy with the ISW term

[7] Note that in general $n_{\rm gwb} \neq n_t$, see the discussion after eq. (3.3).

JCAP10(2023)025

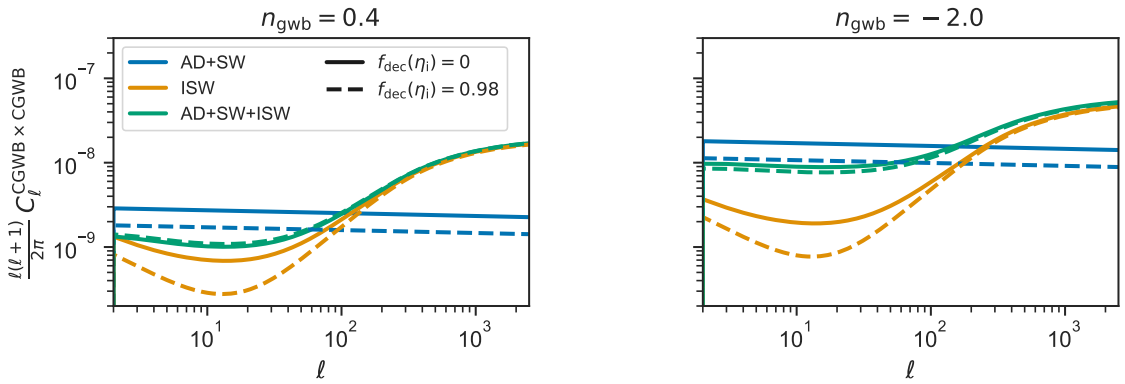

Figure 1. Plot of the contributions to the dimensionless angular power spectrum of CGWB anisotropies seeded by curvature perturbations: AD+SW contribution (blue), ISW contribution (orange) and total AD+SW+ISW contribution (green). Solid lines assume a fraction of relativistic decoupled species — defined in eq. (2.37) — $f_{\rm dec}(\eta_{\rm in}) = 0$, and dashed lines $f_{\rm dec}(\eta_{\rm in}) = 0.98$. We show two examples of GWB with different spectral indices, $n_{\rm gwb} = 0.4$ (left panel) and $n_{\rm gwb} = -2.0$ (right panel), and adiabatic initial conditions.

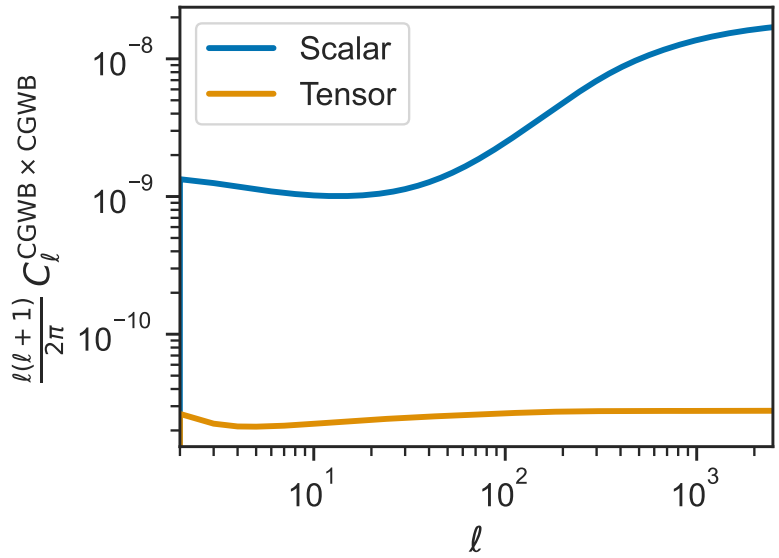

Figure 2. Plot of the contributions to the angular power spectrum of the CGWB for adiabatic initial conditions and $n_{\rm gwb}(q) = 0.4$: scalar (blue), tensor (orange). The primordial tensor spectrum has been computed for the tensor-to-scalar ratio (defined in (3.3)) $r = 0.03$ and $n_{\rm t}(k) = -0.003$. All the spectra assume $f_{\rm dec}(\eta_{\rm in}) = 0$.

of the scalar part, $C_{\ell,T}$ is not suppressed at small angular scales, because the CGWB is sensitive to the variations of T_h also during the radiation-dominated era. As expected [34], the anisotropies induced by large-scale tensor perturbations are subdominant w.r.t. the scalar ones.

2.4 Relativistic decoupled species at early times

The transfer functions of eq. (2.35) show that the angular power spectrum of the CGWB depends on the value of the scalar metric fluctuations (ϕ, ψ) — or, equivalently, of the transfer functions (T_ϕ, T_ψ) — at the very early time $\eta_{\rm in}$ and at all subsequent times. In section 2.2,

JCAP10(2023)025

we argued that the evolution of such perturbations on super-Hubble scales can be followed analytically between $\eta_{\rm in}$ and $\eta_{\rm min} \sim 0.1$ Mpc.

This evolution is discussed in reference [34]. It depends mainly on variations in the fractional energy density of relativistic and decoupled particles species $f_{\rm dec}(\eta)$, defined as

$$f_{\rm dec}(\eta) \equiv \frac{\bar{\rho}_{\rm r}^{\rm dec}(\eta)}{\bar{\rho}_{\rm tot}(\eta)} \,. \tag{2.37}$$

As a matter of fact, these species have a non-vanishing anisotropic stress $\sigma_{\rm dec}$ that determines the difference between the scalar metric perturbations, as shown by the transverse-traceless part of the Einstein equation in the Newtonian gauge,

$$k^2(\phi - \psi) = 16\pi G\, a^2 \bar{\rho}_{\rm r}^{\rm dec}\, \sigma_{\rm dec} \,. \tag{2.38}$$

The solution of the perturbation equations on super-Hubble scales and for the adiabatic mode gives [34, 51]

$$\begin{aligned} \psi(\eta, \vec{k}) &= -\frac{2}{3}\left[1 + \frac{4}{15} f_{\rm dec}(\eta)\right]^{-1} \mathcal{R}(\vec{k}) \,, \\ \phi(\eta, \vec{k}) &= -\frac{2}{3}\left[1 + \frac{4}{15} f_{\rm dec}(\eta)\right]^{-1} \left[1 + \frac{2}{5} f_{\rm dec}(\eta)\right] \mathcal{R}(\vec{k}) \,. \end{aligned} \tag{2.39}$$

The knowledge of $f_{\rm dec}(\eta_{\rm in})$ is important to set properly the value of the transfer function $T_\psi(\eta_{\rm in}, k)$ in $\Delta_\ell^{\rm AD}$ and $\Delta_\ell^{\rm SW}$. In addition, any variation of $f_{\rm dec}(\eta)$ over time leads to a non-zero derivative $(\phi' + \psi')$, and thus to a contribution to the ISW transfer function $\Delta_\ell^{\rm ISW}$ of eq. (2.35). Note that the ISW transfer function of GW anisotropies features an integral from the very early time $\eta_{\rm in}$ defined in section 2.2 until today. This is very different from the ISW transfer function of CMB anisotropies, in which the integral runs only from the time of photon decoupling $\eta_{\rm dec}$ until today.[8]

In its standard version, the `CLASS` code infers from user input the value $f_{\rm dec}(\eta_{\rm min})$ at the initial time at which perturbations are integrated, $\eta_{\rm min} \sim 0.1$ Mpc. At this time, which corresponds to a temperature much smaller than that of neutrino decoupling, $T_{\rm min} \ll T_\nu^{\rm dec} \sim 1\,$MeV, neutrinos are expected to free-stream. For a standard cosmology with three neutrinos, a simple calculation involving the neutrino-to-photon temperature ratio gives approximately $f_{\rm dec}(\eta_{\rm min}) = \bar{\rho}_\nu(\eta_{\rm min})/\bar{\rho}_{\rm r}(\eta_{\rm min}) \simeq 0.4$. For models with a non-standard neutrino density or with additional free-streaming relics (e.g. dark radiation particles originating from a dark sector), `CLASS` adapts this value consistently as a function of input parameters (like the neutrino temperature, the effective number of free-streaming ultra-relativistic relics, etc.[9]) The value of $f_{\rm dec}(\eta_{\rm min})$ is used to set initial conditions for metric perturbations, and then, these fluctuations are evolved according to the Einstein equations. This approach is clearly sufficient for the calculation of CMB anisotropies, but not for that of GW anisotropies, since it neglects any variation of $f_{\rm dec}(\eta)$ between $\eta_{\rm in}$ and $\eta_{\rm min}$.

In `GW_CLASS`, the user passes the value of $f_{\rm dec}(\eta_{\rm in})$ in a given model as an input parameter `f_dec_ini`. This value is taken into account for calculating $T_\psi(\eta_{\rm in}, k)$ in $\Delta_\ell^{\rm AD}$ and $\Delta_\ell^{\rm SW}$.

[8] To be precise, the ISW integral of CMB anisotropies is performed over $e^{-\kappa}(\phi' + \psi')$, where κ is the photon optical depth. In very good approximation, $e^{-\kappa}$ vanishes for $\eta < \eta_{\rm dec}$, which means that the lower boundary of the integral can be set effectively to $\eta_{\rm dec}$ — although EBSs do not perform such an approximation.

[9] In the code, $f_{\rm dec}(\eta_{\rm min})$ is dubbed `fracnu`, but it does take into account any free-streaming relativistic relics beyond standard neutrinos.

JCAP10(2023)025

The code also computes $f_{\rm dec}(\eta_{\rm min})$ like in the standard version: this number is still used to initialise all perturbations at $\eta_{\rm min}$. Finally, the integral in $\Delta_\ell^{\rm ISW}$ is decomposed in two parts. The first part, referred to as the primordial (prim) ISW — with an integral from $\eta_{\rm in}$ to $\eta_{\rm min}$ — is performed analytically [34], giving

$$\begin{aligned}\Delta_\ell^{\rm ISW-prim} &\equiv \int_{\eta_{\rm in}}^{\eta_{\rm min}} d\eta\, j_\ell[k(\eta_0-\eta)]\,\left[T'_\psi(\eta,k)+T'_\phi(\eta,k)\right]\\ &\simeq j_\ell[k(\eta_0-\eta_{\rm in})]\left[T_\psi(\eta,k)+T_\phi(\eta,k)\right]_{\eta_{\rm in}}^{\eta_{\rm min}}\\ &= j_\ell[k(\eta_0-\eta_{\rm in})]\frac{2}{15}\frac{f_{\rm dec}(\eta_{\rm in})-f_{\rm dec}(\eta_{\rm min})}{1+\frac{4}{15}f_{\rm dec}(\eta_{\rm min})}T_\psi(\eta_{\rm in},k)\,,\end{aligned} \tag{2.40}$$

where in the second line we used the fact that $k\eta_{\rm in}$ and $k\eta_{\rm min}$ are both much smaller than one (see section 2.2) to approximate $j_\ell[k(\eta_0-\eta)]$ as $j_\ell[k(\eta_0-\eta_{\rm in})]$, in order to pull this factor out of the integral. The second part — with an integration from $\eta_{\rm min}$ to η_0 — is performed numerically like in the standard version of the code, and both terms are added up to form $\Delta_\ell^{\rm ISW}$.

From a theoretical prospective, the most natural value for $f_{\rm dec}(\eta_{\rm in})$ should be zero, because standard model particles are expected to be strongly interacting in the early universe, at the time when the GW background forms. This is the default setting in `GW_CLASS`.

The CGWB is sensitive not just to the relativistic and decoupled degrees of freedom at high temperatures, $f_{\rm dec}(\eta_{\rm in})$, but in principle also to any ingredient changing the evolution of metric perturbations in the very early universe. Another example is provided by the equation of state of the cosmic fluid driving the expansion of the Universe at $\eta_{\rm prod}$ [53]. More specifically, deviations from the standard equation of state of a relativistic fluid at early times, $w=1/3$, would affect both the SW and the primordial ISW with expressions analogous to eqs. (2.39) and (2.40).

We should stress that the sensitivity of the anisotropies of the CGWB to parameters that influence the evolution of the metric perturbations — like $f_{\rm dec}(\eta_{\rm in})$ — strongly depends on initial conditions and on the frequency dependence of the monopole. In the case of adiabatic initial conditions, the dependence of the CGWB on the $f_{\rm dec}(\eta_{\rm in})$ can be summarized as

$$T_\Gamma^{\rm AD}(\eta_{\rm in},k,q)+T_\Phi(\eta_{\rm in},k)+\frac{\Delta_\ell^{\rm ISW-prim}(\eta_{\rm in},k)}{j_\ell(k(\eta_0-\eta_{\rm in}))}\propto\frac{\frac{6-n_{\rm gwb}(q)}{4-n_{\rm gwb}(q)}+\frac{2}{5}f_{\rm dec}(\eta_{\rm in})}{1+\frac{4}{15}f_{\rm dec}(\eta_{\rm in})}\,. \tag{2.41}$$

In the limit $n_{\rm gwb}\to 0$, the factor on the right-hand side is independent of the number of relativistic and decoupled degrees of freedom (or of the equation of state of the universe at early times, as pointed out by [53]). However, we will explicitly show in further sections that, in the majority of the frequency bins accessible by future interferometers, the tensor tilt $n_{\rm gwb}$ is different from zero (in particular it must be larger than zero if we focus on inflationary mechanisms which respect CMB bounds) for signals that are detectable by current and future GW interferometers.

Figure 1 shows the impact of varying $f_{\rm dec}(\eta_{\rm in})$ on two examples of CGWB spectra. In the left panel, assuming purely adiabatic initial conditions with $n_{\rm gwb}=0.4$, we see that the effect of increasing $f_{\rm dec}(\eta_{\rm in})$ from 0 to 0.98 is large on the individual AD+SW and ISW contributions, but nearly cancels out in the total AD+SW+ISW spectrum. In the right panel, assuming purely adiabatic initial conditions, but with a different tilt $n_{\rm gwb}=-2.0$, the effect of $f_{\rm dec}(\eta_{\rm in})$ on the total spectrum is enhanced.

JCAP10(2023)025

The enhancement factor can be easily inferred from our code, but it is difficult to predict analytically. Indeed, on the one hand, the scaling of the AD+SW contribution with $f_{\rm dec}(\eta_i)$ is exactly given by $[1+4/15\, f_{\rm dec}(\eta_{\rm in})]^{-2}$, because this term is proportional to the square of T_ψ at the time $\eta_{\rm in}$. On the other hand, for the ISW term, the factor found in eq. (2.40), which described the primordial ISW contribution, needs to be summed up at large scales with the early ISW contribution. The latter is caused by the variation of scalar metric perturbations around equality, as discussed at the end of section 2.3, and needs to be computed numerically. In any case, the most important message that can be inferred from figure 1 is that, even in the case of adiabatic initial conditions, the total (AD+SW+ISW) angular power spectrum is sensitive to $f_{\rm dec}(\eta_i)$, with a dependence that can be enhanced for non-zero values of the monopole tilt $n_{\rm gwb}$ of the CGWB. In [34], the adiabatic initial condition of the CGWB has not been considered, in order to do a model-independent discussion of the imprint of the relativistic and decoupled species on the CGWB anisotropies. This is the reason why the damping of the angular power spectrum for larger values of $f_{\rm dec}(\eta_{\rm in})$ is more enhanced in [34] than in figure 1.

3 Cosmological Gravitational Wave Background Sources

As stated above, the physical observable that we can measure with interferometers is the SGWB density contrast [32, 33, 47] defined in eqs. (2.9), (2.13),

$$\delta_{\rm GW}\left(\eta_0,\, \vec{x}_0,\, f,\, \hat{n}\right) = \left(4 - \frac{\partial \ln \bar{\Omega}_{\rm GW}\left(\eta_0,\, f\right)}{\partial \ln f}\right) \Gamma\left(\eta_0,\, \vec{x}_0,\, f,\, \hat{n}\right), \tag{3.1}$$

where we used the observed GW frequency $f = \frac{c}{2\pi\, a_0}\, q$ instead of the comoving graviton momentum q. The value of the pre-factor in eq. (3.1) is model dependent, so we need to know the underlying source of GWs. Our goal is to estimate the angular power spectrum of $\delta_{\rm GW}$ in models that have a monopole amplitude detectable by the future ground-based interferometer network ET+CE.

Among several possible cosmological sources of GWs, three mechanisms are very promising because they relate to different aspects of early universe models: inflation with a blue tilt, first-order phase transitions, and second-order-induced GWs. The detection of inflationary GWs with interferometers would bring information on the inflationary potential at completely different scales than the measurement of tensor modes in the CMB; GWs from a first-order phase transition would probe physics beyond the Standard Model, at energies not accessible with colliders; Finally, second-order-induced GWs could be related to Primordial Black Holes, which may explain a fraction or (for some mass range) the totality of the Dark Matter [54, 55].

Below we briefly describe the GW sourcing mechanisms implemented in `GW_CLASS`. In principle, it is straightforward to implement in `GW_CLASS` other exotic mechanism that could generate a CGWB, such as cosmic strings [3].

3.1 CGWB from inflation with adiabatic initial conditions

For GWs produced by quantum fluctuations during inflation, the current value of the average GW energy density $\bar{\Omega}_{\rm GW}$ is related to the primordial tensor spectrum P_T through (see appendix D for details)

$$\bar{\Omega}_{\rm GW}(q) = \frac{1}{12 H_0^2 a_0^2} \frac{\eta_{\rm eq}^2}{2\eta_0^4} P_T(q)\,. \tag{3.2}$$

JCAP10(2023)025

Here we expressed the average GW energy density as function of comoving momentum q instead of frequency $f = \frac{c}{2\pi q}$. This relation takes into account the evolution of the tensor modes that re-entered the Hubble scale during radiation domination [56]. It depends on the value of conformal time at equality between matter and radiation, $\eta_{\rm eq}$, and today, η_0. Note that eq. (3.2) takes into account the evolution of GWs during radiation and matter domination, but not during dark energy domination. However, as explained [57], the impact of the latter stage is negligible at high frequencies (as long as $f \gg 10^{-18}\,$Hz). Besides, eq. (3.2) neglects the damping of tensor modes propagating in a universe containing free-streaming particles with non-zero anisotropic stress [58–60]. This additional effect should lead to a suppression factor (close to 0.8^2 in the minimal cosmological model, when the damping is only due to active neutrinos).

The primordial tensor spectrum $P_T(k) = 4\,P_{h_\lambda}(k)$ is a familiar object in CMB physics, usually expressed as a function of a Fourier wavenumber k, since it is related to the Fourier transform of the tensor mode of metric fluctuations, $h_{ij}(\eta_{\rm in}, \vec{x})$. The quantity P_T in eq. (3.2) is the same quantity, evaluated however at a much smaller wavenumber, matching the wavelength of GWs probed by GW detectors. Like in the rest of this paper, we use k to denote comoving wavenumbers associated to inhomogeneities on cosmological scales, and q to denote comoving wavenumbers describing GW wavelengths, that is, comoving momenta of gravitons. However, the fluctuations of tensor perturbations on cosmological scales, whose variance is encoded on $P_T(k)$, comes from the existence of very large wavelengths in the graviton phase-space distribution Γ. Thus, in this case, k and q have the same physical interpretation. This means that $P_T(k)$ in eq. (2.24) and $P_T(q)$ in eq. (3.2) represent fundamentally the same function, just evaluated on different scales (cosmological scales in the $P_T(k)$ case, and wavelengths to which GW detectors are sensitive in the $P_T(q)$ case).

The primordial tensor spectrum is commonly parametrized in terms of a tensor-to-scalar ratio r and tensor tilt $n_{\rm t}$,

$$P_T(k) = r A_s \left(\frac{k}{k_*}\right)^{n_{\rm t}}, \tag{3.3}$$

where A_s is the amplitude of scalar perturbations at the CMB pivot scale $k_* = 0.01\,$Mpc. The most recent bounds on these parameters have been evaluated by combining several CMB and GW experiments [61], finding $r < 0.028$ and $-1.37 < n_{\rm t} < 0.42$ at 95% CL.

Since $P_T(k)$ and $P_T(q)$ are fundamentally the same function, we could assume the same value for the $P_T(k)$ spectral index $n_{\rm t}$ and for the $P_T(q)$ spectral index $n_{\rm gwb}$. We note however that the power-law ansatz of eq. (3.3) is not necessarily valid across the huge interval ranging from CMB scales to detectable GW wavelengths. To deal with situations in which the tensor tilt is scale-dependent, we defined $n_{\rm gwb}$ as a free input parameter independent of $n_{\rm t}$ in `GW_CLASS`. Depending on physical assumptions, the user can either set $n_{\rm gwb} = n_{\rm t}$ (subject to the Planck bounds) or $n_{\rm gwb} \neq n_{\rm t}$ (accounting for the variation of the tensor tilt between cosmological scales and detector scales).[10] We recall that the value of $n_{\rm gwb}$ matters because it enters the overall pre-factor in the expression of $C_\ell^{\rm CGWB\times CGWB}$, see eq. (2.34).

In a given cosmological model with known cosmological parameters, including $f_{\rm dec}(\eta_{\rm in})$, no further assumptions are needed to compute the SGWB power spectrum induced by single-field inflation: the code can readily evaluate eq. (2.34) (with the non-adiabatic power spectrum $P_\Gamma^{\rm NL}$ set to zero).

[10] In the parametrization described in appendix F.2, the option $n_{\rm gwb} = n_{\rm t}$ corresponds to the case `inflationary_gwb` and the option $n_{\rm gwb} \neq n_{\rm t}$ to the case `analytic_gwb`.

JCAP10(2023)025

3.2 Generic non-adiabatic CGWB

Among others, `GW_CLASS` offers a generic parametrization of a possible non-adiabatic contribution to the CGWB. This parametrization does not necessarily relate to known physical mechanisms, but is useful for tests and order-of-magnitude estimates.

With non-adiabatic perturbations, the initial GW spectrum $P_\Gamma^{\rm NAD}(k,q)$ may depend on two independent arguments k and q. Indeed, in the general case, k refers to spatial modulations of the GW phase-space density on cosmological scales, and q to the frequency spectrum of GWs. If we do not assume that tensor fluctuations are entirely generated by inflation, there is no general reason to assume that the dependence on k and q are the same.

In this case, we will assume that at the detector frequency $q = 2\pi f/c$, the initial GW spectrum $P_\Gamma^{\rm NAD}(k,q)$ depends on cosmological wavenumbers through

$$P_\Gamma^{\rm NAD}(k,q) = A_{\rm gwi}(q)\,\exp\left[n_{\rm gwi}(q)\,\log\frac{k}{k_*} + \frac{1}{2}\alpha_{\rm gwi}(q)\left(\log\frac{k}{k_*}\right)^2\right], \tag{3.4}$$

where $A_{\rm gwi}(q)$ is the spectrum amplitude, $n_{\rm gwi}(q)$ the spectral index and $\alpha_{\rm gwi}(q)$ the running (gwi stands for Gravitational Wave Initial), all evaluated at the pivot scale k_*. A more general parametrization of the initial GW spectrum could be easily implemented in `GW_CLASS`. The spectral index $n_{\rm gwi}$, referring to k-dependence of the Γ power spectrum, should not be confused with $n_{\rm gwb}$, which refers to frequency dependence of the background GW density (or monopole) $\bar{\Omega}_{\rm GW}(q)$.

If we assume that this non-adiabatic CGWB contribution is not correlated with the adiabatic contribution, the non-adiabatic spectrum $C_\ell^{\rm CGWB\times CGWB}$ featured in the second line of eq. (2.34) (defined at the detector frequency q) can be computed for a given set of parameters $\{A_{\rm gwi}, n_{\rm gwi}, \alpha_{\rm gwi}, k_*, n_{\rm gwb}, f_{\rm dec}(\eta_{\rm in})\}$.

3.3 Primordial black holes

Given the nonlinear nature of gravity, secondary GWs are produced by quadratic contributions in the scalar perturbations that act as a source in the transverse and traceless part of the Einstein equations [62–68] (see [69] for a recent review). A significant amount of GWs can be generated only when the amplitude of the scalar perturbation (spectrum) at small scales is much larger than at CMB scales. This can happen, e.g., if the inflation evolution shows some deviation from scale invariance [70], for instance in an ultra-slow-roll phase (see e.g., [71–73] for recent discussions about the possibility to generate PBH in single-field models.), or in multi-field models [74–76]. When such large density perturbations collapse they may lead to the formation of Primordial Black Holes (PBHs) with masses $\sim (0.001 - 1000)M_\odot$, which encompass the actual mass range probed by present GW detectors. The SGWB energy density has been computed for different kinds of the primordial scalar spectra [77]. In the (idealized) monochromatic case, with a primordial scalar spectrum featuring a Dirac delta-function, $\mathcal{P}_{\mathcal{R}_s}(q) = A_*\, q_*\, \delta(q - q_*)$, it has been shown that the SGWB energy density can be computed analytically and results [50, 78][11]

$$\bar{\Omega}_{\rm GW}(\eta_0, f) = \frac{1}{a_0^2 H_0^2 \eta_0^2}\frac{A_*^2}{15552}\frac{f^2}{f_*^2}\left[\frac{4f_*^2}{f^2} - 1\right]^2 \theta(2f_* - f)\; \mathcal{I}^2\left(\frac{f_*}{f}, \frac{f_*}{f}\right) \tag{3.5}$$

[11] This expression is valid during radiation domination.

JCAP10(2023)025

where θ is the Heaviside step function, and

$$\mathcal{I}^2\left(\frac{f_*}{f},\frac{f_*}{f}\right) = \frac{729}{16}\left(\frac{f}{f_*}\right)^{12}\left(3-\frac{2f_*^2}{f^2}\right)^4\left\{\left[4\left(2-3\frac{f^2}{f_*^2}\right)^{-1}-\log\left(\left|1-\frac{4f_*^2}{3f^2}\right|\right)\right]^2+\pi^2\theta\left(\frac{2f_*}{\sqrt{3}f}-1\right)\right\}. \quad (3.6)$$

The peak GW frequency f_* is related to the spike scale q_* by

$$f_* = \frac{c}{2\pi a_0}\, q_* \,. \quad (3.7)$$

In absence of primordial non-gaussianity, this model would generate negligible GW anisotropies beyond the unavoidable adiabatic initial conditions discussed previously. However, the authors of [50] have shown that if some (local) underlying non-Gaussianity is present in the primordial curvature perturbation, then this generates intrinsic primordial GW anisotropies — corresponding to non-adiabatic modes in the parametrization of eq. (2.34). Reference [50] assumes curvature perturbations with a local non-Gaussianity parametrized during matter domination by,

$$\mathcal{R}(\vec{k}) = \mathcal{R}_g(\vec{k}) + \frac{3}{5}\, f_{\rm NL} \int \frac{d^3p}{(2\pi)^3}\, \mathcal{R}_g\left(\vec{p}\right)\, \mathcal{R}_g(\vec{k}-\vec{p}) \,, \quad (3.8)$$

where the subscript g refers to the Gaussian part of the perturbations, and $f_{\rm NL}$ is assumed to be scale-independent. In this case, the CGWB energy density acquires large-scale (beyond those following from the "separate universe" picture, which accounts for the adiabatic mode), captured by [50]

$$\Omega_{\rm GW}(\eta,\vec{x},q) = \bar{\Omega}_{\rm GW}\left(\eta,\, q\right)\left[1+\frac{24}{5}\, f_{\rm NL}\int \frac{d^3k}{(2\pi)^3}\, \mathrm{e}^{i\vec{k}\cdot\vec{x}}\, \mathcal{R}_g\left(\vec{k}\right)\right], \quad (3.9)$$

where the term $\bar{\Omega}_{\rm GW}\left(\eta,\, q\right)$ is given by (3.5). Then the fluctuations of the graviton phase-space distribution have a non-adiabatic monopole term

$$\Gamma_0^{\rm NAD}(\eta_{\rm in},\vec{x},q) = \frac{3}{5}\tilde{f}_{\rm NL}\left(q\right) \int \frac{d^3k}{(2\pi)^3}\, \mathrm{e}^{i\vec{k}\cdot\vec{x}}\, \mathcal{R}_g\left(\vec{k}\right) \,, \quad (3.10)$$

where

$$\tilde{f}_{\rm NL}\left(q\right) \equiv \frac{8\, f_{\rm NL}}{4-\frac{\partial \ln \bar{\Omega}_{\rm GW}}{\partial \ln q}} = \frac{8\, f_{\rm NL}}{4-n_{\rm gwb}(q)} \,. \quad (3.11)$$

In Fourier space, this initial condition reads

$$\Gamma_0^{\rm NAD}(\eta_{\rm in},\vec{k},q) = \frac{3}{5}\tilde{f}_{\rm NL}(q)\mathcal{R}_g(\vec{k}) \,, \quad (3.12)$$

where $\mathcal{R}_g(\vec{k})$ represents the Gaussian curvature perturbation on large (cosmological) scales, whose power spectrum is given by $P_{\mathcal{R}}(k)$ in the notations of previous sections.

Interestingly, since this non-adiabatic contribution depends on the curvature perturbation, it is fully correlated with the adiabatic mode. Then the adiabatic, non-adiabatic and cross-correlation spectra are related to each other through

$$P_\Gamma^{\rm NAD}(k,q) = \frac{9}{25}\tilde{f}_{\rm NL}^2(q)P_{\mathcal{R}}(k) \,, \quad (3.13)$$

$$P^{\times}(k,q) = \frac{6}{5}\tilde{f}_{\rm NL}(q)P_{\mathcal{R}}(k) \,. \quad (3.14)$$

JCAP10(2023)025

The non-adiabatic initial condition induced by $f_{\rm NL}$ may amplify GW anisotropies in a very significant way, since for the PBH scenario the ratio of non-adiabatic to standard AD+SW contributions to the anisotropy spectrum scales like

$$\frac{C_\ell^{\rm NAD}}{C_\ell^{\rm AD+SW}} \sim \left(\frac{\frac{3}{5}\frac{8\,f_{\rm NL}}{4-n_{\rm gwb}(q)}}{\frac{2}{3}\left[-\frac{2}{4-n_{\rm gwb}(q)}+1\right]} \right)^2 = \left\{ \frac{36 f_{\rm NL}}{5[2-n_{\rm gwb}(q)]} \right\}^2 , \tag{3.15}$$

where we used $T_\psi = -\frac{2}{3}$ during radiation domination with $f_{\rm dec} = 0$ and eq. (2.35). In the case in which $f_{\rm NL} = 1$ and $n_{\rm gwb}(q) = 0$, we find

$$\frac{C_\ell^{\rm NAD}}{C_\ell^{\rm AD+SW}} \approx 13\,. \tag{3.16}$$

This qualitative relation shows that even with $f_{\rm NL}$ of order one, the non-adiabatic contribution dominates the spectrum $C_\ell^{\rm CGWB\times CGWB}$.

3.4 Phase transition

When a PT takes place, the Universe goes from a metastable to a stable state, which represent the configurations of minimal potential energy at high and low temperatures respectively. If latent heat is involved, the PT is of the first order and the phases of the Universe are converted from the false to the true vacuum in a discontinuous way, through the nucleation of bubbles [79]. Such first order PTs can happen in many extensions of the Standard Model (e.g., with additional scalar singlet or doublet, spontaneously broken conformal symmetry, or phase transitions in a hidden sector). In [80], it has been realized for the first time that a large CGWB could be produced during a first-order PT and this is potentially detectable by present and future GW interferometers [9, 40]. In general, three main mechanisms contribute to the generation of GWs [3], by acting as a source in the transverse-traceless part of the Einstein equations:

- **Bubble wall collisions** creating distortions in the plasma. Their action is usually accounted with a method called *envelope approximation* [81–85], consisting in approximating the bubble motion with an infinitesimally thin spherical layer. This is the backbone of the scalar field ϕ contribution to the SGWB signal.

- **Sound waves** generated by the coupling of the scalar field to the plasma during the expansion of the bubbles. These compressional modes constitute an important source of GWs also long after the collision of the bubbles [86–88].

- **Turbulence phenomena** after the bubble collision, which generate vortices in the fluid with a non-vanishing quadrupole moment. The amount of GWs sourced by these eddies from Magneto-Hydro-Dynamics (MHD) turbulence has been computed for instance in [89, 90].

As a consequence, the density of GWs generated by phase transitions can be split into three contributions,

$$\bar{\Omega}_{\rm GW}(f) = \bar{\Omega}_\phi(f) + \bar{\Omega}_{\rm sw}(f) + \bar{\Omega}_{\rm turb}(f)\,. \tag{3.17}$$

JCAP10(2023)025

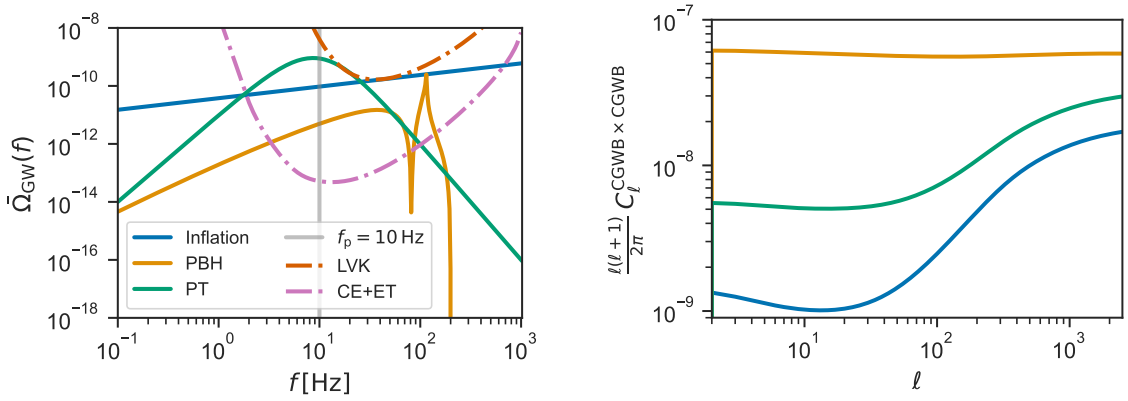

Figure 3. *Left:* Example of frequency spectra for the monopole of the CGWB generated either by: cosmological inflation (with a blue tilt $n_{\rm t} = 0.4$), PBHs (with a peak adjusted to the frequency $f_* = 100\,{\rm Hz}$), or a phase transitions (with a peak adjusted to $f_* = 10$ Hz). *Right:* angular power spectra for these three sources evaluated at $f_{\rm p} = 10\,{\rm Hz}$, assuming adiabatic initial conditions in the inflation case, and non-adiabatic modes in the other two cases. See the text for more details on assumptions and parameters.

Broken power-law

Each of these three contributions can be well described by a broken power law (BPL) spectrum. In `GW_CLASS` we use the same parametrization as in the LIGO analysis of ref. [91],

$$\bar{\Omega}_{\rm GW}^{\rm BPL}(f) = \bar{\Omega}_* \left(\frac{f}{f_*}\right)^{n_1} \left[1 + \left(\frac{f}{f_*}\right)^{\Delta}\right]^{\frac{n_2 - n_1}{\Delta}} \tag{3.18}$$

with $n_1 = 3$ to account causality, n_2 takes the value -4 (resp. -1) for sound waves (resp. bubble collisions), and the contribution from turbulence (MHD) is neglected.

3.5 Spectra for a few examples

In the left panel of figure 3, we plot the monopole of the CGWB generated by three different mechanisms:

- cosmological inflation assuming a power-law tensor spectrum with $r = 0.025$ and $n_{\rm gwb} = n_{\rm t} = 0.4$,
- PBHs with an amplitude $A_* = 2 \times 10^{-5}$ at the peak frequency $f_* = 100\,{\rm Hz}$,
- phase transitions assuming that the GW background is dominated by the sound wave contribution, with $n_1 = 3$, $n_2 = -4$, $\Delta = 2$, $f_* = 10\,{\rm Hz}$ and $\bar{\Omega}_* = 1 \times 10^{-8}$.

We choose these parameters in an optimistic way, that is, compatible with current CMB and interferometric bounds, but leading to a GW background potentially detectable by future interferometers. Thus, in the inflation case, we assumed a blue inflationary spectrum, and in the other two cases, we matched the location of the peaks to the frequency range probed by the CE and ET, while choosing amplitude parameters close to current bounds. The left panel of figure 3 also shows the combined sensitivity of CE+ET and the one of LVK. In all three cases, the signal clearly dominates the noise for $f \sim \mathcal{O}(10\ {\rm Hz})$, showing that such backgrounds would be detectable.

JCAP10(2023)025

In the right panel of the same figure, we show the GW anisotropy angular power-spectra associated to these mechanisms, evaluated at a pivot frequency $f_{\rm p} = 10\,{\rm Hz}$ — that is, close to the maximum sensitivity of the network CE+ET. We assume additionally $f_{\rm dec}(\eta_{\rm ini}) = 0$ and the following initial conditions:

- For cosmological inflation, we take adiabatic initial conditions and $n_{\rm gwb} = n_{\rm t}$;
- For PBHs, on top of adiabatic initial conditions, we consider the non-adiabatic contribution generated by a (local) non-Gaussianity parameter $f_{\rm NL} = 1$, and we infer $n_{\rm gwb}$ at the pivot scale from the background spectrum shown on the left panel ($n_{\rm gwb} \simeq 1.2$);
- For the phase transition, the simplest scenarii are expected to lead to adiabatic initial conditions, but non-adiabatic modes could arise in more complicated cases (see e.g. [92]). For illustrative purposes, we arbitrarily assume here that, on top of adiabatic initial conditions, the CGWB anisotropies include a non-adiabatic mode with the parametrization of eq. (3.4), taking $A_{\rm gwi} = 1 \times 10^{-10}$, $n_{\rm gwi} = 0.0$, and computing $n_{\rm gwb}$ from the background spectrum shown on the left panel ($n_{\rm gwb} \simeq -0.5$).

It is interesting to notice that the three signals considered here produce average monopole terms of the same order of magnitude, but very different anisotropy spectra. The features in the angular power spectra of figure 3 depend on the chosen initial condition and on the tensor tilt of the monopole signal (which is responsible for an enhancement/suppression of the angular power spectrum).

For instance, in our examples, the angular power spectrum of the CGWB for the PT is one order of magnitude larger than that from inflation, because:

- At the chosen frequency $f = 10$ Hz, the AD+SW+ISW contribution to the $C_\ell^{\rm CGWB\times CGWB}$ spectrum is enhanced by a factor 2.5, due to an increase in the factor $(4 - n_{\rm gwb})^2$. To understand this in more details, one can note that, according to eqs. (2.34), (2.35), the SW and ISW terms get multiplied by $(4 - n_{\rm gwb})^2$, while the AD term is independent of $n_{\rm gwb}$. The sign of the SW term is opposite to that of the AD and ISW terms, but in absolute value, the SW term is the largest of the three. Thus, an increase of $(4 - n_{\rm gwb})^2$ does lead to an increase of the total (AD+SW+ISW) contribution.
- Besides, our featured PT model includes a non-adiabatic contribution which is about four times larger than the adiabatic one.

Overall, this explains why the angular power-spectrum of the featured PT model is one order of magnitude larger than the inflation's one. For the PBH case, the enhancement with respect to the inflationary model is produced by similar reasons:

- The decrease in the factor $(4-n_{\rm gwb})^2$ between the two cases reduces the (AD+SW+ISW) contribution by a factor ~ 0.25.
- On the other hand, the non-adiabatic contribution is larger than the adiabatic one by two orders of magnitude, which is consistent with eq. (3.15).

These two factors combine to enhance the PBH spectrum by one to two orders of magnitude compared to the inflationary one.

JCAP10(2023)025

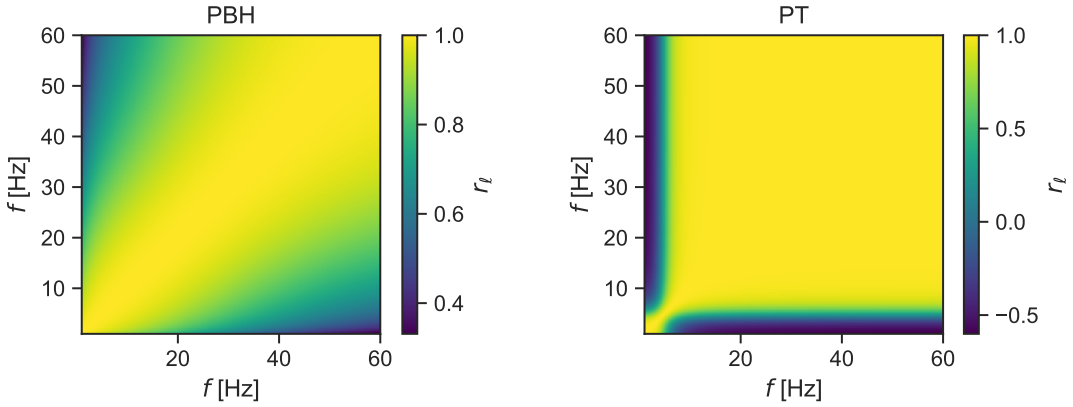

Figure 4. Correlation of the angular power spectrum $r_\ell(q_1, q_2)$ as a function of frequencies for $\ell = 2$, assuming two GW generation mechanisms: PBH with $f_{\rm NL} = 10^{-2}$ (left) and PT (right).

The detectability of these spectra by future experiments will be discussed at length in section 5.

Another potential signal for GW interferometers is given by CSs, which are generated by phase transitions followed by a spontaneous breaking of symmetries, as relics of the previous more symmetric phase of the Universe. Such CSs can oscillate and give rise to a CGWB, that is typically characterized in terms of the string tension $G\mu$ (see e.g. [8, 93] and reference therein). Typically, the distribution of such CSs in the universe is not homogeneous which bring to the generation of anisotropies in the CGWB, which have been computed in [94, 95]. Finally, also preheating models are typically characterized by anisotropies in the SGWB [96, 97]. In this paper we did not considered these last two generation mechanisms leaving a more dedicated analysis to a future study.

4 Cross-correlation spectra

4.1 Cross-correlation of CGWB at different frequencies

In eq. (2.34) we presented the general expression for the CGWB angular-power spectrum that would be inferred from a CGWB map at a given frequency. This expression depends on frequency for two reasons:

- In general, the tensor tilt $n_{\rm gwb}$ depends on frequency f, that is, on momentum q. This function appears in the overall prefactor as well as in the expression of $\Delta_\ell^{\rm AD}$. Note that, in absence of non-adiabatic initial conditions, the factor $(4 - n_{\rm gwb}(q))^2$ cancels in the contribution to $C_\ell^{\rm CGWB\times CGWB}$ proportional to $[\Delta_\ell^{\rm AD}]^2$, but remains present in the terms containing SW and ISW contributions.
- The non-adiabatic primordial spectrum $P_\Gamma^{\rm NAD}(k, q)$ could depend on q — and thus, so is the cross-correlation spectrum $P^\times(k, q)$.

However, in future experiments, the CGWB angular spectrum is likely to be measured from the cross-correlation between pairs of CGWB maps obtained at two different frequencies, in order to reduce stochastic noise. In that case, the CGWB spectrum needs to be generalized to

$$\delta_{\ell\ell'}\ \delta_{mm'}\ C_\ell^{\rm CGWB\times CGWB}(q_1, q_2) \equiv \frac{1}{2}\Big\langle \delta_{{\rm GW},\ell m}(q_1)\delta^*_{{\rm GW},\ell' m'}(q_2) + \delta_{{\rm GW},\ell m}(q_2)\delta^*_{{\rm GW},\ell' m'}(q_1)\Big\rangle\,. \tag{4.1}$$

JCAP10(2023)025

The computation of the angular power spectrum of the cross-correlation of the CGWB at the frequencies q_1 and q_2 is done by using

$$C_\ell^{\mathrm{CGWB}\times\mathrm{CGWB}}(q_1,q_2) = 4\pi\,(4-n_{\mathrm{gwb}}(q_1))\,(4-n_{\mathrm{gwb}}(q_2)) \tag{4.2}$$

$$\int\frac{dk}{k}\Bigg\{P_{\mathcal{R}}(k)\prod_{i=1,2}\left[\Delta_\ell^{\mathrm{AD}}(k,\eta_0,\eta_{\mathrm{in}},q_i)+\Delta_\ell^{\mathrm{SW}}(k,\eta_0,\eta_{\mathrm{in}})+\Delta_\ell^{\mathrm{ISW}}(k,\eta_0,\eta_{\mathrm{in}})\right]$$
$$+\left[j_\ell\left(k\left(\eta_0-\eta_{\mathrm{in}}\right)\right)\right]^2\left[P_\Gamma^{\mathrm{NAD}}(k,q_1,q_2)\right]$$
$$+\sum_{i=1,2,j\neq i}j_\ell\left(k\left(\eta_0-\eta_{\mathrm{in}}\right)\right)\left[\Delta_\ell^{\mathrm{AD}}(q_i)+\Delta_\ell^{\mathrm{SW}}+\Delta_\ell^{\mathrm{ISW}}\right]P^\times(k,q_j)$$
$$+\left[\Delta_\ell^T(k,\eta_0,\eta_{\mathrm{in}})\right]^2\sum_{\lambda=\pm2}P_{h_\lambda}(k)\Bigg\}, \tag{4.3}$$

where the dependence of $\Delta_\ell^{\mathrm{AD}}$ on each q_i is still specified by eq. (2.35). In this generalization, the non-adiabatic spectrum becomes a function of the two frequencies involved in the cross-correlation,

$$P_\Gamma^{\mathrm{NAD}}(k,q_1,q_2) = \frac{1}{2}\Big\langle\Big[\Gamma_0^{\mathrm{NAD}}(\eta_{\mathrm{in}},\vec{k},q_1)\Gamma_0^{\mathrm{NAD}\,*}(\eta_{\mathrm{in}},\vec{k},q_2)$$
$$+\Gamma_0^{\mathrm{NAD}\,*}(\eta_{\mathrm{in}},\vec{k},q_1)\Gamma_0^{\mathrm{NAD}}(\eta_{\mathrm{in}},\vec{k},q_2)\Big]\Big\rangle\,. \tag{4.4}$$

In the literature, when discussing signal-to-noise separation, it has always been assumed that CGWB anisotropy maps at different frequencies are fully correlated [39, 47, 98, 99], such that one could factorize the dependency on q_1 and q_2 as

$$C_\ell^{\mathrm{CGWB}\times\mathrm{CGWB}}(q_1,q_2) = \frac{\mathcal{E}(q_1)\mathcal{E}(q_2)}{\mathcal{E}^2(q_{\mathrm{p}})C_\ell^{\mathrm{CGWB}\times\mathrm{CGWB}}(q_{\mathrm{p}})}\,. \tag{4.5}$$

This condition is equivalent to stating that the correlation factor of the spectra at different frequencies, defined as

$$r_\ell(q_1,q_2) \equiv \frac{C_\ell^{\mathrm{CGWB}\times\mathrm{CGWB}}(q_1,q_2)}{\sqrt{C_\ell^{\mathrm{CGWB}\times\mathrm{CGWB}}(q_1,q_1)C_\ell^{\mathrm{CGWB}\times\mathrm{CGWB}}(q_2,q_2)}}\,, \tag{4.6}$$

is equal to one.

Here we stress that this assumption is only an approximation. For instance, when n_{gwb} is independent of q, and $P_\Gamma^{\mathrm{NAD}}(k,q)$ either vanishes or is independent of q, $r_\ell(q_1,q_2)=1$. This is typically the case when GWs are generated by inflation with purely adiabatic initial conditions and a negligible running of the tensor tilt. However, the condition is broken in other scenarii. Then, our formalism allows to compute explicitly the correlation factor according to eqs. (4.3), (4.6).

We illustrate this for two different cases in figure 4. These cases are similar to the examples picked up in section 3.5 and shown in figure 3. However, in the PBH case, we consider $f_{\mathrm{NL}}=10^{-2}$ instead of $f_{\mathrm{NL}}=1$. This choice is motivated by the fact that at low multipoles, when f_{NL} is very large, the angular power spectrum is dominated by the NAD initial condition. Then, in very good approximation, the frequency dependence can be factorized and $r_\ell(q_1,q_2)\simeq 1$, like for the standard inflationary case.

JCAP10(2023)025

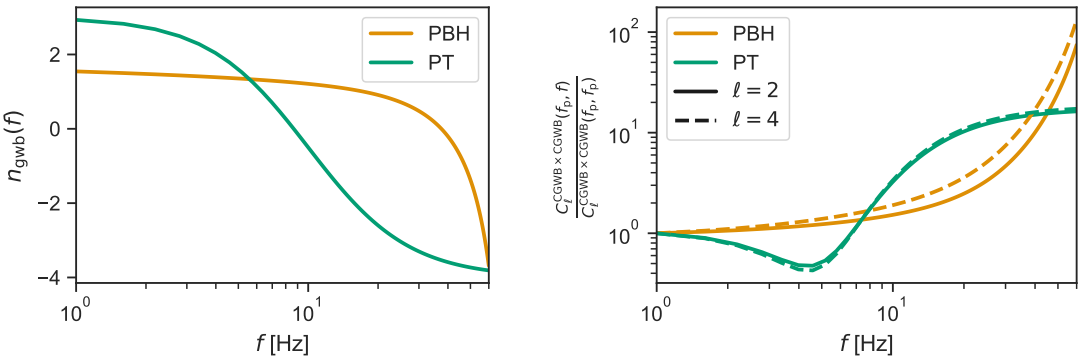

Figure 5. Left: dependence of the tensor tilt $n_{\rm gwb}$ over frequency. Right: dependence of the quadrupole and hexadecapole of the CGWB spectrum $C_\ell^{\rm CGWB\times CGWB}(q,q)$ over frequency (using the one-to-one correspondence between momentum q and frequency f), normalized at the pivot frequency $f_p = 1\,\text{Hz}$.

In figure 5 we show the angular power spectrum evaluated at $q_1 = q_2$ for different frequencies, normalized at the pivot frequency $f_p = 1\,\text{Hz}$. This shows how the anisotropies coming from different sources — or from a given source but from different multipoles — depend differently on frequency. This behaviour is potentially useful for an efficient component separation, as discussed in [44].

4.2 Cross-correlation of SGWB with CMB

Since CMB photons and gravitons share the same geodesics, along which they get red-shifted or blue-shifted by the same metric fluctuations, we expect a significant correlation between CMB temperature anisotropies and GW energy density anisotropies. This cross-correlation has been studied in detail in [35] (sticking to the perturbations induced by scalar fluctuations on cosmological scales, which provide the dominant contribution; see also [37] where the anisotropies induced by tensor perturbations have been included too). An additional amount of correlation between the CMB and the CGWB, which is not considered in this work, could be caused by the existence of a non-trivial primordial scalar-tensor-tensor non-Gaussianity [100].

The multipoles of GW anisotropies can be inferred from a line-of-sight integral according to eqs. (2.16)–(2.20). For the multipoles $a_{\ell m}$ of CMB temperature fluctuations induced by adiabatic scalar perturbations, the equivalent integral reads [101]

$$a_{\ell m} = 4\pi\,(-i)^\ell \int \frac{d^3k}{(2\pi)^3}\, e^{i\vec{k}\cdot\vec{x}_0}\, Y^*_{\ell m}(\hat{k})\, \mathcal{R}(\vec{k})\, \Theta^S_\ell(k,\eta_0)\,, \tag{4.7}$$

$$\begin{aligned}\Theta^S_\ell(k,\eta_0) = \int_{\eta_{\rm min}}^{\eta_0} d\eta \Big[& g(\eta)\,\Big(T_{\Theta_0}(\eta,k) + T_\psi(\eta,k)\Big) j_\ell[k(\eta_0-\eta)] && \text{(SW)}\\ & + g(\eta)\; k^{-1} T_{\theta_b}(\eta,k) j'_\ell[k(\eta_0-\eta)] && \text{(DOP)}\\ & + e^{-\kappa(\eta)}\;\frac{\partial[T_\psi(\eta,k)+T_\phi(\eta,k)]}{\partial\eta} j_\ell[k(\eta_0-\eta)]\Big]\,, && \text{(ISW)}\end{aligned}$$

where $\kappa(\eta)$ is the photon optical depth, $g(\eta)$ the visibility function, $T_{\Theta_0}(\eta,k)$ the transfer function of the photon temperature monopole, and $T_{\theta_b}(\eta,k)$ the transfer function of the divergence of the baryon bulk velocity. The line-of-sight integral features three terms standing

JCAP10(2023)025

for the Sachs-Wolfe (SW), Doppler (DOP) and Integrated Sachs-Wolfe (ISW) contributions. Assuming adiabatic scalar perturbations only, we can write the CMB×CGWB cross-correlation angular power spectrum as

$$\delta_{\ell\ell'}\delta_{mm'}C_\ell^{\rm CMB\times CGWB}(q) \equiv \frac{1}{2}\langle \delta_{{\rm GW},\ell m}(\eta,q)\, a^*_{\ell' m'}(\eta) + \delta^*_{{\rm GW},\ell m}(\eta,q)\, a_{\ell' m'}(\eta)\rangle\,, \tag{4.8}$$

where the adiabatic scalar contribution to $\delta_{{\rm GW},\ell m}$ can be inferred from eq. (2.35):

$$\begin{aligned}\delta_{{\rm GW},\ell m} = 4\pi\,(-i)^\ell(4-n_{\rm gwb})\int \frac{d^3k}{(2\pi)^3}\, e^{i\vec{k}\cdot\vec{x}_0}\, Y^*_{\ell m}(\hat{k})\,\mathcal{R}(\vec{k}) \\ \times\left[\Delta^{\rm AD}_\ell(k,\eta_0,\eta_{\rm in}) + \Delta^{\rm SW}_\ell(k,\eta_0,\eta_{\rm in}) + \Delta^{\rm ISW}_\ell(k,\eta_0,\eta_{\rm in})\right]\,.\end{aligned} \tag{4.9}$$

This cross-correlation spectrum can be expanded as the sum of six terms,

$$C_\ell^{\rm CMB\times CGWB} = C_\ell^{\rm SW\times SW} + C_\ell^{\rm SW\times ISW} + C_\ell^{\rm ISW\times SW} + C_\ell^{\rm ISW\times ISW} + C_\ell^{\rm DOP\times SW} + C_\ell^{\rm DOP\times ISW}\,, \tag{4.10}$$

each of them involving at last one line-of-sight integral for the CMB part.[12] Below, we give approximate expressions for these six terms, based on the instantaneous decoupling approximation $g(\eta) = \delta(\eta-\eta_*)$, where η_* is the conformal age of the universe at the time of photon decoupling:[13]

$$\begin{aligned}
\frac{C_\ell^{\rm SW\times SW}}{4-n_{\rm gwb}} &= 4\pi\int\frac{dk}{k}P_{\mathcal{R}}(k) j_\ell[k(\eta_0-\eta_*)] j_\ell[k(\eta_0-\eta_{\rm in})] \\
&\quad\times\left[T_{\Theta_0}(\eta_*,k)+T_\psi(\eta_*,k)\right]\left[T^{\rm AD}_\Gamma(\eta_{\rm in},k,q)+T_\psi(\eta_{\rm in},k)\right]\,, \\
\frac{C_\ell^{\rm SW\times ISW}}{4-n_{\rm gwb}} &= 4\pi\int\frac{dk}{k}P_{\mathcal{R}}(k) j_\ell[k(\eta_0-\eta_*)]\left[T_{\Theta_0}(\eta_*,k)+T_\psi(\eta_*,k)\right] \\
&\quad\times\int_{\eta_{\rm in}}^{\eta_0} d\eta\left[T'_\psi(\eta,k)+T'_\phi(\eta,k)\right] j_\ell[k(\eta_0-\eta)]\,, \\
\frac{C_\ell^{\rm ISW\times SW}}{4-n_{\rm gwb}} &= 4\pi\int\frac{dk}{k}P_{\mathcal{R}}(k) j_\ell[k(\eta_0-\eta_{\rm in})]\left[T^{\rm AD}_\Gamma(\eta_{\rm in},k,q)+T_\psi(\eta_{\rm in},k)\right] \\
&\quad\times\int_{\eta_*}^{\eta_0} d\eta\left[T'_\psi(\eta,k)+T'_\phi(\eta,k)\right] j_\ell[k(\eta_0-\eta)]\,, \\
\frac{C_\ell^{\rm ISW\times ISW}}{4-n_{\rm gwb}} &= 4\pi\int\frac{dk}{k}P_{\mathcal{R}}(k)\int_{\eta_*}^{\eta_0} d\eta\left[T'_\psi(\eta,k)+T'_\phi(\eta,k)\right] j_\ell[k(\eta_0-\eta)] \\
&\quad\times\int_{\eta_{\rm in}}^{\eta_0} d\tilde{\eta}\left[T'_\psi(\tilde{\eta},k)+T'_\phi(\tilde{\eta},k)\right] j_\ell[k(\eta_0-\tilde{\eta})]\,, \\
\frac{C_\ell^{\rm DOP\times SW}}{4-n_{\rm gwb}} &= 4\pi\int\frac{dk}{k}P_{\mathcal{R}}(k)\, j'_\ell[k(\eta_0-\eta_*)]\; j_\ell[k(\eta_0-\eta_{\rm in})] \\
&\quad\times k^{-1}T_{\theta_b}(\eta_*,k)\left[T^{\rm AD}_\Gamma(\eta_{\rm in},k,q)+T_\psi(\eta_{\rm in},k)\right]]\,,
\end{aligned}$$

[12] Here, for simplicity of notations, when referring to the SW of the CGWB, we include also the monopole of the (adiabatic) initial anisotropies, called AD in previous equations. Such a combination of AD+SW was referred to as the Free Streaming Monopole (FSM) in the notations of [35].

[13] This assumption implies that the optical depth is given by the Heaviside function $\kappa(\eta) = H(\eta-\eta_0)$.

JCAP10(2023)025

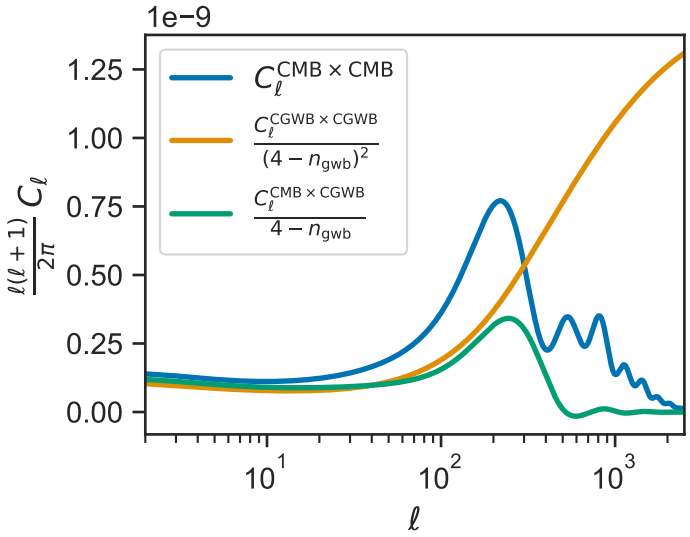

Figure 6. Angular power spectrum of the CMB, of the CGWB with adiabatic initial condition, $n_{\mathrm{gwb}} = 0.4$ and $f_{\mathrm{dec}}(\eta_{\mathrm{in}}) = 0$, and cross-correlation between the two.

$$\frac{C_\ell^{\mathrm{DOP}\times\mathrm{ISW}}}{4-n_{\mathrm{gwb}}} = 4\pi \int \frac{dk}{k} P_{\mathcal{R}}(k)\, j'_\ell[k(\eta_0-\eta_*)]\; k^{-1} T_{\theta_b}(\eta_*,k) \times \int_{\eta_{\mathrm{in}}}^{\eta_0} d\eta \Big[T'_\psi(\eta,k) + T'_\phi(\eta,k)\Big] j_\ell[k(\eta_0-\eta)]\,. \tag{4.11}$$

Note that `GW_CLASS` does not rely on the instantaneous decoupling approximation and always computes the full CMB line-of-sight integral.

In figure 6, we compare the angular power spectra of CMB temperature auto-correlation, of the CGWB auto-correlation (sourced by inflation), and the cross-correlation spectrum. For a more straightforward comparison, in this figure, we divide the CGWB auto-correlation spectrum by $(4-n_{\mathrm{gwb}})^2$ and the cross-spectrum by $(4-n_{\mathrm{gwb}})$. In this case, the three spectra receive a contribution from nearly the same SW term, which explains their similar order of magnitude on large angular scales.

The six contributions of eq. (4.11) to the cross-correlation spectrum are plotted in figure 7, as well as the total cross-correlation spectrum. The overall behavior of each term can be understood qualitatively as follows.

SW × SW contribution. This term gets contributions from Fourier modes propagating at precisely η_* for the CMB perturbations and η_{in} for the GW perturbations. Thus, they originate from two different last scattering spheres, with a comoving radius given respectively by $r_* = \eta_0 - \eta_*$ and $r_{\mathrm{in}} = \eta_0 - \eta_{\mathrm{in}}$. Note that the decoupling times are extremely different, $\eta_* \gg \eta_{\mathrm{in}}$, but the radii of the two spheres are not, since $r_{\mathrm{in}} - r_* = \eta_* - \eta_{\mathrm{in}}$ is much smaller than $r_* \sim r_{\mathrm{in}} \sim \eta_0$.

One may naively expect that the correlation between fluctuations observed on two different last scattering spheres are negligible. In reality, this is not the case. Indeed, primordial perturbations with a comoving wavelength $2\pi/k$ larger than the radii difference $(\eta_* - \eta_{\mathrm{ini}})$ imprint nearly the same patterns on the two spheres, and lead potentially to strong correlations. The correlation induced by each of these wavelengths is seen today mainly under an angle $\theta \simeq \frac{\pi}{k\eta_0}$, and contributes mainly to the multipole $\ell \simeq k\eta_0$. Thus, we expect the

JCAP10(2023)025

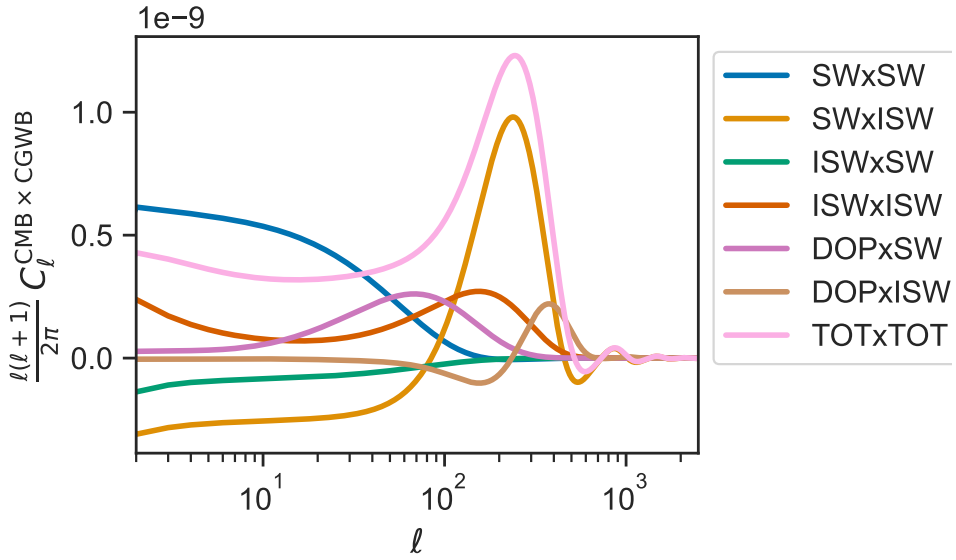

Figure 7. Contributions to the angular power spectrum of the cross-correlation between the CMB and the CGWB.

angular spectrum to be significant for $\ell \ll \frac{2\pi\,\eta_0}{\eta_*-\eta_{\rm in}} \sim 300$. Conversely, primordial perturbations with a comoving wavelength $2\pi/k$ smaller than $(\eta_* - \eta_{\rm ini})$ imprint different patterns on the two spheres and should leave negligible correlations. Thus, the angular spectrum should be suppressed for $\ell \gg \frac{2\pi\,\eta_0}{\eta_*-\eta_{\rm in}}$.

This expectation can be confirmed analytically. In the expression of $C_\ell^{\rm SW\times SW}$ in eq. (4.11), the transfer functions T_{Θ_0}, T_ψ, $T_\Gamma^{\rm AD}$, which are independent of k on super-Hubble scales, can be pulled out of the integral in first approximation. We can do the same with the primordial curvature spectrum $P_{\mathcal{R}}(k) \simeq A_s$, assuming a tilt $n_{\rm s}$ close to one. Then, the shape of $C_\ell^{\rm SW\times SW}$ as a function of ℓ depends on

$$I_\ell = \int \frac{dk}{k}\, j_\ell[k(\eta_0-\eta_*)]\, j_\ell[k(\eta_0-\eta_{\rm in})]\,. \tag{4.12}$$

A calculation summarized in appendix E shows that this integral scales like

$$I_\ell \propto \frac{1}{\sqrt{\ell}\left(\ell+\frac{1}{2}\right)}\left(\frac{\eta_0-\eta_*}{\eta_0-\eta_{\rm in}}\right)^\ell \simeq \frac{1}{\sqrt{\ell}\left(\ell+\frac{1}{2}\right)}\left(1-\frac{\eta_*-\eta_{\rm in}}{\eta_0}\right)^\ell \simeq \frac{1}{\sqrt{\ell}\left(\ell+\frac{1}{2}\right)} e^{-\frac{\eta_*-\eta_{\rm in}}{\eta_0}\ell}, \tag{4.13}$$

which, as expected, gets suppressed exponentially for $\ell \gg \frac{\eta_0}{\eta_*-\eta_{\rm in}}$.

We do observe this small-scale suppression in figure 7. On large angular scales, the amplitude of $C_\ell^{\rm SW\times SW}$ is related to the positive value of $[T_{\Theta_0}+T_\psi][T_\Gamma^{\rm AD}+T_\psi]$ on super-Hubble scales.

SW × ISW contribution. In this term, CMB perturbations contribute at the time η_* and GW perturbations at all times in the range $\eta_{\rm in} \le \eta' \le \eta_0$. The correlation between the CMB and GW perturbations peaks when the two types of perturbations are probed on the same sphere, that is, when $\eta' \sim \eta_*$. Thus, this term depends on the product of the transfer functions $[T_{\Theta_0}(\eta_*,k)+T_\psi(\eta_*,k)][T'_\psi(\eta_*,k)+T'_\phi(\eta_*,k)]$, all evaluated around the time

JCAP10(2023)025

of photon decoupling. The behaviour of this product as a function of k should determine the shape of $C_\ell^{\mathrm{SW}\times\mathrm{ISW}}$ as a function of ℓ, using the angular projection relation $\theta \sim \frac{\pi}{k\eta_0}$ or $\ell \sim k\eta_0$.

The factor $[T_{\Theta_0}(\eta_*, k) + T_\psi(\eta_*, k)]$ is constant on very large scales ($k\eta_* \ll 1$), and then has damped oscillations. The factor $[T'_\psi(\eta_*, k) + T'_\phi(\eta_*, k)]$, also responsible for the early ISW effect in the CMB auto-correlation spectrum, has a broad peak on scales similar to those of the first acoustic peak. As a result, $C_\ell^{\mathrm{SW}\times\mathrm{ISW}}$ has a plateau on large angular scales, a peak coinciding with the first acoustic oscillation, and then smaller damped oscillations. The plateau and the peak have different signs because $[T_{\Theta_0} + T_\psi]$ crosses zero near $k \sim 10^{-2}\,h/\mathrm{Mpc}$ at $\eta \sim \eta_*$ (due to the onset of acoustic oscillations).

ISW × SW contribution. In this term, CMB perturbations contribute at all times in the range $\eta_* \leq \eta \leq \eta_0$ and GW perturbations at the precise time η_{in}. Since these times never overlap, the correlation coming from this term is always very small. It is not exactly zero for the same reason as in the SW×SW case: on the largest angular scales, the same primordial fluctuations contribute to the two last scattering spheres. Even though, the correlation is very small because the transfer function $[T'_\psi(\eta_*, k) + T'_\phi(\eta_*, k)])$ is negligible in the super-Hubble limit (in which ϕ and ψ are nearly constant in time). Thus, the $C_\ell^{\mathrm{ISW}\times\mathrm{SW}}$ contribution is sub-dominant.

ISW × ISW contribution. In this term, CMB perturbations contribute at times in the range $\eta_* \leq \eta \leq \eta_0$ and GW perturbations are all times in the range $\eta_{\mathrm{in}} \leq \eta' \leq \eta_0$. The correlation comes mainly from all overlapping times $\eta \simeq \eta'$ with $\eta_* \leq \eta \leq \eta_0$. Actually, up to the prefactor $(4 - n_{\mathrm{gwb}})$, this term is nearly identical to the ISW × ISW contribution to the CMB auto-correlation spectrum. Like the latter, it includes a tilted plateau at small ℓ's, corresponding to the late ISW effect, and a peak close to the scale of the first acoustic peak, corresponding to the early ISW effect.

DOP × SW contribution. The discussion of this term is qualitatively similar to the SW × SW case. The main difference is that the transfer function associated to the Doppler term, T_{θ_b}, vanishes on super-Hubble scales, unlike $[T_{\Theta_0} + T_\psi]$. Thus, this term only has a broad peak for $\ell \sim 100$.

DOP × ISW contribution. A reasoning similar to the SW × ISW case shows that the correlation now depends on the product of the transfer functions $T_{\theta_b}(\eta_*, k)\,[T'_\psi(\eta_*, k) + T'_\phi(\eta_*, k)])$, all evaluated around the time of photon decoupling. Compared to the SW transfer function $[T_{\Theta_0}(\eta_*, k) + T_\psi(\eta_*, k)]$, the Doppler transfer function $T_{\theta_b}(\eta_*, k)$ vanishes on scales larger than the sound horizon, and has oscillations on smaller scales, but with a phase shift compared to the SW case. Instead, the transfer functions $[T'_\psi(\eta_*, k) + T'_\phi(\eta_*, k)]$ are suppressed on scales smaller than the sound horizon. As a result, $C_\ell^{\mathrm{DOP}\times\mathrm{ISW}}$ has two small peaks on intermediate scales (comparable to the scales of the first two acoustic peaks in the CMB spectrum, but with a different phase).

Total contribution. The total contribution $C_\ell^{\mathrm{CMB}\times\mathrm{CGWB}}$ is dominated by the SW×SW and SW×ISW contributions. It exhibits a tilted plateau on large angular scales, a peak on intermediate scales, and a few damped oscillations. Because of its origin in the SW × ISW contribution, the main peak does not originate simply for the first oscillation of the photon density transfer function, and reaches its maximum at a slightly larger ℓ than the first CMB peak.

JCAP10(2023)025

5 Sensitivity forecasts

In this section, we forecast the sensitivity of the ET+CE network to the information contained in the CGWB anisotropies. As a network configuration we assumed an ET triangular detector with 10-km arm-length placed in Sardinia, and 2 L-shaped CE detectors of 40 and 20 km arms placed in the actual two LIGO detectors. Present and future GW interferometers, both on the ground and in space, are limited in angular sensitivity. Space-based interferometers that are expected to have high (angular) sensitivities, are the Big Bang Observer (BBO) [13] and the DECI-hertz interferometer Gravitational wave Observatory (DECIGO) [102] or network of detectors [103]. So we use such reference sensitivities for our analysis, even if we are focusing on ground-based detectors. Having in mind that future noise upgrades of both ET and CE, could bring the sensitivity close to such values. Of course, the `GW_CLASS` code can be easily used with other GW detectors like LISA and/or Taiji. Additionally, to showcase the theoretical limit on the constraining power of CGWB anisotropies, we consider a cosmic-variance-limited detection up to $\ell_{\rm max} = 2500$, called CV. Our forecasts rely on assuming a mock likelihood and fitting mock data with a Monte-Carlo-Markov-Chain (MCMC) method. Our pipeline is implemented as an extension of the Bayesian inference package `MontePython` [42, 43].

5.1 Detector noise

To perform a forecast on mock data, we need to make assumptions concerning instrumental noise.

For this purpose, we rely on previous investigations of CGWB anisotropy map reconstruction techniques [26, 39, 47, 98, 99, 104]. The problem consists in finding optimal algorithms to go from raw data to CGWB maps at a given frequency. For GW interferometers, the raw data consists in a measurement of the time-delay required by light to complete a flight across the arms as a function of frequency and time — with each point in the timeline corresponding to a given orientation of the detector. The target is a map of CGWB density fluctuations at a given frequency, $\bar{\Omega}_{\rm CGWB}(q)\,\delta_{\rm CGWB}(q,\hat{n})$, see eq. (2.8). The map can be expanded in harmonic space as $\bar{\Omega}_{\rm CGWB}(q)\,a_{\ell m}^{\rm CGWB}$, where $a_{\ell m}^{\rm CGWB}$ is a Gaussian random field of zero mean and of covariance given — in absence of detector noise — by the angular power spectrum $C_\ell^{\rm CGWB\times CGWB}(q)$ of eq. (2.34).

Previous works approached this problem under the assumption that the dependence of the monopole $\bar{\Omega}_{\rm CGWB}(q)$ and of the power spectrum $C_\ell^{\rm CGWB\times CGWB}(q)$ over frequency are known, and also, that the correlation between anisotropies at different frequencies is exactly one or, equivalently, that the frequency dependence of the anisotropies can be factorized out of the stochastic part,

$$a_{\ell m}^{\rm CGWB}(q) = \frac{\mathcal{E}(q)}{\mathcal{E}(q_{\rm p})} a_{\ell m}^{\rm CGWB}(q_{\rm p})\,, \tag{5.1}$$

where $q_{\rm p}$ is an arbitrary pivot scale. In section 4.2, we mentioned that this assumption is not exact, but in the forecasts presented in this work, we will stick to this approximation.

The measurement of the map in presence of detector noise and of other types of signals or foregrounds is a typical component separation problem. Refs. [17, 39, 47, 98, 99] show how to build an unbiased estimator of the map at the pivot scale using a linear combination of raw data at different frequencies, with weights chosen to minimize the covariance of the map. This

JCAP10(2023)025

covariance can be split in two contributions: the spectrum of the signal, $C_\ell^{\mathrm{CGWB}\times\mathrm{CGWB}}(q_\mathrm{p})$, and the noise spectrum $N_\ell^{\mathrm{GW}}(q_\mathrm{p})$. The latter depends on:

- the assumed frequency dependence of the monopole $\bar{\Omega}_{\mathrm{CGWB}}(q)$ and of the angular power spectrum $\mathcal{E}(q)$,
- the characteristics of the detector,
- the number of years of observations.

Estimates of the angular noise spectrum can be performed using the code `schNell` [99]. The output of the code is the noise spectrum of the density fluctuation $\bar{\Omega}_{\mathrm{CGWB}}(q)\, a_{\ell m}^{\mathrm{CGWB}}$ rather than that of the density contrast $a_{\ell m}^{\mathrm{CGWB}}$. Thus, N_ℓ^{GW} is given by the `schNell` output divided by $\bar{\Omega}_{\mathrm{GW}}^2$. In the original version of the code, it was possible to compute the angular power spectrum of the noise only for monopoles that scale like a power law, $\bar{\Omega}_{\mathrm{CGWB}}(q) \propto q^{n_{\mathrm{gwb}}}$. We have generalized the algorithm for stochastic backgrounds with a non-trivial frequency dependence, like the CGWBs sourced by a PT or PBHs described in section 3. We have also implemented in the code the sensitivity of the network ET+CE.

The results are displayed in figures 8, 10, and 12 for various CGWB sourcing mechanisms. In each figure, the left plot compares each detector Power Law Sensitivity (PLS) to the monopole $\bar{\Omega}_{\mathrm{CGWB}}(q)$, while the right plot compares the noise spectrum $N_\ell^{\mathrm{GW}}(q_\mathrm{p})$ of each detector to the angular power spectrum $C_\ell^{\mathrm{CGWB}\times\mathrm{CGWB}}(q_\mathrm{p}, q_\mathrm{p})$. In the plots, the PLS curves and the noise spectra have been computed for $\mathrm{SNR}_{\mathrm{thr}} = 1$ and five years of observation. Thus, on the left plots, when the monopole of a CGWB is tangent to the PLS curve of a given detector (network), this CGWB could be detected with a signal-to-noise ratio (SNR) of one after five years of observation. On the right plots, when the angular power spectrum stays above the noise spectrum at a given multipole ℓ, the SNR for the measurement of this multipole would be larger than one after five years. For a longer time of observation, the noise spectrum can be simply rescaled by the square root of the observing time, $N_\ell^{\mathrm{GW}} \propto 1/\sqrt{T_{\mathrm{obs}}}$. We stress again that the PLS and noise curves depend on the frequency dependence of the signal, and thus, they slightly differ between each of figures 8, 10, and 12.

5.2 Mock likelihood

We model our data as a vector $\vec{a} = \left\{a_{\ell m}^{\mathrm{CMB}}, a_{\ell m}^{\mathrm{GW}}\right\}$ with a Gaussian likelihood $\mathcal{L}$ given by

$$\mathcal{L}(\vec{a}|\Theta) = \frac{1}{\sqrt{(2\pi)^2 \left|\bar{\mathbf{C}}(\Theta)\right|}} \exp\left(-\frac{1}{2}\vec{a}^\dagger \left[\bar{\mathbf{C}}(\Theta)\right]^{-1} \vec{a}\right) . \tag{5.2}$$

The covariance matrix $\bar{\mathbf{C}}$ contains the theoretical prediction for the auto-correlation and cross-correlation spectrum of CMB and GW multipoles, respectively $\bar{C}_\ell^{\mathrm{CMB}\times\mathrm{CMB}}$, $\bar{C}_\ell^{\mathrm{CGWB}\times\mathrm{CGWB}}$, $\bar{C}_\ell^{\mathrm{CMB}\times\mathrm{CGWB}}$. According to the discussion of the previous section, the reconstructed map and the angular power spectrum of the cosmological background are evaluated at the pivot frequency f_p. These spectra assume particular values of the model parameters $\Theta = (\theta_1, \theta_2, \ldots)$. The auto-correlation spectra also include the noise spectrum N_ℓ^{CMB} (resp. N_ℓ^{GW}) of the assumed CMB (resp. GW) instrument. The determinant of the covariance matrix is denoted $\left|\bar{\mathbf{C}}(\Theta)\right|$.

It is well-known that such a likelihood can be written in a much more compact way in terms of the covariance matrix of the data, $\hat{\mathbf{C}} = \langle \vec{a}^\dagger \vec{a} \rangle$. In the case of a forecast, this matrix

JCAP10(2023)025

contains the power spectra of the fiducial model $\hat{C}_\ell^{\rm CMB\times CMB}$, $\hat{C}_\ell^{\rm CGWB\times CGWB}$, $\hat{C}_\ell^{\rm CMB\times CGWB}$, computed with fiducial parameter values, plus the noise spectra. After some calculations, one gets the following effective chi square:

$$\chi^2_{\rm eff} \equiv -2\ln\mathcal{L} = \sum_\ell (2\ell+1)\left[\frac{|D_\ell|}{\left|\bar{C}_\ell\right|} + \ln\frac{\left|\bar{C}_\ell\right|}{\left|\hat{C}_\ell\right|} - 2\right], \tag{5.3}$$

where, for each ℓ, we defined the theory, data and mixed determinants:

$$\left|\bar{C}_\ell\right| = \left(\bar{C}_\ell^{\rm CMB\times CMB} + N_\ell^{\rm CMB}\right)\left(\bar{C}_\ell^{\rm CGWB\times CGWB} + N_\ell^{\rm GW}\right) - \left(\bar{C}_\ell^{\rm CMB\times CGWB}\right)^2, \tag{5.4}$$

$$\left|\hat{C}_\ell\right| = \left(\hat{C}_\ell^{\rm CMB\times CMB} + N_\ell^{\rm CMB}\right)\left(\hat{C}_\ell^{\rm CGWB\times CGWB} + N_\ell^{\rm GW}\right) - \left(\hat{C}_\ell^{\rm CMB\times CGWB}\right)^2, \tag{5.5}$$

$$\begin{aligned}|D_\ell| = &\left(\bar{C}_\ell^{\rm CMB\times CMB} + N_\ell^{\rm CMB}\right)\left(\hat{C}_\ell^{\rm CGWB\times CGWB} + N_\ell^{\rm GW}\right)\\ &+ \left(\hat{C}_\ell^{\rm CMB\times CMB} + N_\ell^{\rm CMB}\right)\left(\bar{C}_\ell^{\rm CGWB\times CGWB} + N_\ell^{\rm GW}\right)\\ &- 2\bar{C}_\ell^{\rm CMB\times CGWB}\,\hat{C}_\ell^{\rm CMB\times CGWB}.\end{aligned} \tag{5.6}$$

In the case of a forecast including only a GW detector, without CMB cross-correlation, the effective chi square simplifies to:

$$\chi^2_{\rm eff} = \sum_\ell (2\ell+1)\left[\frac{\hat{C}_\ell^{\rm CGWB\times CGWB} + N_\ell^{\rm GW}}{\bar{C}_\ell^{\rm CGWB\times CGWB} + N_\ell^{\rm GW}} + \ln\frac{\bar{C}_\ell^{\rm CGWB\times CGWB} + N_\ell^{\rm GW}}{\hat{C}_\ell^{\rm CGWB\times CGWB} + N_\ell^{\rm GW}} - 1\right]. \tag{5.7}$$

For the CMB noise spectrum $N_\ell^{\rm CMB}$, we will always assume the Planck temperature sensitivity — thus our forecasts assume a cosmic-variance limited measurement of CMB temperature anisotropies up to approximately $\ell = 1800$ [105].

5.3 CGWB produced by inflation with a blue tilt

In this section, we assume that the universe can be described by the standard ΛCDM model with fiducial cosmological parameter values fixed to the Planck 2018 best fit, with two additional assumptions:

- in order to get a sizeable CGWB, we assume that inflation takes place at an energy scale close to the current limit set by Planck+Bicep+Keck [61], with a tensor-to-scalar ratio $r = 0.025$ and a power-law spectrum with a blue tilt $n_{\rm t} = 0.4$. These optimistic assumptions allow us to consider a large GW background of the order of $\bar{\Omega}_{\rm GW}(f) \sim \mathcal{O}(10^{-10})$ at the frequency range best probed by LVK, CE and ET, see figure 8, left plot. The assumption that the tensor spectrum follows a single power-law from CMB scales down to interferometer scales is not necessarily realistic, but it is not important either in the context of this forecast: any model with adiabatic initial conditions leading to the same $\bar{\Omega}_{\rm GW}(f)$ in the vicinity of $f_{\rm p} = 10$ Hz would lead to similar results.

- In standard analyses of cosmological data (not including CGWB anisotropies), the number $f_{\rm dec}(\eta_{\rm in})$ has no impact on observables. Instead, once we include CGWB anisotropy data, this parameter does play a role. In the case of GWs produced by inflation, $\eta_{\rm in}$ accounts for the Hubble-crossing time of the pivot frequency, see eq. (2.26).

JCAP10(2023)025

Thus, we include $f_{\rm dec}(\eta_{\rm in})$ as an additional free cosmological parameter in our analysis. In our forecast, we choose a fiducial value $f_{\rm dec}(\eta_{\rm in}) = 0$, and we float this parameter during parameter inference in order to estimate the sensitivity of the mock data to this quantity.

When `MontePython` is launched for the first time in the context of a forecast, it uses `GW_CLASS` to compute the fiducial temperature, GW and cross-correlation spectra (taking fiducial parameter values from the input parameter file). When it is launched for the second time, it assumes that the fiducial spectra account for the spectra of the mock data, and it fits this data using the mock likelihood of section 5.2, while floating the free parameters of the model. In our case, the free parameters (with flat priors) are

$$\{h,\ \omega_{\rm m},\ \omega_{\rm b},\ \ \ln 10^{10} A_s,\ n_{\rm s},\ \tau_{\rm reio},\ f_{\rm dec}(\eta_{\rm in})\},$$

accounting for the Hubble rate, the density of non-relativistic matter and baryons, the primordial curvature spectrum amplitude and tilt, the optical depth to reionization and the number of decoupled relativistic degrees of freedom after inflation. Note that we are not including $\{r, n_{\rm t}\}$ to the list, because our mock data consists only in CMB temperature and CGWB maps. These observables have negligible sensitivity to the amplitude of tensor modes and to their spectral index. Of course, without a CGWB in the first place, there would be no CGWB anisotropies to measure. However, the anisotropies themselves come dominantly from scalar fluctuations.[14] In order to constrain $\{r, n_{\rm t}\}$, one would need to include CMB polarisation data (for large scales) and/or the measurements of the monopole $\bar{\Omega}_{\rm GW}(f) \sim \mathcal{O}(10^{-10})$ by GW interferometers (for small scales). Forecasts of the sensitivity of such data sets to $\{r, n_{\rm t}\}$ can easily be found in the literature. Instead, the goal of this paper is to focus on the information contained in the CGWB anisotropies and in their correlation with the CMB temperature. Thus, we may consider $\{r, n_{\rm t}\}$ as fixed parameters in the forecast, assuming that their value would be inferred directly from the monopole measured by GW interferometers. We also note that $\{\omega_{\rm b}, \tau_{\rm reio}\}$ are kept free in our analysis because they are determined from the CMB temperature spectrum — as however they have no direct sizeable effect on the GW spectrum.

In the left plot of figure 8, our assumed monopole $\bar{\Omega}_{\rm GW}(f)$ is compared to the sensitivity of LVK, CE+ET, CE+ET+ET100 and CE+ET+ET1000. Intuitively, one expects that CGWB anisotropies could be observed by an instrument only if the background was detected with a very high signal-to-noise, typically of the order of $\sim 10^5$. According to the left plot of figure 8, this would be the case only for CE+ET+ET100 and CE+ET+ET1000. This expectation is confirmed by the right plot, in which we compare the GW auto-correlation spectrum with the detector noise $N_\ell^{\rm GW}$ of each detector, computed with a modified version of the `schNell` code as described in section 5.1. We see that with the combination CE+ET, the signal is still a few orders of magnitude below the noise, while with the upgraded ET100 and ET1000 detectors the first few multipoles have a signal-to-noise larger than one (up to $\ell = 4$ for CE+ET+ET100 and $\ell = 5$ for CE+ET+ET1000). Thus, we will perform a sensitivity forecast only for CE+ET+ET1000 and for a cosmic-variance-limited experiment. All the analysis has been done assuming five years of continuous observation.

[14] Equation (2.24) shows that the CGWB anisotropy spectrum gets a contribution from tensor modes. However, this effect is sub-dominant, thus we can safely neglect the tensor contribution in all our forecasts (in `GW_CLASS`, switching tensor modes on/off is an option).

JCAP10(2023)025

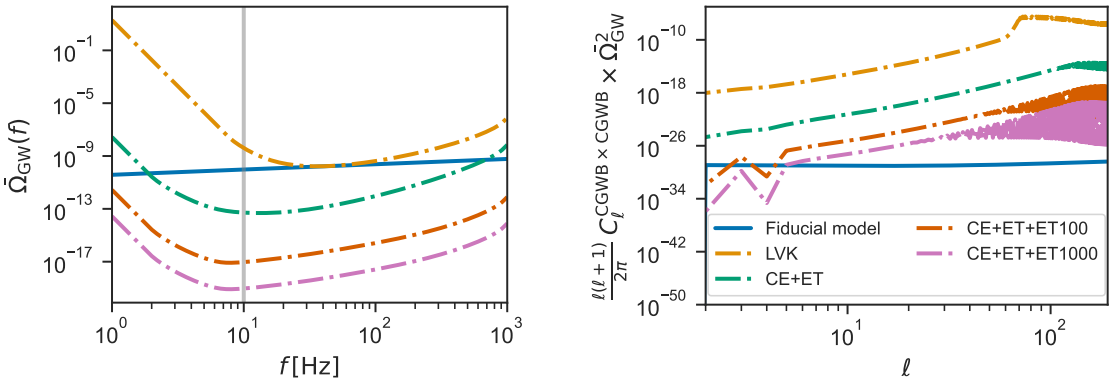

Figure 8. Fiducial model for the forecast assuming a CGWB produced by inflation with a blue tilt. We use a power-law CGWB with $\bar{\Omega}_{\rm GW} = 9.5 \times 10^{-11}$ and $n_{\rm gwb} = 0.4$, corresponding to a CGWB generated by inflation with a blue tiled tensor spectrum: $r = 0.025$ and $n_{\rm t} = 0.4$. The fiducial values of all other parameters can be found in table 1. Left: Fiducial model (solid lines) and instrumental sensitivity (dot-dashed lines) for the CGWB background energy density (or monopole) $\bar{\Omega}_{\rm GW}(f)$. The vertical line shows the pivot frequency $f_{\rm p} = 10\,$Hz. Right: Power spectrum for the anisotropies in the CGWB, $C_\ell^{\rm CGWB\times CGWB}$ (solid lines) and detector noise $N_\ell^{\rm GW}$ (dot-dashed lines). Since the detector noise scales like $\bar{\Omega}_{\rm GW}^{-2}$, we multiplied all spectra by $\bar{\Omega}_{\rm GW}^2$.

In table 1 and figure 9, we show our forecasted errors and confidence contours for:

- Planck (CMB temperature) alone, using a simplified version of the Planck likelihood dubbed `fake_planck_realistic` in `MontePython`, to which any fiducial model can be passed instead of the real Planck data,
- Planck plus mock GW anisotropy data from CE+ET+ET1000, including the CMB×GW cross-correlation,
- the same for Planck plus ideal cosmic-variance-limited GW anisotropy data up to $\ell = 2500$, dubbed CV ($\ell_{\rm max} = 2500$).

We first discuss the difference between the Planck alone and Planck+CV ($\ell_{\rm max} = 2500$) forecasted errors:

- The overall amplitude of the CMB (resp. GW spectrum) is fixed by $e^{-2\tau_{\rm reio}} A_s$ (resp. A_s). Planck temperature data is sensitive to $\tau_{\rm reio}$ only through a small steplike feature at large angular scales, and is thus unable to measure each of $\tau_{\rm reio}$ or $A_{\rm s}$ accurately. The combination of the two CMB temperature and GW spectra gives independent measurements of these two parameters, explaining why their errors shrink strongly in the combined case. We should remember however that this forecast does not include CMB polarisation data, which would also provide a good determination of $\tau_{\rm reio}$. Nevertheless, the sensitivity of the joint temperature+GW forecast, $\sigma(\tau_{\rm reio}) = 0.0014$, is about three times better than with Planck temperature+polarisation data, and twice better than in forecasts with future temperature+polarisation data from CMB-Stage-IV + LiteBIRD [106]. The cosmic-variance-limited temperature+GW error is even competing with the sensitivity of $\tau_{\rm reio}$ measurements from future 21cm surveys like HERA or SKA [107]. This shows that an ideal CGWB detector would bring decisive information for the measurement of $\{A_{\rm s}, \tau_{\rm reio}\}$ — and also potentially of the neutrino mass through the removal of parameter degeneracies [106, 108].

JCAP10(2023)025

Parameter	Fiducial	[Prior]	Planck + CE+ET+ET1000	Planck + CV($\ell_{\rm max} = 2500$)	Planck alone
h	0.6736	[0.5 - 0.8]	0.6741 ± 0.0096	0.6756 ± 0.0068	0.674 ± 0.010
ω_m	0.143	[0.1 - 0.2]	0.1429 ± 0.0020	0.1426 ± 0.0014	0.1429 ± 0.0021
$\ln 10^{10} A_s$	3.044	[1.7 - 5]	3.044 ± 0.015	3.0413 ± 0.0053	3.044 ± 0.016
n_s	0.965	[0.9 - 1]	0.9654 ± 0.0051	0.9662 ± 0.0028	$0.9653^{+0.0051}_{-0.0057}$
ω_b	0.02237	[0.02 - 0.025]	0.02238 ± 0.00020	0.02240 ± 0.00016	0.02238 ± 0.00022
$\tau_{\rm reio}$	0.0544	[0.02 - 0.08]	0.0547 ± 0.0071	0.0536 ± 0.0012	0.0545 ± 0.0073
$f_{\rm dec}(\eta_{\rm in})$	0	[0 - 1]	< 0.597	< 0.159	—

Table 1. Forecasted errors on parameters extracted from temperature anisotropy data from Planck, alone or in combination with mock GW anisotropy data from two futuristic GW detectors: CE+ET+ET1000, and an ideal cosmic-variance-limited instrument CV($\ell_{\rm max} = 2500$). We assume a CGWB produced by inflation with a blue tilt, like in figure 8.

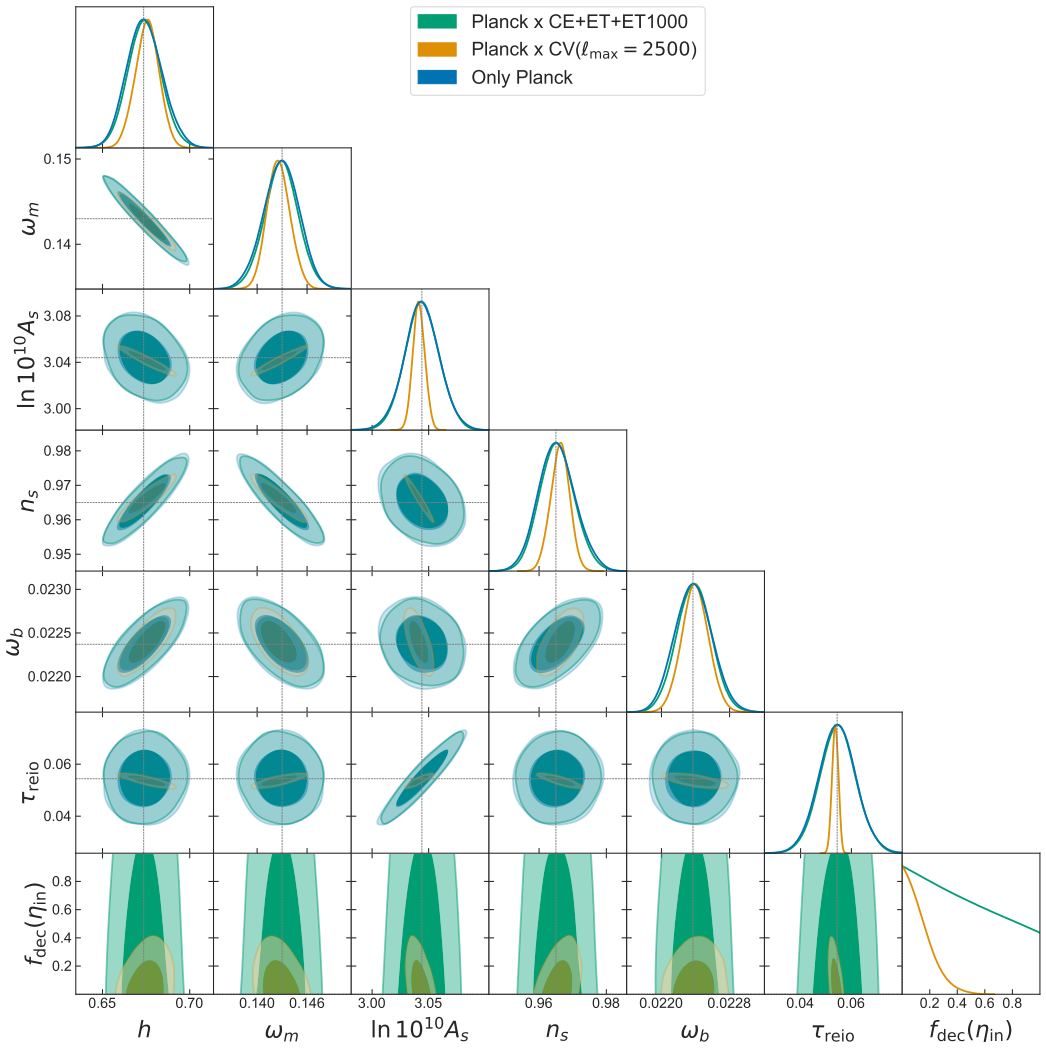

Figure 9. For the same forecast as in table 1, one-dimensional posteriors and two-dimensional 68% / 95% confidence limits on the reconstructed cosmological parameters.

JCAP10(2023)025

- The Hubble rate and matter density parameters affect the shape of the CMB and GW spectra (tilt of the plateau due to the ISW effect, scale and shape of the acoustic oscillations in the CMB case, scale and shape of the raising of the GW spectrum for modes crossing the Hubble rate during radiation domination). Our forecast shows that the errors on $\{h, \omega_{\rm m}\}$ shrink roughly by a factor $\sqrt{2}$ in the combined fit, which suggests that the map of CMB temperature anisotropy and GW anisotropies contain roughly the same amount of information on h and $\omega_{\rm m}$.

- The overall tilt of all spectra depends on $n_{\rm s}$. Thus, one may expect that the error on the tilt also shrinks by $\sqrt{2}$ in the combined case. The gain is actually a bit larger. This is due to the fact that the GW spectrum is not affected by acoustic oscillations and Silk damping, and thus, is a more direct probe of the primordial spectrum shape over a larger multipole range.

- The baryon density parameter $\omega_{\rm b}$ only affects the CMB spectrum. Still, its forecasted error decreases a tiny bit in the joint forecast. This comes for degeneracies between $\omega_{\rm b}$ and other parameters that are better determined by the GW data.

- The parameter $f_{\rm dec}(\eta_{\rm in})$ only affects the GW spectrum. With ideal GW anisotropy data, we get an error bar of about $\sigma(f_{\rm dec}(\eta_{\rm in})) = 0.17$, showing that this parameter can in principle be measured.

These results quantify the amount of information that can be extracted from the data with an extremely futuristic instrument. We now restore detector noise and compare the results obtained with Planck alone and with the combination Planck+CE+ET+ET1000. Table 1 and figure 9 show that the error bars are similar in these two cases, even for $f_{\rm dec}(\eta_{\rm in})$, which is unconstrained by Planck+CE+ET+ET1000 (see the flat posterior in figure 9). We have seen in table. 1 that a hypothetical ET1000 detector would measure the first few multipoles of the GW anisotropy spectrum with a signal-to-noise larger than one, and thus, would contain a non-zero amount of information on cosmological parameters like e.g. $A_{\rm s}$ or $n_{\rm s}$. However, the forecast shows that this amount is too small and that error bars are always dominated by the CMB temperature data.

We can conclude that for a CGWB produced by inflation with a blue tilt, even a detector with a noise level 10^3 better than the Einstein telescope would be unable to extract relevant information from the GW anisotropy map. In the next section, we will check whether similar conclusions apply to other mechanisms for the generation of the CGWB.

5.4 CGWB produced by PBHs

We now consider the GWB generation mechanism discussed in section 3.3, associated to primordial black hole formation caused by a sharp peak in the primordial spectrum with an underlying local non-Gaussian statistics. Our fiducial model has a peak at a scale corresponding to the frequency $f_* = 100\,{\rm Hz}$, with an amplitude $A_* = 2 \times 10^{-5}$ and a local non-Gaussianity parameter $f_{\rm NL} = 1$. We assume again a fiducial value $f_{\rm dec}(\eta_{\rm in}) = 0$. We consider that the CGWB is measured at a frequency $f_{\rm p} = 10\,{\rm Hz}$, and we estimate the tilt $n_{\rm gwb} = \frac{\partial \ln \bar{\Omega}_{\rm GW}}{\partial \ln f}$ from the background spectrum shown on the left-hand side of figure 10.

Figure 10 shows that for such a fiducial model, CE+ET could detect the CGWB monopole, but the sensitivity of CE+ET+ET100 is needed to start probing the first multipoles of the anisotropy spectrum. For this reason, we perform our forecast for this combination only.

JCAP10(2023)025

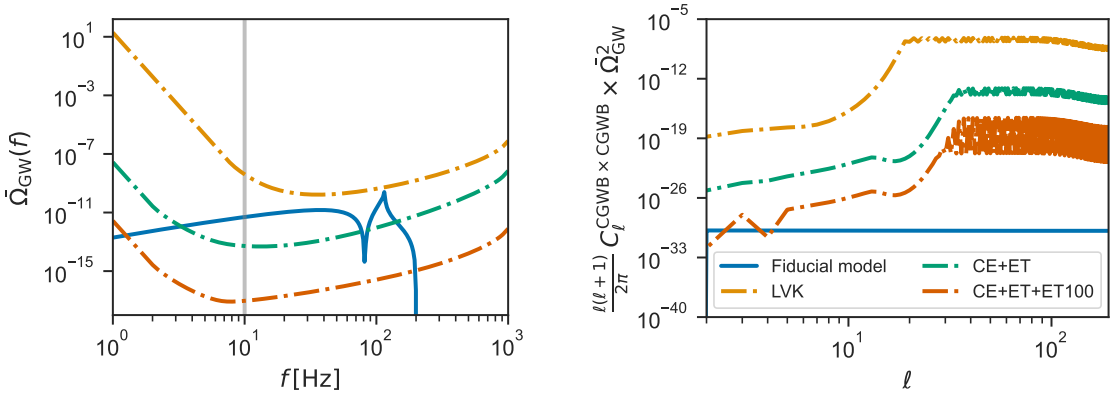

Figure 10. Fiducial model for the forecast assuming a CGWB produced by PBHs, with a fiducial local non-Gaussianity parameter $f_{\rm NL} = 1$. Left: Fiducial model (solid line) and detector sensitivity (dot-dashed lines) for the CGWB background energy density (i.e., monopole) $\bar{\Omega}_{\rm GW}(f)$. The vertical line shows the pivot frequency $f_{\rm p} = 10\,{\rm Hz}$. Right: Angular power spectrum for the CGWB anisotropies $C_\ell^{\rm CGWB\times CGWB}$ and detector noise $N_\ell^{\rm GW}$. Since the detector noise scales like $\bar{\Omega}_{\rm GW}^{-2}$, we multiplied all spectra by $\bar{\Omega}_{\rm GW}$.

Parameter	Fiducial	[Prior]	CE+ET+ET100
$f_{\rm NL}$	1	[-11.1 - 9.3]	$1.17^{+0.23}_{-0.41}$, $-1.74^{+0.42}_{-0.23}$
$f_{\rm dec}(\eta_{\rm in})$	0	[0 - 1]	—

Table 2. Forecasted errors on the cosmological parameters affecting only the CGWB anisotropies, assumed to be measured by the GW detector combination CE+ET+ET100. We assume a CGWB produced by PBHs like in figure 10.

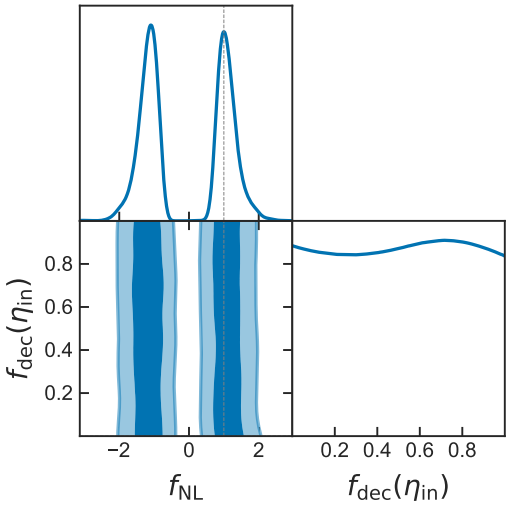

Figure 11. For the same forecast as in table 2, one-dimensional posteriors and two-dimensional 68% / 95% confidence limits on the reconstructed cosmological parameters.

JCAP10(2023)025

Having seen in the last section that the measurement of the first few multipoles of the CGWB is not sufficient for bringing new information on the ΛCDM parameters, we fix them to the Planck best-fit values. We also fix A_* and k_*, assuming that they would be inferred from data on the GW monopole. Thus, in our forecast, we only fluctuate the parameters that can be probed solely by the angular power spectra involving CGWB anisotropies, namely, ($f_{\rm NL}$ and $f_{\rm dec}(\eta_{\rm in})$).

The forecast results are shown in table 2 and figure 11. As can be seen in figure 11, there is an ambiguity in the reconstructed value of $f_{\rm NL}$. This can be understood by noticing that the dominant non-adiabatic contribution to the C_ℓ's, $C_\ell^{\rm NAD}$, is sourced by $P_\Gamma^{\rm NAD}(k,q)$ and proportional to $f_{\rm NL}^2$ (see eq. 3.13). The degeneracy between models with opposite values of $f_{\rm NL}$ is lifted by the cross-correlation between the adiabatic and non-adiabatic modes, sourced by $P^\times(k,q)$ and proportional to $f_{\rm NL}$ (see eq. 3.14). Since the non-adiabatic and cross-correlation terms depend differently on ℓ, with perfect data, it would be possible to determine uniquely the value and the sign of $f_{\rm NL}$. However, the experiment of CE+ET+ET100 is only able to observe the first multipoles until $\ell \sim 4$ (see right plot of figure 10). Thus, the ambiguity cannot be removed, and the fit to the fiducial model (with $f_{\rm NL} = 1$) is compatible with two values (close to -2 and 1).

The results displayed in figure 11 show that, in order to measure $f_{\rm dec}(\eta_{\rm in})$, it would also be necessary to measure more multipoles.

In conclusion, for the CGWB assumed here, the combination CE+ET+ET100 would be able to detect the anisotropies and use them to measure the order of magnitude of $|f_{\rm NL}|$, but a better sensitivity would be required to discriminate between the two reconstructed values of $f_{\rm NL}$ and to determine $f_{\rm dec}(\eta_{\rm in})$.

A complementary way to constrain non-Gaussianity using the SGWB×CMB signal is through the astrophysical background anisotropies. A recent forecast for next generation detectors has been done in [109].

5.5 CGBW produced by a PT with uncorrelated power-law non-adiabatic fluctuations

Like in section 3.5, we now assume a CGWB produced by sound waves during a phase transition with parameters $n_1 = 3$, $n_2 = -4$, $\Delta = 2$ and $\Omega_* = 1.0 \times 10^{-8}$. The left plot in figure 12 shows that, for this model, the monopole would be marginally detectable by LVK and well detectable by CE+ET. However, at a pivot frequency of $f_p = 10\,\text{Hz}$, the CE+ET signal-to-noise ratio would be of the order of 10^4, that is, not sufficient to detect CGWB anisotropies in presence of adiabatic initial conditions only. To get detectable CGWB anisotropies, we need to consider a more sensitive network like CE+ET+ET100 and/or assume that CGWB anisotropies are produced with intrinsic fluctuations beyond the adiabatic mode.

We thus assume like in section 3.5 that the PT seeds non-adiabatic GW fluctuations, uncorrelated with the adiabatic one and parametrized with a power-law spectrum like in eq. (3.4). We assume that this spectrum is scale-invariant ($n_{\rm gwi} = 0$) with a fiducial amplitude parameter given either by $A_{\rm gwi} = 1.0 \times 10^{-10}$ or $A_{\rm gwi} = 1.0 \times 10^{-7}$. In the first case, the adiabatic and non-adiabatic modes have the same order of magnitude, while in the second case the non-adiabatic mode strongly dominates and enhances the total perturbation spectrum by three orders of magnitude. Next, we assume that the background is mapped at the pivot frequency $f_p = 10\,\text{Hz}$, and we infer $n_{\rm gwb}$ from the monopole frequency spectrum. Finally, we assume a fiducial value for the fraction of relativistic decoupled species $f_{\rm dec}(\eta_{\rm in}) = 0$. The

JCAP10(2023)025

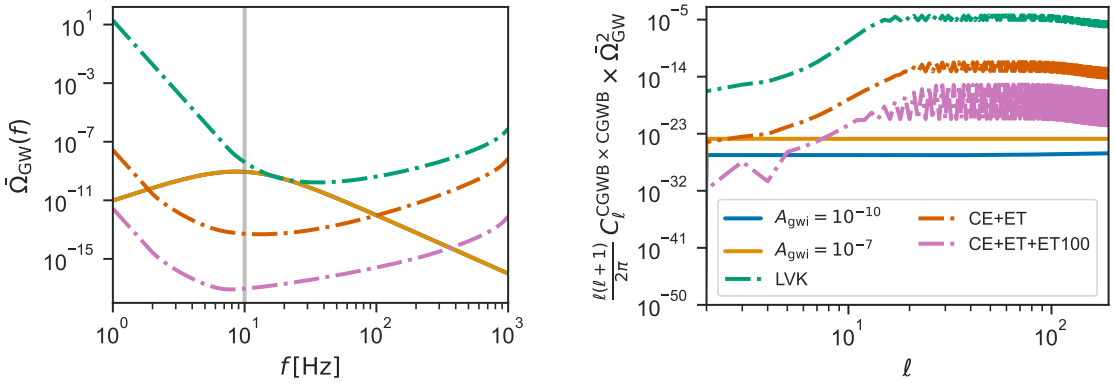

Figure 12. Fiducial model for the forecast assuming a CGWB produced by sound waves during a PT. Left: fiducial model (solid lines) and experimental sensitivity (dot-dashed line) for the monopole $\bar{\Omega}_{\rm GW}(f)$. The vertical line shows the pivot frequency $f_{\rm p} = 10\,{\rm Hz}$. Right: Power spectrum for the CGWB anisotropies $C_\ell^{\rm CGWB\times CGWB}$ and detector noise $N_\ell^{\rm GW}$, both multiplied by $\bar{\Omega}_{\rm GW}^{-2}$. For the anisotropy spectrum, we assume an uncorrelated non-adiabatic contribution with amplitude $A_{\rm gwi}$. The two curves correspond to the two fiducial models assumed here, featuring two different values of $A_{\rm gwi}$.

Parameter	Fiducial	[Prior]	CE+ET+ET100
$\ln 10^{10} A_{\rm gwi}$	0	[-10 - 10]	< 0.927
$n_{\rm gwi}$	0	[-2 - 2]	> 0.0344
$f_{\rm dec}(\eta_{\rm in})$	0	[0 - 1]	—
$\ln 10^{10} A_{\rm gwi}$	6.9	[-10 - 30]	6.6 ± 3.1
$n_{\rm gwi}$	0	[-2 - 2]	-0.06 ± 0.65
$f_{\rm dec}(\eta_{\rm in})$	0	[0 - 1]	—

Table 3. Forecasted errors on the cosmological parameters affecting only the CGWB anisotropy spectrum for the detector combination CE+ET+ET100. Like in figure 12, we assume a CGWB produced by sound waves during a PT, with an uncorrelated non-adiabatic contribution of amplitude $A_{\rm gwi} = 1.0 \times 10^{-10}$ (upper half) or 1.0×10^{-7} (lower half).

right plot in figure 12 shows that with the first fiducial model, CE+ET+ET100 could detect multipoles up to $\ell = 5$, while for the second model it could probe anisotropies up to $\ell = 7$.

The results of the two forecasts are presented in table 3 and figure 13. For the fiducial model with a small non-adiabatic contribution, the detector is only able to place an upper limit on the amplitude $A_{\rm gwi}$, which means that there would be no statistically significant detection of the anisotropies. For the model with an enhanced intrinsic GW fluctuations, there is a clear measurement of the amplitude of the non-adiabatic spectrum, and the detector could even put strong limits on its spectral index. We conclude that for a CGWB generated by a phase transition, the ability of future detectors to extract information from the spectrum of GW anisotropies depends mainly on the existence and amplitude of intrinsic GW fluctuations, beyond the unavoidable inhomogeneities corresponding to the adiabatic mode.

JCAP10(2023)025

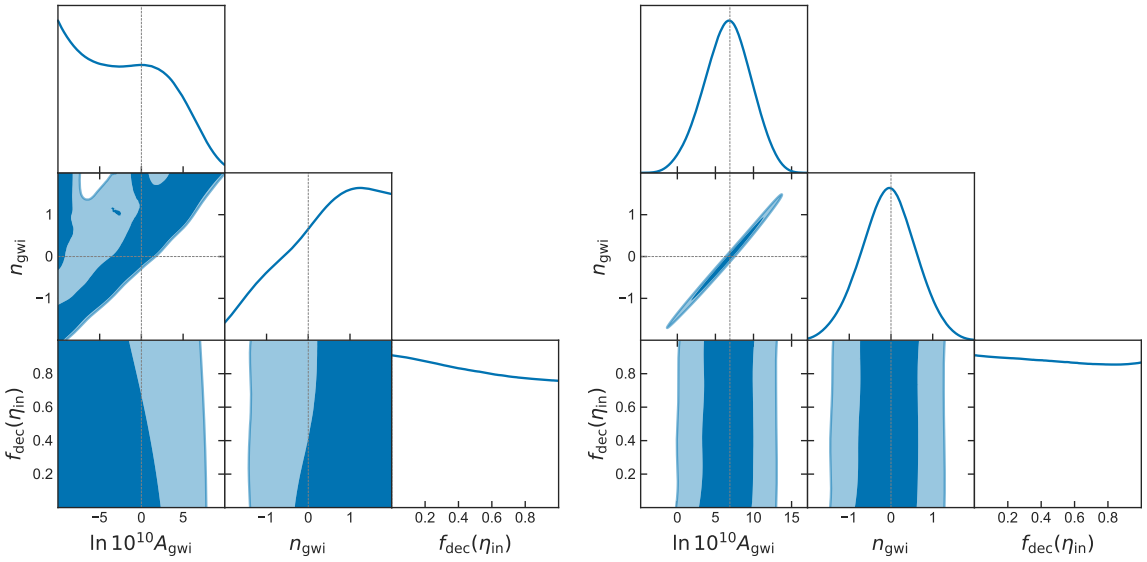

Figure 13. For the same forecasts as in table 3 (PT case with two fiducial values of $A_{\rm gwi} = 1.0 \times 10^{-10}$ (left) or 1.0×10^{-7} (right)), one-dimensional posteriors and two-dimensional 68% / 95% confidence limits on the reconstructed cosmological parameters.

6 Conclusions

The detection of a CGWB is one of the most important objectives in cosmology, as it represents a unique probe of the physics operating at very high energy scales and of the early stages of evolution of the universe. The fact that GWs can be produced at very early times and that gravitons are collisionless below the Planck scale make it possible to inspect the structure of the universe since the time at which gravitons start propagating.

Analogously to the CMB photons, primordial GWs are dominated by a homogeneous and isotropic contribution (the monopole) and exhibit tiny anisotropies of at least 1 part per 10^4. In this paper we introduce a new version of `CLASS`, called `GW_CLASS`, which computes the angular power spectrum of the CGWB and its cross-correlation with the CMB.

Although the features of the CGWB monopole depend heavily on the attributes of their generation mechanism, the CGWB anisotropy spectrum includes contributions that depend very weakly on the model. Indeed, some observable graviton fluctuations are always sourced by the modulation of the monopole by adiabatic curvature fluctuations, and then, additionally, by the propagation of the GWs through the large-scale perturbations of the universe. These contributions have essentially the same shape for all sourcing mechanisms, up to small differences triggered by the different times $\eta_{\rm in}$ at which the GW propagation starts, and by different values of the spectral index $n_{\rm gwb}$ of the monopole, which plays a role in the GW amplitude-to-energy-density conversion factor. These universal mechanisms tend to seed GW amplitude fluctuations of the same order of magnitude as curvature perturbations, that is, 1 part in 10^5. Once converted into GW density fluctuations, the anisotropies are typically of the order of 1 part in 10^4.

The default contribution to the GW anisotropy spectrum includes some SW and ISW terms that are similar to those affecting the CMB temperature spectrum, but with slightly different features, since gravitons start propagating long before the last scattering of photons and the radiation-matter equality. In `GW_CLASS`, we carefully follow the evolution of the

JCAP10(2023)025

anisotropy source functions at early times in order to account for the primordial ISW effect that operates before recombination. This allows us to compute the observable effect of parameters that regulate the evolution of the background metric of the universe, such as the fractional energy density of relativistic and decoupled species $f_{\rm dec}(\eta_{\rm in})$ or the equation of state of the universe at $\eta_{\rm in}$. The measurement of CGWB anisotropies would provide a unique handle on complementary parameters which do not leave a direct signature on the monopole. We have included the effect of $f_{\rm dec}(\eta_{\rm in})$ in `GW_CLASS`, in order to study its detectability with future experiments.

Beyond these unavoidable contributions, there is a possibility that CGWB fluctuations get enhanced in a model-dependent way by some initial intrinsic inhomogeneities in the graviton phase-space distribution that could be imprinted by each particular generation mechanism. While the adiabatic mode is independent of frequency, the non-adiabatic mode requires a long and detailed model-dependent computation. In general, it should be parametrized as a non-factorizable function of the frequency of the GWs and of the wavelength of the large-scale perturbation considered. We include in `GW_CLASS` a few possible parametrizations of this model-dependent contribution, that we call the non-adiabatic mode. Our implementation takes into account the fact that the non-adiabatic mode can be arbitrarily correlated with the adiabatic mode.

In this work, we have considered and compared for the first time the angular power spectrum of the CGWB sourced by different mechanisms. In particular, we have described the anisotropies sourced by inflation, Primordial Black Holes (PBH) and Phase Transitions (PTs), with adiabatic and non-adiabatic initial conditions. These three mechanisms are considered to be the most promising candidates to produce GWs with amplitudes large enough to be detected by future ground- and space-based interferometers. In each of these three cases, we have reviewed the impact of initial conditions and of the spectral tilt $n_{\rm gwb}$ on the CGWB angular power spectrum, making clear how these two attributes can change by orders of magnitude the amplitude of the fluctuations in the energy density of the CGWB. This example illustrates how stochastic backgrounds are sensitive to the non-adiabatic initial conditions and to interesting cosmological parameters, such as $f_{\rm NL}$. In `GW_CLASS`, it is possible to select any of these backgrounds through various possible parametrization of the non-adiabatic initial conditions.

In previous literature, the correlation of the CGWB at different frequencies has always been considered equal to one. In other words, the dependence of the angular power spectrum on frequency and multipole was assumed to be factorizable. This is however not the case when non-adiabatic initial conditions are taken into account, or when the tensor tilt changes with the frequency. A non-exact correlation of the spectrum has important consequences from a theoretical and experimental point of view, because it affects significantly the way in which we can perform the data analysis of future GW interferometers. Furthermore, a different frequency scaling of the GW anisotropies w.r.t. the monopole will be a crucial ingredient for performing component separation, reducing uncertainties in the reconstruction of GW maps. In this work, we show for the first time how to compute the correlation of the CGWB angular power spectra at different frequencies using `GW_CLASS`. `GW_CLASS` evaluates efficiently the angular power spectrum at multiple different frequencies for the auto- and cross-correlation.

We also studied in details the correlation between the CGWB and CMB anisotropy spectra. We provided a physical and mathematical interpretation of the angular power spectrum of the cross-correlation, in terms of projection effects from the last scattering surfaces of gravitons to that of photons. We found that the distance between these surfaces

JCAP10(2023)025

plays an important role at small scales. In particular, since photons and gravitons share their geodesics, there is a large correlation between their spectra on large angular scales (in absence of non-adiabatic perturbations). In the future, it would be possible to take advantage of this property to maximize the amount of information that can be extracted by a joint analysis of CMB and CGWB maps.

In order to establish the amount of information that can be extracted from CGWB observations by future experiments, we have presented some forecasts on the detectability of the CGWB angular power spectrum. Our forecasts show the sensitivity of future detectors to cosmological parameters through joint fits of mock CGWB and CMB data. Under the reasonable assumption that the correlation of the angular power spectrum of the CGWB at different frequencies is one, we have quantified the noise spectrum $N_\ell^{\rm GW}$ in CGWB maps reconstructed with various detectors. This noise depends on the amplitude of the monopole signal, on the frequency dependence of the monopole and of the anisotropy spectrum, and on the detector sensitivity and orientation.

We have performed several forecasts, considering a CGWB produced either by inflation, PBHs or a PT, as well as various combination of detectors: First, the Einstein Telescope and Cosmic Explorer; Second, a more futuristic case in which the ET sensitivity is enhanced by a factor 100 or 1000, close to expectations for the future space-based interferometers BBO and DECIGO; and finally, a cosmic-variance-limited (CVL) detector.

Our Bayesian analysis shows that a CVL detector could put very tight constraints on the parameters of the minimal ΛCDM model, since the degeneracy between the primordial amplitude A_s and the optical depth to reionization $\tau_{\rm reio}$ is broken by the CGWB. Besides, more realistic CGWB instruments offer a unique way to measure some parameters that are very difficult to probe otherwise, such as the relativistic decoupled density fraction $f_{\rm dec}(\eta_{\rm in})$, the non-Gaussianity parameter $f_{\rm NL}$ or the amplitude of non-adiabatic GW fluctuations generated during a PT. We leave for future works also the application of `GW_CLASS` to other cosmological sources of interest for interferometers.

Acknowledgments

We thank G. Galloni for useful discussions and comments on the draft. FS acknowledges support from both RWTH and MPIK computer clusters and from the IT staff. FS acknowledges membership in the International Max Planck Research School for Astronomy and Cosmic Physics at the University of Heidelberg (IMPRS-HD). NB, DB and SM acknowledge support from the COSMOS network (www.cosmosnet.it) through the ASI (Italian Space Agency) Grants 2016-24-H.0, 2016-24-H.1-2018 and 2020-9-HH.0. AR acknowledges financial support from the Supporting TAlent in ReSearch@University of Padova (STARS@UNIPD) for the project "Constraining Cosmology and Astrophysics with Gravitational Waves, Cosmic Microwave Background and Large-Scale Structure cross-correlations".

JCAP10(2023)025

A Correspondence between notations

We specify here the correspondence between the notations of previous papers on CGWB anisotropies [32–35] and those of this work, which are closer to the notations of the `CLASS` code and papers (e.g. [29, 45]):

quantity	previous	current
scalar metric perturbations in Newtonian gauge	Φ, Ψ	ψ, ϕ
comoving curvature perturbation	ζ	$\mathcal{R}$
tensor metric perturbations	χ_{ij}	h_{ij}
tensor field (with polarisation $\lambda = \pm 2$)	ξ_λ	h_λ
tensor transfer function	χ	T_h
anisotropic stress of decoupled species	$2\mathcal{N}_2$	$\sigma_{\rm dec}$
adiabatic transfer function of the graviton p.s.d. Γ	Ξ	$T_\Gamma^{\rm AD}$

B Adiabatic initial condition for the monopole

When we consider a system made of different particle species, it is useful to introduce the comoving density perturbation of each given species. This quantity is defined in a gauge invariant way as [110]

$$\Delta_{c,j} = \delta_j^{\rm bol} - 3(1+w_j)\mathcal{H}\left(v_\parallel + \omega_\parallel\right) , \tag{B.1}$$

where we have introduced the equation-of-state-parameter $w_j \equiv p_j/\rho_j$ of the species j, the longitudinal part of the total velocity $v_\parallel$, related to individual velocities v_j through

$$v_\parallel \equiv \frac{\sum_j (\rho_j + p_j) v_{\parallel\, j}}{\sum_j (\rho_j + p_j)} , \tag{B.2}$$

and the longitudinal component $\omega_\parallel$ of the metric perturbation δg_{0i}, which vanishes in the Newtonian gauge. The energy density perturbation[15] $\delta_j^{\rm bol}$ in the Newtonian gauge is connected to the one evaluated in the comoving/synchronous gauge by exploiting the fact that, in the Newtonian gauge, $\omega_\parallel = 0$. Thus, in this gauge,

$$\delta_j^{\rm bol} = \Delta_{c,j} + 3(1+w_j)\mathcal{H} v_\parallel . \tag{B.3}$$

The total comoving density is defined as

$$\Delta \equiv \sum_j \frac{\rho_j}{\rho} \Delta_{c\, j} . \tag{B.4}$$

It can be computed using the Poisson equation,

$$8\pi G \rho\, \Delta = -\frac{2k^2}{a^2}\phi \to \Delta = -\frac{2k^2}{3\mathcal{H}^2}\phi . \tag{B.5}$$

[15] We write $\delta_j^{\rm bol}$ to distinguish between the "bolometric" perturbation in the energy density, integrated over all the frequencies of the spectrum, and the perturbation in the energy density in a frequency bin, defined for the CGWB in eq. (2.13).

JCAP10(2023)025

For super-horizon modes, the ratio $k/\mathcal{H}$ goes to zero, therefore

$$|\Delta| \ll |\phi| \,. \tag{B.6}$$

The comoving density perturbation of a given species is related to the total comoving density perturbation through the relative entropy perturbation between pairs of species S_{ij},

$$\Delta_{c,i} = \frac{1+w_i}{1+w}\Delta + \sum_j \frac{\rho_j + p_j}{\rho + p} S_{ij} \,. \tag{B.7}$$

Therefore, if we consider adiabatic perturbations such that $S_{ij} = 0$, we get $\Delta_{ci} = \Delta$. Then, we can infer $\delta_j^{\rm bol}$ from eq. (B.3) provided that we find an expression for $v_\parallel$. The $(0,i)$ component of the Einstein equations gives

$$(\phi' + \mathcal{H}\psi) = -4\pi G a^2 v_\parallel \sum_j (\rho_j + p_j) \to v_\parallel = -\frac{\phi' + \mathcal{H}\psi}{2\mathcal{H}^2} \,, \tag{B.8}$$

which means that, for relativistic particles with $w_j = 1/3$, the initial density perturbation is

$$\delta_j^{\rm bol} = 4\mathcal{H} v_\parallel = -\frac{2}{\mathcal{H}} (\phi' + \mathcal{H}\psi) \,. \tag{B.9}$$

In the case of the CMB, it is immediate to connect the perturbation of the energy density to the perturbation of the distribution function, because, under the assumption that the spectrum of photon is thermal, it is possible to show that the temperature fluctuations do not depend on q, finding $\delta_{\rm CMB}^{\rm bol} = 4\Theta_0$, where Θ is the fractional temperature fluctuation of CMB photons. Since the energy spectrum of the CGWB is generally non-thermal, the relative perturbation of the energy density that appears in the Einstein equations is not the relative energy perturbation at the frequency q defined in eq. (2.13), but the bolometric density perturbation of the CGWB, which corresponds to the density perturbation at a frequency q weighted over all the GW spectrum. These two density perturbations are connected by the following integral

$$\delta_{\rm GW}^{\rm bol}(\eta, k) = \frac{\int \frac{d^3q}{a^4(\eta)} q \bar{f}_{\rm GW}(q) \delta_{\rm GW}(\eta, k, q)}{\int \frac{d^3q}{a^4(\eta)} q \bar{f}_{\rm GW}(q)} \,. \tag{B.10}$$

The adiabatic initial condition for the bolometric energy overdensity is equivalent to an integral equation for the energy density perturbation at the frequency q,

$$\int \frac{d^3q}{a^4(\eta)} q \bar{f}_{\rm GW}(q) \left[\delta_{\rm GW}(\eta, k, q) + \frac{2}{\mathcal{H}} \left(\phi'(\eta, k) + \mathcal{H}(\eta)\psi(\eta, k) \right) \right] = 0 \,. \tag{B.11}$$

In order to have a reasonable solution for any distribution function $\bar{f}_{\rm GW}(q)$, the relative perturbation of the energy density at the frequency q cannot depend on the frequency, therefore it is possible to use the relation $\delta_{\rm GW}^{\rm bol} = \delta_{\rm GW}$, finding

$$\delta_{\rm GW}(\eta_{\rm in}, k, q) = \delta_{\rm GW}(\eta_{\rm in}, k) = -\frac{2}{\mathcal{H}} \left[\phi'(\eta_{\rm in}, k) + \mathcal{H}(\eta_{\rm in})\psi(\eta_{\rm in}, k) \right] \,. \tag{B.12}$$

A physical motivation for this result is that gravitons are decoupled and we can think of them as a collection of independent species, each corresponding to a given momentum bin, and not interacting with the other bins. The adiabatic initial condition in each redshift bin gives then

$$\delta_{\rm GW}(\eta_{\rm in}, k, q) = \delta_{\rm GW}(\eta_{\rm in}, k, q') \to \delta_{\rm GW}(\eta_{\rm in}, k, q) = \delta_{\rm GW}(\eta_{\rm in}, k) = \delta_{\rm GW}^{\rm bol}(\eta_{\rm in}, k) \,. \tag{B.13}$$

JCAP10(2023)025

To compute the initial conditions for the Boltzmann equation, we use the relation between $\delta_{\rm GW}$ and Γ evaluated at initial time,

$$\delta_{\rm GW}(\eta_{\rm in},k)=\left(4-\frac{\partial\ln\bar{\Omega}_{\rm GW}(\eta_{\rm in},\,q)}{\partial\ln\,q}\right)\Gamma_0(\eta_{\rm in},k,q)\,, \tag{B.14}$$

which implies that

$$\Gamma_0(\eta_{\rm in},k,q)=-\frac{2}{\mathcal{H}(\eta_{\rm in})}\frac{1}{\left(4-\frac{\partial\ln\bar{\Omega}_{\rm GW}(\eta_{\rm in},q)}{\partial\ln\,q}\right)}\left[\phi'(\eta_{\rm in},k)+\mathcal{H}(\eta_{\rm in})\psi(\eta_{\rm in},k)\right]\,. \tag{B.15}$$

The source function for the initial condition contribution to the angular power spectrum is given by

$$\delta^{\rm I}_{\rm GW}(\eta_0,k,q)=-\frac{2}{\mathcal{H}(\eta_{\rm in})}\left(4-\frac{\partial\ln\bar{\Omega}_{\rm GW}(\eta_0,\,q)}{\partial\ln\,q}\right)\frac{\phi'(\eta_{\rm in},k)+\mathcal{H}(\eta_{\rm in})\psi(\eta_{\rm in},k)}{\left(4-\frac{\partial\ln\bar{\Omega}_{\rm GW}(\eta_{\rm in},q)}{\partial\ln\,q}\right)}\,. \tag{B.16}$$

Similarly to the CMB case, if one neglects ϕ' (and in this case consider a scale-invariant power tensor spectrum) the initial condition is $\delta_\gamma=4\theta_\gamma=-2\psi$. If there are no variations in the number of relativistic and decoupled species at $\eta_{\rm in}$, $\phi'(\eta_{\rm in},k)$ is negligible and we find the initial condition

$$\delta^{\rm I}_{\rm GW}(\eta_{\rm in},k)=-2\psi(\eta_{\rm in},k)\,. \tag{B.17}$$

As shown in appendix C, there is no Doppler term in the case of the CGWB, because gravitons are decoupled. Therefore, the source function of the adiabatic initial condition defined in eq. (2.31) is

$$T^{\rm AD}_\Gamma(\eta_{\rm in},k,q)=-\frac{2}{4-n_{\rm gwb}(q)}T_\psi(\eta_{\rm in},k)=-\frac{2}{4-n_{\rm gwb}(q)}\frac{2}{3}\left[1+\frac{4}{15}f_{\rm dec}(\eta_{\rm in})\right]^{-1}\,. \tag{B.18}$$

C Adiabatic initial condition for the dipole

The initial condition for the dipole/Doppler term has been derived for instance in [46]. We compute it by combining the two Einstein equations

$$k^2\phi(\eta,k)+3\mathcal{H}\left[\phi'(\eta,k)+\mathcal{H}(\eta)\psi(\eta,k)\right]=-16\pi Ga^2(\eta)\sum_{i=\rm all}\rho_i(\eta)f^i_0(\eta,k)\,, \tag{C.1}$$

$$k^2\phi(\eta,k)=-16\pi Ga^2(\eta)\sum_{i=\rm all}\rho_i\left[f^i_0(\eta,k)+\frac{3\mathcal{H}(\eta)}{k}f^i_1(\eta,k)\right]\,,$$

where the f^i_j represent the j-multipole of the distribution function of the species i. Under adiabatic initial conditions, we have $f^i=f^{i'}$. Therefore, it is easy to see that

$$\begin{aligned}\Gamma_1(\eta_{\rm in},k,q)&=\frac{1}{4-n_{\rm gwb}}f_1(\eta_{\rm in},k,q)\\&=-\frac{1}{4-n_{\rm gwb}}\frac{k}{6\mathcal{H}}\left(\frac{\phi'}{\mathcal{H}}+\psi\right)\to|\Gamma_1(\eta_{\rm in},k,q)|\ll|\psi(\eta_{\rm in},k,q)|\,,\end{aligned} \tag{C.2}$$

which means that the Doppler term in the initial conditions does not contribute to the angular power spectrum of the CMB anisotropies.

JCAP10(2023)025

D Inflationary CGWB

Following [3] we introduce the characteristic GW strain $h_c(\eta, \vec{k})$ describing the variance of tensor perturbations in the metric,

$$\langle h_r(\eta, \vec{k}) h_p^*(\eta, \vec{q}) \rangle = \frac{8\pi^5}{k^3} h_c^2(\eta, k) \delta_{rp} \delta^{(3)}(\vec{k} - \vec{q}) \,. \tag{D.1}$$

We compare this with the definition of the tensor power spectrum $P_T(k)$ for the inflationary GWs/tensor modes $h^{\rm inf}$ [3, eq. (188)]:

$$\begin{aligned}
\langle h_{ij}^{\rm inf}(\vec{k}) \left(h_{ij}^{\rm inf}(\vec{q}) \right)^* \rangle &= \frac{2\pi^2}{k^3} P_T(k) (2\pi)^3 \delta^{(3)}(\vec{k} - \vec{q}) && \text{(D.2)} \\
&= \langle h_{ij}(\eta_{\rm in}, \vec{k}) h_{ij}^*(\eta_{\rm in}, \vec{q}) \rangle && \text{(D.3)} \\
&= \sum_{r\,p} \langle h_r(\eta_{\rm in}, \vec{k}) h_p^*(\eta_{\rm in}, \vec{q}) \rangle \, 2\delta_{rp} && \text{(D.4)} \\
&= 4 \times \frac{8\pi^5}{k^3} h_c^2(\eta_{\rm in}, k) \delta_{rp} \delta^{(3)}(\vec{k} - \vec{q}) \,. && \text{(D.5)}
\end{aligned}$$

Thus, we can identify

$$P_T(k) = 2h_c^2(\eta_{\rm in}, k) \equiv 2 \left(h^{\rm inf}(k) \right)^2 . \tag{D.6}$$

For canonical models of inflation, one obtains [3, eq. (191)]

$$P_T(k) \simeq \frac{2}{\pi^2} \frac{H_k^2}{m_{\rm Pl}^2} \,, \quad \text{for} \quad k = a_k H_k \,. \tag{D.7}$$

Next, we want to connect the GW strain with the spectral GW energy density $\bar{\Omega}_{\rm GW}(k)$. The energy density $\rho_{\rm GW}$ is given by [3, eq. (83)]

$$\rho_{\rm GW} = \frac{\langle \dot{h}_{ij} \dot{h}^{ij} \rangle}{32\pi G} = \frac{\langle h'_{ij} h'^{ij} \rangle}{32\pi G a^2} = \int \frac{dk}{k} \frac{d\rho_{\rm GW}}{d\log k} \,. \tag{D.8}$$

We identify

$$\bar{\Omega}_{\rm GW}(k) = \frac{1}{\rho_{c\,0}} \frac{d\rho_{\rm GW}}{d\log k} \tag{D.9}$$

with the critical energy density today, $\rho_{c\,0} = \frac{3H_0^2}{8\pi G}$. Similar to the characteristic strain, we introduce the amplitude $h_c'^2(\eta, \vec{k})$ [3, eq. (84)]:

$$\langle h'_r(\eta, \vec{k}) h'^*_p(\eta, \vec{q}) \rangle = \frac{8\pi^5}{k^3} \, \delta^{(3)}(\vec{k} - \vec{q}) \, \delta_{rp} \, h_c'^2(\eta, k) \,. \tag{D.10}$$

Thus, we can identify

$$\bar{\Omega}_{\rm GW}(k) = \frac{1}{\rho_{c\,0}} \frac{d\rho_{\rm GW}}{d\log k} = \frac{1}{\rho_{c\,0}} \frac{h_c'^2(\eta_0, k)}{16\pi G \, a^2} = \frac{h_c'^2(\eta_0, k)}{6H_0^2 a^2} \,. \tag{D.11}$$

Next, using the free evolution equation of GWs in an FLRW universe [3, eq. (64)],

$$H_r''(\eta, \vec{k}) + \left(k^2 - \frac{a''}{a} \right) H_r(\eta, \vec{k}) = 0 \,, \tag{D.12}$$

JCAP10(2023)025

with $H_r(\eta,\vec{k}) = a(\eta)h_r(\eta,\vec{k})$, we find that the full solution for $a \propto \eta^n$ is given by [3, eq. (66)]

$$h_r(\eta,\vec{k}) = \frac{A_r(\vec{k})}{a(\eta)}\,\eta\, j_{n-1}(k\eta) + \frac{B_r(\vec{k})}{a(\eta)}\,\eta\, y_{n-1}(k\eta)\,. \tag{D.13}$$

The evolution on super-Hubble scales can be assumed to be constant, so $h^{\rm inf}(k)$ provides the correct initial condition for the evolution of tensor perturbations after Hubble crossing $k = a_k H_k$. Here, we only consider modes that re-enter the horizon during radiation domination (RD), $k > k_{\rm eq} = \frac{1}{\eta_{\rm eq}}$, corresponding to $f > 1.3 \times 10^{-17}\,$Hz.

During RD ($n = 1$), the evolution is given by [3, eq. (201)]

$$h_r^{\rm RD}(\eta,\vec{k}) = h^{\rm inf}(k) j_0(k\eta)\,. \tag{D.14}$$

This equation can be matched to the one describing the propagation of GWs during matter domination (MD) ($n = 2$), which we write as [3, eq. (204)]

$$h_r^{\rm MD}(\eta,\vec{k}) = \tilde{A}(\vec{k})\frac{j_1(k\eta)}{k\eta} + \tilde{B}(\vec{k})\frac{y_1(k\eta)}{k\eta}\,, \tag{D.15}$$

using a more convenient parametrization of the prefactors compared to eq. (D.13). Matching the solutions at matter-radiation equality, $\eta_{\rm eq}$, gives [3, eqs. (207), (208)]

$$\tilde{A}(k) = h^{\rm inf}(k)\left[\frac{3}{2} - \frac{\cos(2x)}{2} + \frac{\sin(2x)}{x}\right]\,, \tag{D.16}$$

$$\tilde{B}(k) = h^{\rm inf}(k)\left[\frac{1}{x} - x - \frac{\sin(2x)}{2} + \frac{\cos(2x)}{x}\right]\,, \tag{D.17}$$

with $x = k\,\eta_{\rm eq}$. Now, the full solution today (assuming η_0 is still during MD) can simply be written as [3, eq. (209)]

$$h_r(\eta_0,\vec{k}) = T(\eta_0,k)h^{\rm inf}(k)\,, \tag{D.18}$$

where $T(\eta_0,k)$ is the transfer function [3, eq. (210)]

$$T(\eta_0,k) = \frac{\tilde{A}(k)}{h^{\rm inf}(k)}\frac{j_1(k\eta_0)}{k\eta_0} + \frac{\tilde{B}(k)}{h^{\rm inf}(k)}\frac{y_1(k\eta_0)}{k\eta_0}\,. \tag{D.19}$$

Using this notation, the GW energy density eq. (D.11) can be written as [3, eq. (212)]

$$\bar{\Omega}_{\rm GW}(k) = \frac{1}{6H_0^2a_0^2}\left[T'(\eta_0,k)\right]^2\left(h^{\rm inf}(k)\right)^2 = \frac{1}{12H_0^2a_0^2}\left[T'(\eta_0,k)\right]^2 P_T(k)\,. \tag{D.20}$$

For sub-horizon scales $k \ll 1/\eta_0$ and averaging the oscillations $\sin \approx \cos \approx \frac{1}{\sqrt{2}}$, we only have to consider the leading terms in leading terms in $k\eta_0 \ll 1$ and $k\eta_{\rm eq} \ll 1$:

$$T(\eta_0,k) \underset{k\eta_0\ll 1}{\longrightarrow} \frac{k\eta_{\rm eq}}{(k\eta_0)^2}\sin(k\eta_0) \approx \frac{1}{\sqrt{2}}\frac{\eta_{\rm eq}}{k\eta_0^2}\,, \tag{D.21}$$

and [3, eq. (214)]

$$T'(\eta_0,k) \underset{k\eta_0\ll 1}{\longrightarrow} \frac{k\eta_{\rm eq}}{(k\eta_0)^2}k\cos(k\eta_0) \approx \frac{1}{\sqrt{2}}\frac{\eta_{\rm eq}}{\eta_0^2} = k\,T(\eta_0,k)\,. \tag{D.22}$$

In summary, we have

$$\bar{\Omega}_{\rm GW}(k) = \frac{1}{12H_0^2a_0^2}\frac{\eta_{\rm eq}^2}{2\eta_0^4}P_T(k)\,. \tag{D.23}$$

JCAP10(2023)025

E Correlation between two last scattering spheres

The cross-correlation angular power spectrum $C_\ell^{\rm CMB\times CGWB}$ quantifies the correlation between two last scattering spheres with slightly different radii, which depends on the calculation of the integral

$$I_\ell = \int \frac{dk}{k}\, j_\ell[k(\eta_0-\eta_1)]\, j_\ell[k(\eta_0-\eta_2)]\,. \tag{E.1}$$

In our case, η_0 is the conformal age of the universe, while $\eta_1 = n_*$ (resp. $\eta_2 = \eta_{\rm in}$) represents the conformal time at CMB (resp. GW) decoupling. Thus, we are interested in the case $\eta_0 \gg \eta_1 \gg \eta_2$, with $(\eta_1-\eta_2) \ll \eta_0$.

The general solution of this integral can be found by using

$$\begin{aligned} I_\ell &= \int \frac{dk}{k} j_\ell[k(\eta_0-\eta_1)] j_\ell[k(\eta_0-\eta_2)] = \int \frac{dx}{x} j_\ell\left(x\frac{\eta_0-\eta_1}{\eta_0-\eta_2}\right) j_\ell(x) \\ &= \frac{\pi}{2}\sqrt{\frac{\eta_0-\eta_2}{\eta_0-\eta_1}} \int \frac{dx}{x^2} J_{\ell+1/2}\left(x\frac{\eta_0-\eta_1}{\eta_0-\eta_2}\right) J_{\ell+1/2}(x)\,, \end{aligned} \tag{E.2}$$

valid for $\eta_2 < \eta_1 < \eta_0$ and defining $x = k(\eta_0-\eta_2)$. We have also used

$$j_\ell(x) = \sqrt{\frac{\pi}{2x}} J_{\ell+1/2}(x)\,. \tag{E.3}$$

The solution is found in [111]:

$$\begin{aligned} \int \frac{dx}{x^2} J_{\ell+1/2}\left(x\frac{\eta_0-\eta_1}{\eta_0-\eta_2}\right) J_{\ell+1/2}(x) = \frac{1}{4}\left(\frac{\eta_0-\eta_1}{\eta_0-\eta_2}\right)^{\ell+1/2} \frac{\Gamma(\ell)}{\Gamma(3/2)\Gamma(\ell+3/2)} \\ \times F\left[\ell, -\frac{1}{2}; \ell+3/2; \left(\frac{\eta_0-\eta_1}{\eta_0-\eta_2}\right)^2\right], \end{aligned} \tag{E.4}$$

where the last term is given by the hypergeometric series (which converges in our case)

$$F(\alpha,\beta;\gamma;z) = 1 + \frac{\alpha\cdot\beta}{\gamma\cdot 1} z + \frac{\alpha(\alpha+1)\beta(\beta+1)}{\gamma(\gamma+1)\cdot 1\cdot 2} z^2 + \frac{\alpha(\alpha+1)(\alpha+2)\beta(\beta+1)(\beta+2)}{\gamma(\gamma+1)(\gamma+2)\cdot 1\cdot 2\cdot 3} z^3 + \dots \tag{E.5}$$

By using $\Gamma(\ell+3/2) = (\ell+1/2)\Gamma(\ell+1/2)$, we can write I_ℓ as

$$I_\ell = \frac{\pi}{8}\left(\frac{\eta_0-\eta_1}{\eta_0-\eta_2}\right)^\ell \frac{1}{\ell+1/2}\frac{\Gamma(\ell)}{\Gamma(3/2)\Gamma(\ell+1/2)} F\left[\ell, -\frac{1}{2}; \ell+3/2; \left(\frac{\eta_0-\eta_1}{\eta_0-\eta_2}\right)^2\right]. \tag{E.6}$$

Thus, I_ℓ can be expressed as a convergent series in $y = \left(\frac{\eta_0-\eta_1}{\eta_0-\eta_2}\right)$, where y is slightly smaller than one. The leading contribution is given by the lowest-order term in the series,

$$I_\ell \simeq \frac{\pi}{8}\left(\frac{\eta_0-\eta_1}{\eta_0-\eta_2}\right)^\ell \frac{1}{\ell+1/2}\frac{\Gamma(\ell)}{\Gamma(3/2)\Gamma(\ell+1/2)}\,, \tag{E.7}$$

which, in the large-ℓ limit, scales like

$$I_\ell \propto \left(\frac{\eta_0-\eta_1}{\eta_0-\eta_2}\right)^\ell \frac{1}{\sqrt{\ell}(\ell+1/2)}\,. \tag{E.8}$$

JCAP10(2023)025

F The GW_CLASS code

In this appendix, we present GW_CLASS in more detail. GW_CLASS will be made publicly available on GitHub as a new branch.[16] Like in the base version of CLASS, GW_CLASS can be called using either the command line with a parameter file (.param) or through the Python interface classy. The basic input and output specific to GW_CLASS are described in appendix F.1, including the flags activating the CGWB computation and the format of the output files. Appendix F.2 gives a complete overview of all CGWB sources (that is, generation mechanisms) covered by GW_CLASS and of their parametrization. The most important modifications to the base CLASS code are summarized in appendix F.3, and a few precision tests establishing the validity and accuracy of our implementation are presented in appendix F.4.

F.1 GW_CLASS input and output

Input. A comprehensive overview of the most important parameters specific to GW_CLASS is given in table 4.

To activate the computation of the CGWB at a given (list of) frequencies f_gwb, one should include either gwCl or OmGW in the field output, e.g. with output = gwCl, OmGW. The key gwCl activates the computation of the angular power spectrum $C_\ell^{\mathrm{CGWB}\times\mathrm{CGWB}}$ using the line of sight integral, as described in section 2, while OmGW activates the computation of the spectral energy density $\bar{\Omega}_{\mathrm{GW}}(f)$ for a given source model (specified through the field gwb_source_type). Note that GW_CLASS is designed primarily for the computation of $C_\ell^{\mathrm{CGWB}\times\mathrm{CGWB}}$. Still, the computation of $\bar{\Omega}_{\mathrm{GW}}(f)$ is included, because the calculation of the $C_\ell^{\mathrm{CGWB}\times\mathrm{CGWB}}$'s at a given frequency f_i depend on it through the parameters $n_{\mathrm{gwb}}(f_i)$ and $\bar{\Omega}_{\mathrm{GW}}(f_i)$. As a consequence, the key gwCl only works in combination with OmGW.

GW_CLASS automatically computes the cross-correlations angular spectrum $C_\ell^{\mathrm{CMB}\times\mathrm{CGWB}}(f_i)$ at all frequencies f_i specified by f_gwb if at least tCl and gwCl are simultaneously included in the output field, e.g. with output = tCl, gwCl, OmGW.

The minimum and maximum frequency f_{min} and f_{max} give the range for $\bar{\Omega}_{\mathrm{GW}}(f)$, while the pivot frequency f_{pivot} determines the pivot scale for $\bar{\Omega}_{\mathrm{GW}}(f)$. The CGWB anisotropies and their cross-correlations are evaluated at all frequencies $\mathbf{f}_{\mathrm{gwb}} = (f_1, \ldots, f_i, \ldots, f_j, \ldots, f_N)$. The parameter convert_gwb_to_energydensity controls whether the power spectrum $C_\ell^{\mathrm{CGWB}\times\mathrm{CGWB}}$ is the anisotropy spectrum of the density δ_{GW} (when set to yes, default) or of the graviton phase-space-distribution perturbation Γ (when set to no).[17]

The different terms contributing to the power spectrum $C_\ell^{\mathrm{CGWB}\times\mathrm{CGWB}}$ can be switched on/off thanks to the field gravitational_wave_contributions in the same way as, in the base version of CLASS, different contributions to C_ℓ^{CMB} can be switched on/off with the field temperature_contributions.

The user can adjust the GW initial conditions with several input fields. The initial conformal time defined in (2.26) is assumed to be $\eta_{\mathrm{ini}} = 0$ Mpc. The number of relativistic decoupled degrees of freedom $f_{\mathrm{dec}}(\eta_{\mathrm{in}})$ at that time is specified through f_dec_ini. In the text, we argued that a natural choice for this parameter is f_dec_ini=0 (default). However,

[16] The branch will be available under the name GW_CLASS at https://github.com/lesgourg/class_public/ once this paper has been accepted. The GW_CLASS branch will be up-to-date with the current base version of CLASS, that is, with the master branch.

[17] GW_CLASS computes the line-of-sight integral in terms of Γ, since this is more convenient (see section 2). The conversion to the energy density contrast δ_{GW} is achieved by multiplying the transfer functions with $(4 - n_{\mathrm{gwb}})$.

JCAP10(2023)025

Parameter	GW_CLASS
Compute $C_\ell^{\mathrm{CGWB}\times\mathrm{CGWB}}$ and $\bar{\Omega}_{\mathrm{GW}}(f)$	`output = gwCl, OmGW`
Compute cross correlations with CMB	`output = tCl, gwCl, OmGW`
Pivot frequency f_{pivot} [Hz]	`f_pivot = 1`
Minimum frequency f_{min} [Hz]	`f_min = 1e-3`
Maximum frequency f_{max} [Hz]	`f_max = 1e2`
Observed CGWB frequencies f [Hz]	`f_gwb = f_pivot`
can be a list of N frequencies	`f_gwb = 1.0, 2.5, ..., 1e2`
Convert to GWB energy density	`convert_gwb_to_energydensity = yes/no`
Contributions to $C_\ell^{\mathrm{CGWB}\times\mathrm{CGWB}}$	`gravitational_wave_contributions =`
SW	`tsw,`
primordial ISW ($z \gg \mathcal{O}(10^5)$)	`pisw,`
early ISW ($z \sim 10^3$)	`eisw,`
late ISW ($z \sim \mathcal{O}(1)$)	`lisw,`
adiabatic initial contribution	`ad,`
non-adiabatic initial contribution	`ini`
Split redshift for early/late ISW	`early_late_isw_redshift = 50`
$f_{\mathrm{dec}}(\eta_{\mathrm{in}})$	`f_dec_ini = 0`
CGWB source type	`gwb_source_type =`
Power-law	`analytic_gwb`
Inflationary CGWB	`inflationary_gwb`
External CGWB	`external_gwb`
CGWB from PBHs	`PBH_gwb`
CGWB from PT	`PT_gwb`

Table 4. Most important parameters specific to GW_CLASS (and implemented default value when relevant).

to deactivate the effect of early decoupled species, one can set `f_dec_ini = -1`. In this case, GW_CLASS will assume no decoupled species beyond those still present at recombination, that is, ordinary neutrinos plus possible extra relativistic relics passed in input for the CMB anisotropy calculations. Then, GW_CLASS will automatically infer $f_{\mathrm{dec}}(\eta_{\mathrm{in}})$ from the usual "effective number of neutrinos" N_{eff}, base on input values for the density of ultra-relativistic relics `ur` and light relics `ncdm`. The type of CGWB source (or generation mechanism) can be set with the parameter `gwb_source_type`. Each type leads to a different parametrization for $\bar{\Omega}_{\mathrm{GW}}(f)$. More details on the different sources are given in appendix F.2 and in Chap. 3. On top of choosing a given source type, the user can activate intrinsic/non-adiabatic initial perturbations for the CGWB, labelled `gwi` in GW_CLASS. The corresponding parameters are summarized in table 5.

JCAP10(2023)025

Parameter	GW_CLASS
initial condition: adiabatic mode GW intrinsic/non-adiabatic initial mode other isocurvature modes (baryon isocurvature, ...)	ic = ad, gwi, bi, ...
amplitude $A_{\rm gwi}$ or $\ln 10^{10} A_{\rm gwi}$ spectral index $n_{\rm gwi}$ running $\alpha_{\rm gwi}$	A_gwi = 0. ln10^{10}A_gwi n_gwi = 0. alpha_gwi = 0.
cross-correlations fraction with adiabatic mode its spectral index its running	c_ad_gwi = 0. n_ad_gwi = 0. alpha_ad_gwi = 0.

Table 5. Parameters describing a possible intrinsic/non-adiabatic initial mode for GWs in GW_CLASS, see section 3.2 (the right column also shows the implemented default values). The syntax is very similar to that for ordinary isocurvature modes in the base version of CLASS.

Output. As usual in CLASS, the output consists either in files (when running on a terminal) or python dictionaries (when calling the functions of the classy python module). GW_CLASS can output the angular power spectra C_ℓ (possibly including CMB, CGWB and cross-correlation spectra at all frequencies f_gwb), the energy density spectra $\bar{\Omega}_{\rm GW}(f)$, and finally, if non-adiabatic modes are enabled, the primordial spectrum $P^{\rm NAD}(k)$. Table 6 gives an overview of the labels corresponding to column names in the output files or to keys in output python dictionaries.

F.2 CGWB sources in GW_CLASS

Table 7 summarizes the different schemes implemented in GW_CLASS to describe the various sources (or generation mechanisms) for the GW background. These schemes are labelled by the flag gwb_source_type.

The simplest possible parametrization of the CGWB energy density $\bar{\Omega}_{\rm GW}(f)$ is a power-law. In GW_CLASS this case is activated with the flag gwb_source_type = analytic_gwb. It assumes a parametrization of $\bar{\Omega}_{\rm GW}(f)$ with a syntax very similar to that of the scalar power spectrum in the case analytic_Pk:

$$\bar{\Omega}_{\rm GW}(f) = \bar{\Omega}_* \left(\frac{f}{f_{\rm pivot}} \right)^{n_{\rm gwb} + \frac{1}{2}\alpha_{\rm gwb} \log \frac{f}{f_{\rm pivot}}} . \tag{F.1}$$

Details on this parametrization are provided in table 7.

Second, one can assume that $\bar{\Omega}_{\rm GW}(f)$ is given by the primordial tensor spectrum generated by inflation, whose parametrization is already implemented in the base version of CLASS. In that case, one should switch to gwb_source_type = inflationary_gwb, check that tensor modes are activated with the usual CLASS syntax (modes = t, ...) and adjust the tensor-to-scalar ratio, tensor spectral index and tensor running, as described in section 3.1 and table 7. As indicated, GW_CLASS uses $n_{\rm gwb} = n_{\rm t}$ in this parametrization.

JCAP10(2023)025

Output	Terminal	`classy`
Power spectrum C_ℓ	`cl.dat`	`classy.raw_cl(l_max)`
multipole ℓ	`l`	`ell`
$C_\ell^{\mathrm{CMB}\times\mathrm{CMB}}$	`TT`	`tt`
$C_\ell^{\mathrm{CGWB}\times\mathrm{CGWB}}(f_i, f_j)$	`G[i]-G[j]`	`gg` (only $i = j = 1$)
$C_\ell^{\mathrm{CMB}\times\mathrm{CGWB}}(f_i)$	`T-G[i]`	`tg` (only $i = 1$)
Alternative `classy` function	–	`classy.cgwb_cl(l_max)`
multipole ℓ		`ell`
frequencies f_i [Hz]		`f_gwb [Hz]`
$C_\ell^{\mathrm{CGWB}\times\mathrm{CGWB}}(f_i, f_j)$		`gg` (3D-array `[i][j][ell]`)
$C_\ell^{\mathrm{CMB}\times\mathrm{CGWB}}(f_i)$		`tg` (2D-array `[i][ell]`)
Spectral energy density $\bar{\Omega}_{\mathrm{GW}}(f)$	`OmegaGW.dat`	`classy.get_omega_gw()`
frequency f [Hz]	`f [Hz]`	`f [Hz]`
$\bar{\Omega}_{\mathrm{GW}}(f)$	`Omega_GW(f)`	`Omega_GW(f)`
Alternative `classy` function		`classy.Omega_GW(f)`
Spectral tilt $n_{\mathrm{gwb}}(f)$	–	`classy.n_gwb(f)`
Primordial spectrum $P(k)$	`primordial_Pk.dat`	`classy.get_primordial()`
wave number k [1/Mpc]	`k [1/Mpc]`	`k [1/Mpc]`
scalar spectrum $P_{\mathcal{R}}(k)$	`P_scalar(k)`	`P_scalar(k)`
CGWB isocurvature $P_{NAD}(k)$	`P_gwi(k)`	`P_gwi(k)`
scalar $\times$ CGWB cross correlation	`ad x gwi`	`ad x gwi`
tensor spectrum $P_T(k) = 4P_{h_\lambda}(k)$	`P_tensor(k)`	`P_tensor(k)`

Table 6. Output files with their column names and output dictionaries with their associated keys.

Third, with the option `gwb_source_type = external_gw`, it is also possible to pass to `GW_CLASS` a spectrum $\bar{\Omega}_{\mathrm{GW}}(f)$ that has been tabulated in a file or that is being computed on-the-fly by an external code. This works in a similar way as for the primordial scalar/tensor spectra when the flag `external_Pk` is activated in the base version of `CLASS` (see table 7).[18]

Fourth, one can activate the sourcing of GW anisotropies by PBHs with non-Gaussian statistics described in section 3.3 with `gwb_source_type = PBH_gwb`. In this case, the parameters listed in table 7 match the definitions given in section 3.3.

Fifth, the user may switch to GW anisotropies originating from a phase transition (see section 3.4) with `gwb_source_type = PT_gwb`. The parameters shown in table 7 for this case are explained in section 3.4.

[18] `GW_CLASS` also allows to pass a tabulated non-adiabatic mode `gwi` together with the primordial power spectrum.

JCAP10(2023)025

gwb_source_type	Parameter	GW_CLASS
analytic_gwb	Amplitude $\bar{\Omega}_*$ quad or $\ln\left(10^{10}\bar{\Omega}_*\right)$ tilt $n_{\rm gwb}$ running $\alpha_{\rm gwb}$	Omega_gwb = 1e-10 ln10^{10}Omega_gwb n_gwb = 0. alpha_gwb = 0.
inflationary_gwb	activate tensor modes tensor to scalar ratio r $n_{\rm t}(=n_{\rm gwb})$ α_t	modes = t (, s) r = 1. n_t = scc alpha_t = scc
external_gwb	command for $P(k)$ command for $\bar{\Omega}_{\rm GW}(f)$ argument1 ... argument10	command command_gwb custom1 ... custom10
PBH_gwb	A_* or $\ln(10^{10}A_*)$ f_* in [Hz] $f_{\rm NL}$	A_star = 2e-5 ln10^{10}A_star f_star = 10. f_NL = 0.
PT_gwb	$\bar{\Omega}_*$ f_* [Hz] n_1 n_2 Δ	OmegaPT_star = 1e-7 fPT_star = 1. nPT_1 = 3. nPT_2 = -4. deltaPT = 2.

Table 7. Input parameters for the different CGWB sources.

F.3 Numerical implementation

The main modification in GW_CLASS consists in the implementation of new source functions for the scalar and tensor perturbations of the CGWB. For the ISW contribution to scalar and tensor perturbations, these source functions are defined in the perturbation module:

```
//Newtonian gauge
// Integrand to be multiplied by j_ell for the ISW
gwb0 = switch_gwb_isw * 2.*phi_prime;

// Integrand to be multiplied by j^(1)_ell for the ISW
gwb1 = switch_gwb_isw * k* (psi-phi);

//Synchronous gauge
// Integrand to be multiplied by j_ell for the ISW
gwb0 = switch_gwb_isw * 2. * (eta_prime
        - a_prime_over_a_prime * alpha
        - a_prime_over_a * alpha_prime);

// Integrand to be multiplied by j^(1)_ell for the ISW
```


JCAP10(2023)025

```
    gwb1 = switch_gwb_isw * k * (alpha_prime
            + 2. * a_prime_over_a * alpha
            - eta);

    //Tensor modes
    gwb2 = -switch_gwb_isw * gwdot;
```

Listing 1. Implementation of the source function `gwb0`, `gwb1` and `gwb2` in `perturbation.c:perturbations_sources()`

These source functions are integrated along the line of sight within the `transfer` module. Since the other source functions are only meant to be evaluated at $\eta_{\rm in}$ or $\eta_{\rm min}$,[19] and do not need to be integrated over the line of sight, they are more conveniently defined directly within the `transfer` module, in the lines:

```
    // Combination of PISW and EISW: terms proportional to Phi
    gwb_sw0 = (-switch_gwb_pisw)
            * phi[tau_ini_gwb] * ((1. + 2./5. * f_dec_ini) / (1. + 4./15. *
    f_dec_ini)) / ((1. + 2./5. * f_dec_late) / (1. + 4./15. * f_dec_late)) //
    this product gives phi(eta_ini) in the notations of the paper
            + (switch_gwb_pisw + switch_gwb_eisw)
            * phi[tau_ini_gwb]; // this is directly phi(eta_min) in the
    notations of the paper

    // Combination of SW, PISW, EISW: terms proportional to Psi
    gwb_sw1 = (switch_gwb_sw - switch_gwb_pisw)
            * psi[tau_ini_gwb] * (1. + 4./15. * f_dec_late) / (1. + 4./15. *
    f_dec_ini) // this product gives psi(eta_ini)
            + (switch_gwb_pisw - switch_gwb_eisw)
            * psi[tau_ini_gwb]; // this is directly psi(eta_min)

    // Adiabatic inital condition
    gwb_ad = switch_gwb_ad
            * psi[tau_ini_gwb] * (1. + 4./15. * f_dec_late) / (1. + 4./15. *
    f_dec_ini); // this product gives psi(eta_ini)

    gwb_ini = switch_gwb_ini * 1.;
```

Listing 2. Implementation of the source function `gwb_sw0`, `gwb_sw1`, `gwb_ad` and `gwb_ini` in `transfer.c:transfer_sources()`

The source functions `gwb0`, `gwb_sw0`, `gwb_sw1`, `gwb_ad`, `gwb_ini` are then multiplied with the spherical Bessel function $j_\ell(k(\eta_{\rm in}-\eta_0))$ (associated to the flag `SCALAR_TEMPERATURE_0` in the code), while `gwb1` uses the derivative of this function $j_\ell^{(1)}(k(\eta_{\rm in}-\eta_0))$ (with flag `SCALAR_TEMPERATURE_1`) and `gwb2` uses the Bessel function usually associated to tensor modes (with flag `TENSOR_TEMPERATURE_2`). Afterwards, in the `harmonic` module, all terms are gathered to form the complete transfer function, possibly including non-adiabatic and/or tensor modes.

In order to enable the computation of the source functions at early time $\eta \sim \eta_{\rm min}$, the time sampling of the source functions needs to be extended to an earlier time in `GW_CLASS` than in the base code. This time is set by a precision parameter `start_sources_at_tau_gwb` with default value 0.1 Mpc. Starting from this time, the source functions are sampled at every interval $\Delta\eta = \frac{a}{a'} \times \epsilon$, where ϵ is set like in the base version of `CLASS` by the precision parameter `perturbations_sampling_stepsize`.

[19] In this paper, we always denote conformal time as η, but inside the code it is denoted as `tau`.

JCAP10(2023)025

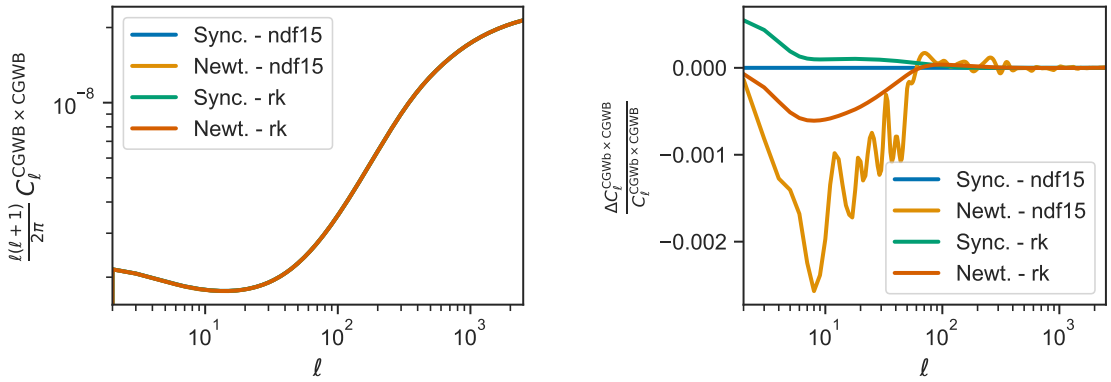

Figure 14. Comparison of `GW_CLASS` in two different gauges and using two different ODE evolvers. Left: power spectrum $C_\ell^{\mathrm{CGWB}\times\mathrm{CGWB}}$, right: relative difference.

The energy density $\bar{\Omega}_{\mathrm{GW}}$ is implemented in the `primordial` module as a new variable `lnOmGW`, together with the logarithmic frequency `lnf`. The non-adiabatic initial spectrum $P^{\mathrm{NAD}}(k)$ is associated to a new type of initial condition with index `index_ic_gwi`, defined on equal footing with usual isocurvature modes (baryon isocurvature, CDM isocurvature, etc.)

F.4 Precision tests

We have performed an extended series of precision tests. First, we have compared in a systematic way the output of two versions of `GW_CLASS` developed independently by two of us. Second, we have checked the convergence of our results against precision parameter settings. We only highlight here the result of our most important tests.

Figure 14 shows the comparison of the CGWB anisotropy spectrum in the Newtonian (Newt.) and synchronous (Sync.) gauge, using the two Ordinary Differential Equation (ODE) evolvers of `CLASS`, `ndf15` and `rk`. We find that percent precision is achieved, although the Newtonian gauge is slightly less precise than the synchronous one.

It is worth highlighting the important role played by the precision parameter that controls the k_{max} value in `GW_CLASS`, called `k_max_tau0_over_l_max_gwb`. This parameter fixes the ratio $R \equiv [k_{\mathrm{max}}\tau_0/\ell_{\mathrm{max}}]$, such that k_{max} is inferred from the requested multipole ℓ_{max} and from the conformal age of the universe τ_0 computed for each cosmology (denoted as η_0 in this paper). This dimensionless parameter is fixed by default to $R = 2.4$.

Using the default value $R = 2.4$ for the CGWB anisotropy spectrum leads to numerical artifacts for large ℓ, see figure 15. The figure shows the SW contribution alone compared with its analytic solution (based on an analytic integral over the spherical Bessel function, valid for constant source functions on super-Hubble scales). In `GW_CLASS`, the calculation of the $C_\ell^{\mathrm{CGWB}\times\mathrm{CGWB}}$ spectrum relies on a new precision parameter `k_max_tau0_over_l_max_gwb` set by default to $R = 12$. With such a setting, the `GW_CLASS` spectrum is in excellent agreement with the analytic solution. A further increase of this parameter leads to even better accuracy at the expense of drastically increasing the computation time.

Another important precision parameter is η_{min} (`start_sources_at_tau_gwb`), which defines the conformal time at which the ISW contribution to GW perturbations starts to be stored in the `perturbation` module — and thus, starts to be integrated explicitly over the line of sight in the `transfer` module. Starting at too late times $\eta > 1\,\mathrm{Mpc}$ results in loosing contributions to the ISW term, and using imprecise initial conditions for the SW and

JCAP10(2023)025

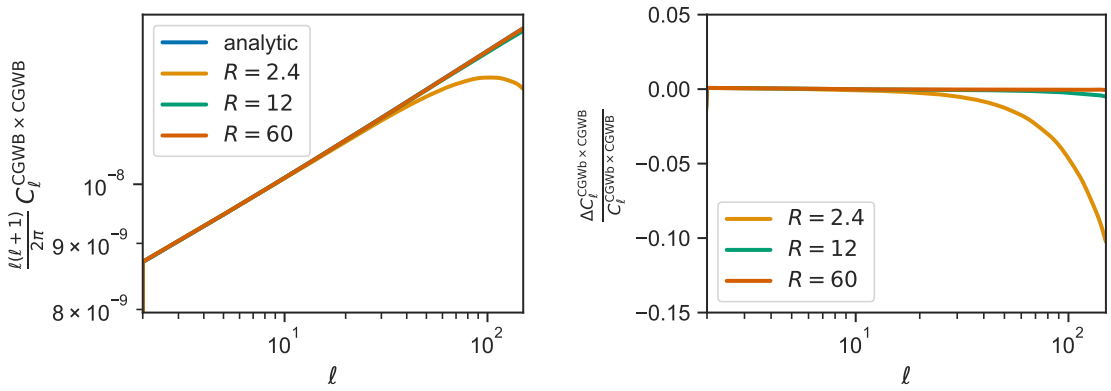

Figure 15. Comparison of the SW effect calculated analytically and with `GW_CLASS` for different choices of $k_{\max}$, controlled by the parameter $R \equiv [k_{\max}\tau_0/\ell_{\max}]$. Left: power spectrum $C_\ell^{\mathrm{CGWB}\times\mathrm{CGWB}}$, right: relative difference.

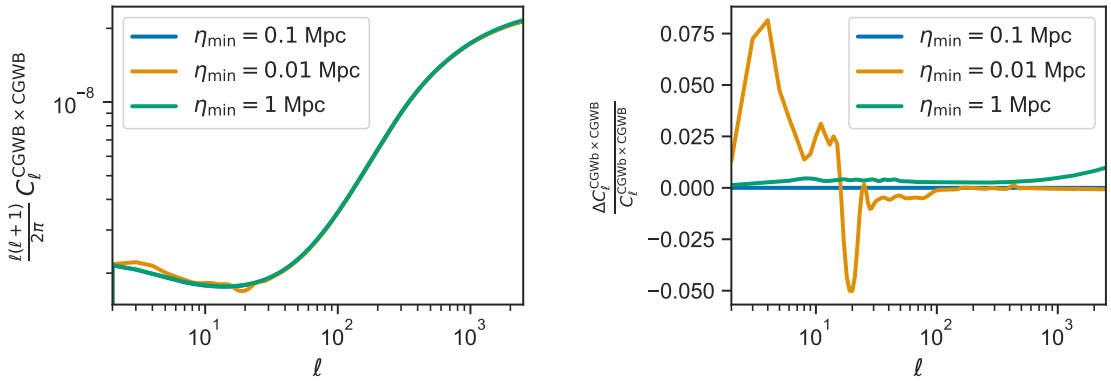

Figure 16. Impact of the parameter $\eta_{\min}$ that governs the starting time for of the line-of-sight integral of the ISW contribution, in the Newtonian gauge and using the `ndf15` evolver. Left: power spectrum $C_\ell^{\mathrm{CGWB}\times\mathrm{CGWB}}$, right: relative difference. The results are more stable in the synchronous gauge.

initial terms. On the other hand, using too early times leads to numerical problems in `CLASS`, which was originally developed for starting to store the CMB source functions slightly before photon decoupling. These problems are especially apparent in the Newtonian gauge, while the synchronous gauge is more stable. In `GW_CLASS`, this parameter is set to 0.1 Mpc. We find that this compromise gives stable and well-converged results in both gauges and using both evolvers. Figure 16 illustrates the impact of changing this parameter.

Finally, we gather in table 8 the default settings for all precision parameters relevant specifically to `GW_CLASS`. These parameters are defined and further explained in `input/precisions.h`.

JCAP10(2023)025

Parameter	GW_CLASS
$R = [k_{\max}\tau_0/\ell_{\max}]$	k_max_tau0_over_l_max_gwb = 12.0
Starting time of GW_CLASS $\eta_{\min}$ [Mpc]	start_sources_at_tau_gwb = 0.1
Logarithmic f spacing	f_per_decade_primordial = 100.
Trigger to neglect transfer function gwb0	transfer_neglect_delta_k_S_gwb0 = 0.3
Trigger to neglect transfer function gwb1	transfer_neglect_delta_k_S_gwb1 = 0.2
Trigger to neglect transfer function gwb2	transfer_neglect_delta_k_T_gwb2 = 0.2

Table 8. Precision parameter defined in precisions.h. These should not be changed, unless one is aware of the consequences.

References

[1] M. Maggiore, *Gravitational Waves. Vol. 2: Astrophysics and Cosmology*, Oxford University Press (2018) [INSPIRE].

[2] M.C. Guzzetti, N. Bartolo, M. Liguori and S. Matarrese, *Gravitational waves from inflation*, *Riv. Nuovo Cim.* **39** (2016) 399 [arXiv:1605.01615] [INSPIRE].

[3] C. Caprini and D.G. Figueroa, *Cosmological Backgrounds of Gravitational Waves*, *Class. Quant. Grav.* **35** (2018) 163001 [arXiv:1801.04268] [INSPIRE].

[4] LISA Cosmology Working Group collaboration, *Cosmology with the Laser Interferometer Space Antenna*, *Living Rev. Rel.* **26** (2023) 5 [arXiv:2204.05434] [INSPIRE].

[5] C. Caprini et al., *Reconstructing the spectral shape of a stochastic gravitational wave background with LISA*, *JCAP* **11** (2019) 017 [arXiv:1906.09244] [INSPIRE].

[6] R. Flauger et al., *Improved reconstruction of a stochastic gravitational wave background with LISA*, *JCAP* **01** (2021) 059 [arXiv:2009.11845] [INSPIRE].

[7] M. Punturo et al., *The Einstein Telescope: A third-generation gravitational wave observatory*, *Class. Quant. Grav.* **27** (2010) 194002 [INSPIRE].

[8] M. Maggiore et al., *Science Case for the Einstein Telescope*, *JCAP* **03** (2020) 050 [arXiv:1912.02622] [INSPIRE].

[9] M. Branchesi et al., *Science with the Einstein Telescope: a comparison of different designs*, *JCAP* **07** (2023) 068 [arXiv:2303.15923] [INSPIRE].

[10] D. Reitze et al., *Cosmic Explorer: The U.S. Contribution to Gravitational-Wave Astronomy beyond LIGO*, *Bull. Am. Astron. Soc.* **51** (2019) 035 [arXiv:1907.04833] [INSPIRE].

[11] M. Evans et al., *A Horizon Study for Cosmic Explorer: Science, Observatories, and Community*, arXiv:2109.09882 [INSPIRE].

[12] LISA collaboration, *Laser Interferometer Space Antenna*, arXiv:1702.00786 [INSPIRE].

[13] V. Corbin and N.J. Cornish, *Detecting the cosmic gravitational wave background with the big bang observer*, *Class. Quant. Grav.* **23** (2006) 2435 [gr-qc/0512039] [INSPIRE].

[14] S. Kawamura et al., *The Japanese space gravitational wave antenna DECIGO*, *Class. Quant. Grav.* **23** (2006) S125 [INSPIRE].

[15] N.J. Cornish, *Mapping the gravitational wave background*, *Class. Quant. Grav.* **18** (2001) 4277 [astro-ph/0105374] [INSPIRE].

[16] C.M.F. Mingarelli, T. Sidery, I. Mandel and A. Vecchio, *Characterizing gravitational wave stochastic background anisotropy with pulsar timing arrays*, *Phys. Rev. D* **88** (2013) 062005 [arXiv:1306.5394] [INSPIRE].

JCAP10(2023)025

[17] C.R. Contaldi et al., *Maximum likelihood map-making with the Laser Interferometer Space Antenna*, *Phys. Rev. D* **102** (2020) 043502 [arXiv:2006.03313] [INSPIRE].

[18] KAGRA et al. collaborations, *Search for anisotropic gravitational-wave backgrounds using data from Advanced LIGO and Advanced Virgo's first three observing runs*, *Phys. Rev. D* **104** (2021) 022005 [arXiv:2103.08520] [INSPIRE].

[19] V. Ferrari, S. Matarrese and R. Schneider, *Stochastic background of gravitational waves generated by a cosmological population of young, rapidly rotating neutron stars*, *Mon. Not. Roy. Astron. Soc.* **303** (1999) 258 [astro-ph/9806357] [INSPIRE].

[20] V. Ferrari, S. Matarrese and R. Schneider, *Gravitational wave background from a cosmological population of core collapse supernovae*, *Mon. Not. Roy. Astron. Soc.* **303** (1999) 247 [astro-ph/9804259] [INSPIRE].

[21] E.S. Phinney, *A practical theorem on gravitational wave backgrounds*, astro-ph/0108028 [INSPIRE].

[22] A.J. Farmer and E.S. Phinney, *The gravitational wave background from cosmological compact binaries*, *Mon. Not. Roy. Astron. Soc.* **346** (2003) 1197 [astro-ph/0304393] [INSPIRE].

[23] T. Regimbau and S.A. Hughes, *Gravitational-wave confusion background from cosmological compact binaries: Implications for future terrestrial detectors*, *Phys. Rev. D* **79** (2009) 062002 [arXiv:0901.2958] [INSPIRE].

[24] X.-J. Zhu et al., *Stochastic Gravitational Wave Background from Coalescing Binary Black Holes*, *Astrophys. J.* **739** (2011) 86 [arXiv:1104.3565] [INSPIRE].

[25] T. Regimbau, *The astrophysical gravitational wave stochastic background*, *Res. Astron. Astrophys.* **11** (2011) 369 [arXiv:1101.2762] [INSPIRE].

[26] G. Mentasti, C. Contaldi and M. Peloso, *Prospects for detecting anisotropies and polarization of the stochastic gravitational wave background with ground-based detectors*, *JCAP* **08** (2023) 053 [arXiv:2304.06640] [INSPIRE].

[27] D. Bertacca et al., *Projection effects on the observed angular spectrum of the astrophysical stochastic gravitational wave background*, *Phys. Rev. D* **101** (2020) 103513 [arXiv:1909.11627] [INSPIRE].

[28] N. Bellomo et al., *CLASS_GWB: robust modeling of the astrophysical gravitational wave background anisotropies*, *JCAP* **06** (2022) 030 [arXiv:2110.15059] [INSPIRE].

[29] D. Blas, J. Lesgourgues and T. Tram, *The Cosmic Linear Anisotropy Solving System (CLASS) II: Approximation schemes*, *JCAP* **07** (2011) 034 [arXiv:1104.2933] [INSPIRE].

[30] V. Alba and J. Maldacena, *Primordial gravity wave background anisotropies*, *JHEP* **03** (2016) 115 [arXiv:1512.01531] [INSPIRE].

[31] C.R. Contaldi, *Anisotropies of Gravitational Wave Backgrounds: A Line Of Sight Approach*, *Phys. Lett. B* **771** (2017) 9 [arXiv:1609.08168] [INSPIRE].

[32] N. Bartolo et al., *Anisotropies and non-Gaussianity of the Cosmological Gravitational Wave Background*, *Phys. Rev. D* **100** (2019) 121501 [arXiv:1908.00527] [INSPIRE].

[33] N. Bartolo et al., *Characterizing the cosmological gravitational wave background: Anisotropies and non-Gaussianity*, *Phys. Rev. D* **102** (2020) 023527 [arXiv:1912.09433] [INSPIRE].

[34] L. Valbusa Dall'Armi et al., *Imprint of relativistic particles on the anisotropies of the stochastic gravitational-wave background*, *Phys. Rev. D* **103** (2021) 023522 [arXiv:2007.01215] [INSPIRE].

[35] A. Ricciardone et al., *Cross-Correlating Astrophysical and Cosmological Gravitational Wave Backgrounds with the Cosmic Microwave Background*, *Phys. Rev. Lett.* **127** (2021) 271301 [arXiv:2106.02591] [INSPIRE].

JCAP10(2023)025

[36] M. Braglia and S. Kuroyanagi, *Probing prerecombination physics by the cross-correlation of stochastic gravitational waves and CMB anisotropies*, *Phys. Rev. D* **104** (2021) 123547 [arXiv:2106.03786] [INSPIRE].

[37] G. Galloni et al., *Test of the statistical isotropy of the universe using gravitational waves*, *JCAP* **09** (2022) 046 [arXiv:2202.12858] [INSPIRE].

[38] J. Lesgourgues, *The Cosmic Linear Anisotropy Solving System (CLASS) I: Overview*, arXiv:1104.2932 [INSPIRE].

[39] B. Allen and A.C. Ottewill, *Detection of anisotropies in the gravitational wave stochastic background*, *Phys. Rev. D* **56** (1997) 545 [gr-qc/9607068] [INSPIRE].

[40] C. Caprini et al., *Science with the space-based interferometer eLISA. II: Gravitational waves from cosmological phase transitions*, *JCAP* **04** (2016) 001 [arXiv:1512.06239] [INSPIRE].

[41] N. Bartolo et al., *Science with the space-based interferometer LISA. IV: Probing inflation with gravitational waves*, *JCAP* **12** (2016) 026 [arXiv:1610.06481] [INSPIRE].

[42] B. Audren, J. Lesgourgues, K. Benabed and S. Prunet, *Conservative Constraints on Early Cosmology: an illustration of the Monte Python cosmological parameter inference code*, *JCAP* **02** (2013) 001 [arXiv:1210.7183] [INSPIRE].

[43] T. Brinckmann and J. Lesgourgues, *MontePython 3: boosted MCMC sampler and other features*, *Phys. Dark Univ.* **24** (2019) 100260 [arXiv:1804.07261] [INSPIRE].

[44] L. Valbusa Dall'Armi, A. Ricciardone and D. Bertacca, *The dipole of the astrophysical gravitational-wave background*, *JCAP* **11** (2022) 040 [arXiv:2206.02747] [INSPIRE].

[45] J. Lesgourgues and T. Tram, *Fast and accurate CMB computations in non-flat FLRW universes*, *JCAP* **09** (2014) 032 [arXiv:1312.2697] [INSPIRE].

[46] S. Dodelson, *Modern Cosmology*, Academic Press, Amsterdam, The Netherlands (2003) [INSPIRE].

[47] LISA Cosmology Working Group collaboration, *Probing anisotropies of the Stochastic Gravitational Wave Background with LISA*, *JCAP* **11** (2022) 009 [arXiv:2201.08782] [INSPIRE].

[48] L. Pizzuti et al., *Boltzmann equations for astrophysical Stochastic Gravitational Wave Backgrounds scattering off of massive objects*, *JCAP* **02** (2023) 054 [arXiv:2208.02800] [INSPIRE].

[49] D. Wands, K.A. Malik, D.H. Lyth and A.R. Liddle, *A new approach to the evolution of cosmological perturbations on large scales*, *Phys. Rev. D* **62** (2000) 043527 [astro-ph/0003278] [INSPIRE].

[50] N. Bartolo et al., *Gravitational wave anisotropies from primordial black holes*, *JCAP* **02** (2020) 028 [arXiv:1909.12619] [INSPIRE].

[51] C.-P. Ma and E. Bertschinger, *Cosmological perturbation theory in the synchronous and conformal Newtonian gauges*, *Astrophys. J.* **455** (1995) 7 [astro-ph/9506072] [INSPIRE].

[52] S. Bashinsky and U. Seljak, *Neutrino perturbations in CMB anisotropy and matter clustering*, *Phys. Rev. D* **69** (2004) 083002 [astro-ph/0310198] [INSPIRE].

[53] A. Malhotra et al., *New universal property of cosmological gravitational wave anisotropies*, *Phys. Rev. D* **107** (2023) 103502 [arXiv:2212.10316] [INSPIRE].

[54] M. Sasaki, T. Suyama, T. Tanaka and S. Yokoyama, *Primordial black holes — perspectives in gravitational wave astronomy*, *Class. Quant. Grav.* **35** (2018) 063001 [arXiv:1801.05235] [INSPIRE].

[55] N. Bartolo et al., *Primordial Black Hole Dark Matter: LISA Serendipity*, *Phys. Rev. Lett.* **122** (2019) 211301 [arXiv:1810.12218] [INSPIRE].

JCAP10(2023)025

[56] C. Caprini and R. Durrer, *Gravitational waves from stochastic relativistic sources: Primordial turbulence and magnetic fields*, *Phys. Rev. D* **74** (2006) 063521 [astro-ph/0603476] [INSPIRE].

[57] Y. Watanabe and E. Komatsu, *Improved Calculation of the Primordial Gravitational Wave Spectrum in the Standard Model*, *Phys. Rev. D* **73** (2006) 123515 [astro-ph/0604176] [INSPIRE].

[58] S. Weinberg, *Damping of tensor modes in cosmology*, *Phys. Rev. D* **69** (2004) 023503 [astro-ph/0306304] [INSPIRE].

[59] D.A. Dicus and W.W. Repko, *Comment on damping of tensor modes in cosmology*, *Phys. Rev. D* **72** (2005) 088302 [astro-ph/0509096] [INSPIRE].

[60] B.A. Stefanek and W.W. Repko, *Analytic description of the damping of gravitational waves by free streaming neutrinos*, *Phys. Rev. D* **88** (2013) 083536 [arXiv:1207.7285] [INSPIRE].

[61] G. Galloni et al., *Updated constraints on amplitude and tilt of the tensor primordial spectrum*, *JCAP* **04** (2023) 062 [arXiv:2208.00188] [INSPIRE].

[62] K. Tomita, *Non-Linear Theory of Gravitational Instability in the Expanding Universe. II*, *Prog. Theor. Phys.* **45** (1971) 1747.

[63] S. Matarrese, O. Pantano and D. Saez, *A general relativistic approach to the nonlinear evolution of collisionless matter*, *Phys. Rev. D* **47** (1993) 1311 [INSPIRE].

[64] S. Matarrese, O. Pantano and D. Saez, *General relativistic dynamics of irrotational dust: Cosmological implications*, *Phys. Rev. Lett.* **72** (1994) 320 [astro-ph/9310036] [INSPIRE].

[65] S. Matarrese, S. Mollerach and M. Bruni, *Second order perturbations of the Einstein-de Sitter universe*, *Phys. Rev. D* **58** (1998) 043504 [astro-ph/9707278] [INSPIRE].

[66] S. Mollerach, D. Harari and S. Matarrese, *CMB polarization from secondary vector and tensor modes*, *Phys. Rev. D* **69** (2004) 063002 [astro-ph/0310711] [INSPIRE].

[67] R. Saito and J. Yokoyama, *Gravitational-Wave Constraints on the Abundance of Primordial Black Holes*, *Prog. Theor. Phys.* **123** (2010) 867 [arXiv:0912.5317] [INSPIRE].

[68] K.N. Ananda, C. Clarkson and D. Wands, *The cosmological gravitational wave background from primordial density perturbations*, *Phys. Rev. D* **75** (2007) 123518 [gr-qc/0612013] [INSPIRE].

[69] G. Domènech, S. Pi and M. Sasaki, *Induced gravitational waves as a probe of thermal history of the universe*, *JCAP* **08** (2020) 017 [arXiv:2005.12314] [INSPIRE].

[70] Y.B. Zel'dovich and I.D. Novikov, *The Hypothesis of Cores Retarded during Expansion and the Hot Cosmological Model*, *Soviet Astron. AJ (Engl. Transl.)* **10** (1967) 602 [INSPIRE].

[71] J. Kristiano and J. Yokoyama, *Ruling Out Primordial Black Hole Formation From Single-Field Inflation*, arXiv:2211.03395 [INSPIRE].

[72] A. Riotto, *The Primordial Black Hole Formation from Single-Field Inflation is Still Not Ruled Out*, arXiv:2303.01727 [INSPIRE].

[73] H. Firouzjahi and A. Riotto, *Primordial Black Holes and Loops in Single-Field Inflation*, arXiv:2304.07801 [INSPIRE].

[74] J. Garcia-Bellido, M. Peloso and C. Unal, *Gravitational waves at interferometer scales and primordial black holes in axion inflation*, *JCAP* **12** (2016) 031 [arXiv:1610.03763] [INSPIRE].

[75] V. Domcke, F. Muia, M. Pieroni and L.T. Witkowski, *PBH dark matter from axion inflation*, *JCAP* **07** (2017) 048 [arXiv:1704.03464] [INSPIRE].

[76] J. Fumagalli, S. Renaux-Petel, J.W. Ronayne and L.T. Witkowski, *Turning in the landscape: A new mechanism for generating primordial black holes*, *Phys. Lett. B* **841** (2023) 137921 [arXiv:2004.08369] [INSPIRE].

JCAP10(2023)025

[77] K. Kohri and T. Terada, *Semianalytic calculation of gravitational wave spectrum nonlinearly induced from primordial curvature perturbations*, *Phys. Rev. D* **97** (2018) 123532 [arXiv:1804.08577] [INSPIRE].

[78] J.R. Espinosa, D. Racco and A. Riotto, *A Cosmological Signature of the SM Higgs Instability: Gravitational Waves*, *JCAP* **09** (2018) 012 [arXiv:1804.07732] [INSPIRE].

[79] E. Witten, *Cosmic Separation of Phases*, *Phys. Rev. D* **30** (1984) 272 [INSPIRE].

[80] C.J. Hogan, *Gravitational radiation from cosmological phase transitions*, *Mon. Not. Roy. Astron. Soc.* **218** (1986) 629 [INSPIRE].

[81] A. Kosowsky and M.S. Turner, *Gravitational radiation from colliding vacuum bubbles: envelope approximation to many bubble collisions*, *Phys. Rev. D* **47** (1993) 4372 [astro-ph/9211004] [INSPIRE].

[82] M. Kamionkowski, A. Kosowsky and M.S. Turner, *Gravitational radiation from first order phase transitions*, *Phys. Rev. D* **49** (1994) 2837 [astro-ph/9310044] [INSPIRE].

[83] C. Caprini, R. Durrer, T. Konstandin and G. Servant, *General Properties of the Gravitational Wave Spectrum from Phase Transitions*, *Phys. Rev. D* **79** (2009) 083519 [arXiv:0901.1661] [INSPIRE].

[84] S.J. Huber and T. Konstandin, *Gravitational Wave Production by Collisions: More Bubbles*, *JCAP* **09** (2008) 022 [arXiv:0806.1828] [INSPIRE].

[85] D.J. Weir, *Revisiting the envelope approximation: gravitational waves from bubble collisions*, *Phys. Rev. D* **93** (2016) 124037 [arXiv:1604.08429] [INSPIRE].

[86] M. Hindmarsh, S.J. Huber, K. Rummukainen and D.J. Weir, *Gravitational waves from the sound of a first order phase transition*, *Phys. Rev. Lett.* **112** (2014) 041301 [arXiv:1304.2433] [INSPIRE].

[87] M. Hindmarsh, S.J. Huber, K. Rummukainen and D.J. Weir, *Numerical simulations of acoustically generated gravitational waves at a first order phase transition*, *Phys. Rev. D* **92** (2015) 123009 [arXiv:1504.03291] [INSPIRE].

[88] M. Hindmarsh, *Sound shell model for acoustic gravitational wave production at a first-order phase transition in the early Universe*, *Phys. Rev. Lett.* **120** (2018) 071301 [arXiv:1608.04735] [INSPIRE].

[89] C. Caprini, R. Durrer and G. Servant, *The stochastic gravitational wave background from turbulence and magnetic fields generated by a first-order phase transition*, *JCAP* **12** (2009) 024 [arXiv:0909.0622] [INSPIRE].

[90] P. Binetruy, A. Bohe, C. Caprini and J.-F. Dufaux, *Cosmological Backgrounds of Gravitational Waves and eLISA/NGO: Phase Transitions, Cosmic Strings and Other Sources*, *JCAP* **06** (2012) 027 [arXiv:1201.0983] [INSPIRE].

[91] A. Romero et al., *Implications for First-Order Cosmological Phase Transitions from the Third LIGO-Virgo Observing Run*, *Phys. Rev. Lett.* **126** (2021) 151301 [arXiv:2102.01714] [INSPIRE].

[92] S. Kumar, R. Sundrum and Y. Tsai, *Non-Gaussian stochastic gravitational waves from phase transitions*, *JHEP* **11** (2021) 107 [arXiv:2102.05665] [INSPIRE].

[93] P. Auclair et al., *Probing the gravitational wave background from cosmic strings with LISA*, *JCAP* **04** (2020) 034 [arXiv:1909.00819] [INSPIRE].

[94] S. Kuroyanagi, K. Takahashi, N. Yonemaru and H. Kumamoto, *Anisotropies in the gravitational wave background as a probe of the cosmic string network*, *Phys. Rev. D* **95** (2017) 043531 [arXiv:1604.00332] [INSPIRE].

JCAP10(2023)025

[95] A.C. Jenkins and M. Sakellariadou, *Anisotropies in the stochastic gravitational-wave background: Formalism and the cosmic string case*, *Phys. Rev. D* **98** (2018) 063509 [arXiv:1802.06046] [INSPIRE].

[96] L. Bethke, D.G. Figueroa and A. Rajantie, *Anisotropies in the Gravitational Wave Background from Preheating*, *Phys. Rev. Lett.* **111** (2013) 011301 [arXiv:1304.2657] [INSPIRE].

[97] L. Bethke, D.G. Figueroa and A. Rajantie, *On the Anisotropy of the Gravitational Wave Background from Massless Preheating*, *JCAP* **06** (2014) 047 [arXiv:1309.1148] [INSPIRE].

[98] G. Mentasti and M. Peloso, *ET sensitivity to the anisotropic Stochastic Gravitational Wave Background*, *JCAP* **03** (2021) 080 [arXiv:2010.00486] [INSPIRE].

[99] D. Alonso et al., *Noise angular power spectrum of gravitational wave background experiments*, *Phys. Rev. D* **101** (2020) 124048 [arXiv:2005.03001] [INSPIRE].

[100] P. Adshead et al., *Multimessenger cosmology: Correlating cosmic microwave background and stochastic gravitational wave background measurements*, *Phys. Rev. D* **103** (2021) 023532 [arXiv:2004.06619] [INSPIRE].

[101] U. Seljak and M. Zaldarriaga, *A line of sight integration approach to cosmic microwave background anisotropies*, *Astrophys. J.* **469** (1996) 437 [astro-ph/9603033] [INSPIRE].

[102] S. Kawamura et al., *Current status of space gravitational wave antenna DECIGO and B-DECIGO*, *PTEP* **2021** (2021) 05A105 [arXiv:2006.13545] [INSPIRE].

[103] G. Orlando, M. Pieroni and A. Ricciardone, *Measuring Parity Violation in the Stochastic Gravitational Wave Background with the LISA-Taiji network*, *JCAP* **03** (2021) 069 [arXiv:2011.07059] [INSPIRE].

[104] G. Mentasti, C.R. Contaldi and M. Peloso, *Intrinsic limits on the detection of the anisotropies of the Stochastic Gravitational Wave Background*, arXiv:2301.08074 [INSPIRE].

[105] PLANCK collaboration, *Planck 2018 results. I. Overview and the cosmological legacy of Planck*, *Astron. Astrophys.* **641** (2020) A1 [arXiv:1807.06205] [INSPIRE].

[106] T. Brinckmann et al., *The promising future of a robust cosmological neutrino mass measurement*, *JCAP* **01** (2019) 059 [arXiv:1808.05955] [INSPIRE].

[107] A. Liu et al., *Eliminating the optical depth nuisance from the CMB with 21 cm cosmology*, *Phys. Rev. D* **93** (2016) 043013 [arXiv:1509.08463] [INSPIRE].

[108] R. Allison et al., *Towards a cosmological neutrino mass detection*, *Phys. Rev. D* **92** (2015) 123535 [arXiv:1509.07471] [INSPIRE].

[109] G. Perna, A. Ricciardone, D. Bertacca and S. Matarrese, *Non-Gaussianity from the Cross-correlation of the Astrophysical Gravitational Wave Background and the Cosmic Microwave Background*, arXiv:2302.08429 [INSPIRE].

[110] H. Kodama and M. Sasaki, *Cosmological Perturbation Theory*, *Prog. Theor. Phys. Suppl.* **78** (1984) 1 [INSPIRE].

[111] I.S. Gradshteyn, I.M. Ryzhik, D. Zwillinger and V. Moll, *Table of integrals, series, and products*, 8th edition, Academic Press, Amsterdam, The Netherlands (2015) [DOI:0123849330].

JCAP10(2023)025